Published for SISSA by Springer

Received: *January 11, 2022*
Accepted: *March 22, 2022*
Published: *May 3, 2022*

Search for higgsinos decaying to two Higgs bosons and missing transverse momentum in proton-proton collisions at $\sqrt{s} = 13$ TeV

The CMS collaboration

E-mail: cms-publication-committee-chair@cern.ch

Abstract: Results are presented from a search for physics beyond the standard model in proton-proton collisions at $\sqrt{s} = 13$ TeV in channels with two Higgs bosons, each decaying via the process $\mathrm{H} \to \mathrm{b\bar{b}}$, and large missing transverse momentum. The search uses a data sample corresponding to an integrated luminosity of 137 fb^{-1} collected by the CMS experiment at the CERN LHC. The search is motivated by models of supersymmetry that predict the production of neutralinos, the neutral partners of the electroweak gauge and Higgs bosons. The observed event yields in the signal regions are found to be consistent with the standard model background expectations. The results are interpreted using simplified models of supersymmetry. For the electroweak production of nearly mass-degenerate higgsinos, each of whose decay chains yields a neutralino ($\tilde{\chi}_1^0$) that in turn decays to a massless goldstino and a Higgs boson, $\tilde{\chi}_1^0$ masses in the range 175 to 1025 GeV are excluded at 95% confidence level. For the strong production of gluino pairs decaying via a slightly lighter $\tilde{\chi}_2^0$ to H and a light $\tilde{\chi}_1^0$, gluino masses below 2330 GeV are excluded.

Keywords: Hadron-Hadron Scattering, Higgs Physics, Supersymmetry

ArXiv ePrint: 2201.04206

Open Access, Copyright CERN,
for the benefit of the CMS Collaboration.
Article funded by SCOAP[3].

https://doi.org/10.1007/JHEP05(2022)014

JHEP05(2022)014

Contents

1 Introduction **1**

2 Analysis strategy **4**

3 The CMS detector **5**

4 Simulated event samples **6**

5 Triggers and event reconstruction **7**

6 Event selection and reconstruction of Higgs boson candidates **10**

7 Background estimation **15**

8 Systematic uncertainties **18**
- 8.1 Background systematic uncertainties (resolved signature) 18
- 8.2 Background systematic uncertainties (boosted signature) 19
- 8.3 Signal systematic uncertainties 21

9 Results and interpretation **23**

10 Summary **31**

The CMS collaboration **43**

JHEP05(2022)014

1 Introduction

The discovery of the Higgs boson (H) at the CERN Large Hadron Collider (LHC) [1–4] provides a new tool for probing physics beyond the standard model (SM). Higgs boson production is expected to be prominent in the decays of a variety of new, heavy particles, such as those arising in theories based on supersymmetry (SUSY) [5–14]. For example, Higgs bosons would be produced in the decays of higgsinos, their supersymmetric partners. A key motivation to search for higgsinos is that in certain models they are generically expected to be among the lightest supersymmetric particles, with masses kinematically accessible at the LHC. This is particularly the case in so-called natural SUSY models [15–17], which are designed to stabilize the electroweak mass scale. Searches for higgsinos are nevertheless challenging, not only because of the wide range of possible physics scenarios, but also because their electroweak coupling to other particles leads to small production cross sections. Higgsino searches are therefore expected to be a long-term part of the LHC physics program.

We search for processes in proton-proton (pp) collisions leading to the production of two Higgs bosons, together with missing momentum transverse to the beam direction ($\vec{p}_{\mathrm{T}}^{\mathrm{miss}}$) and possible additional jets. The Higgs bosons are reconstructed in the decay $\mathrm{H} \to \mathrm{b}\overline{\mathrm{b}}$, which has a branching fraction of 58% [18]. To provide sensitivity to the wide range of kinematic configurations that can arise, the analysis searches both for events containing pairs of $\mathrm{H} \to \mathrm{b}\overline{\mathrm{b}}$ decays in which the b-tagged jets are separately resolved, and for events in which the b jets from a given H boson decay are merged together into a single, wider jet. We refer to the unmerged and merged kinematic configurations as the resolved signature and the boosted signature, respectively, because the merging of b jets typically occurs when the parent Higgs boson has a high momentum.

The search uses an event sample of pp collision data at $\sqrt{s} = 13\,\mathrm{TeV}$, corresponding to an integrated luminosity of $137\,\mathrm{fb}^{-1}$, collected in 2016–2018 by the CMS experiment at the LHC. Searches for this and related decay scenarios have been performed by ATLAS [19–37] and CMS [38–64] using 7, 8, and 13 TeV data. The data for the results reported here include the smaller samples of ref. [45] for the resolved signature and ref. [51] for the boosted signature. Tabulated results are provided in the HEPData record for this analysis [65].

The simplest SUSY framework is the minimal supersymmetric standard model (MSSM), which includes an additional doublet of complex scalar Higgs fields [12–14] beyond the doublet in the SM. The SUSY partners of the gauge and Higgs bosons, referred to as gauginos and higgsinos, respectively, are all spin $J = 1/2$ fermions. In the MSSM, there are four higgsinos, two of which are charged ($\widetilde{\mathrm{H}}^{\pm}$) and two of which are neutral ($\widetilde{\mathrm{h}}^{0}$, $\widetilde{\mathrm{H}}^{0}$). However, the phenomenology of the electroweak sector of the MSSM is complicated by the fact that the partners of the electroweak gauge and Higgs bosons can mix. The resulting physical states are then the electrically neutral mass eigenstates, $\widetilde{\chi}^{0}_{1\text{-}4}$ (where the particles are ordered in mass, with $\widetilde{\chi}^{0}_{1}$ corresponding to the lightest), referred to as neutralinos, and the electrically charged mass eigenstates, $\widetilde{\chi}^{\pm}_{1,2}$ [66], referred to as charginos. In models that conserve R-parity [11, 67], the lightest supersymmetric particle (LSP) is stable, and because of its weak interactions would escape experimental detection. The $\widetilde{\chi}^{0}_{1}$ would be a candidate for the LSP, as would the goldstino ($\widetilde{\mathrm{G}}$), a Nambu-Goldstone particle associated with the spontaneous breaking of global supersymmetry.

Figure 1 shows three models that can lead to the experimental signature considered in this analysis. These scenarios are described using the framework of simplified SUSY models [68–71], in which many of the SUSY particles are assumed to be decoupled or otherwise irrelevant to the process under consideration. In the TChiHH-G simplified model (figure 1, left), the LSP is the goldstino. In a broad range of scenarios in which SUSY breaking is mediated at a low scale, such as gauge-mediated supersymmetry breaking (GMSB) models [72, 73], the goldstino is nearly massless on the scale of the other particles and is the LSP. The $\widetilde{\chi}^{0}_{1}$ is then the next-to-lightest supersymmetric particle (NLSP) [74]. The NLSPs are produced in the cascade decays of several different combinations of neutralinos and charginos, and the goldstino is taken to be approximately massless. An important case arises when the lighter neutralinos $\widetilde{\chi}^{0}_{1,2}$ and charginos $\widetilde{\chi}^{\pm}_{1}$ are dominated by their higgsino content and, as a consequence, are nearly mass degenerate. In this case, all of their cascade decays can lead to the production of the NLSP and soft particles. The NLSP subsequently

JHEP05(2022)014

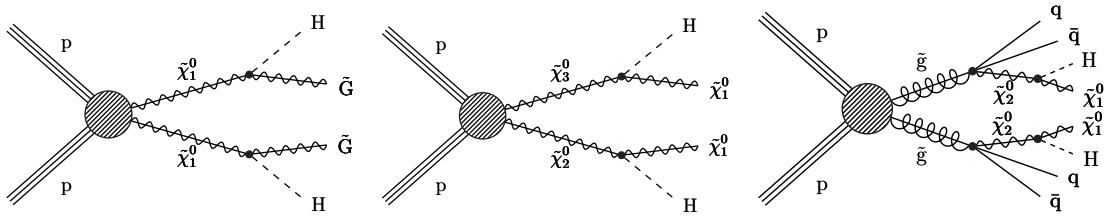

Figure 1. Diagrams for (left) the TChiHH-G signal model, $\tilde{\chi}_1^0\tilde{\chi}_1^0 \to \mathrm{HH}\tilde{\mathrm{G}}\tilde{\mathrm{G}}$, in which the $\tilde{\chi}_1^0$ NLSPs are produced indirectly through the cascade decays of several combinations of neutralinos and charginos, as described in the text; (center) TChiHH, in which the electroweak production of two neutralinos leads to two Higgs bosons and two neutralinos ($\tilde{\chi}_1^0$); (right) T5HH, the strong production of a pair of gluinos, each of which decays via a three-body process to quarks and a neutralino, with the neutralino subsequently decaying to a Higgs boson and a $\tilde{\chi}_1^0$ LSP. In each diagram, the hatched circle represents the sum of processes that can lead to the SUSY particles shown.

decays to the goldstino and a Higgs boson, with a coupling that is suppressed by the SUSY breaking scale [72]. Integrating over the contributions from the allowed combinations of produced charginos and neutralinos ($\tilde{\chi}_1^0\tilde{\chi}_2^0$, $\tilde{\chi}_1^0\tilde{\chi}_1^\pm$, $\tilde{\chi}_2^0\tilde{\chi}_1^\pm$, $\tilde{\chi}_1^\pm\tilde{\chi}_1^\mp$) leads to an effective rate for $\tilde{\chi}_1^0\tilde{\chi}_1^0$ production [75, 76] that is significantly larger than that for any of the individual primary pairs. We assume a branching fraction of 100% for $\tilde{\chi}_1^0 \to \mathrm{H}\tilde{\mathrm{G}}$.

In the TChiHH simplified model (figure 1, center), two higgsinos $\tilde{\chi}_2^0$ and $\tilde{\chi}_3^0$ are produced. The $\tilde{\chi}_1^0$ is the LSP, assumed to be a bino (the superpartner of the SM boson corresponding to the U(1) weak hypercharge gauge field B), while $\tilde{\chi}_2^0$ and $\tilde{\chi}_3^0$, nearly degenerate in mass, are the NLSPs. The other higgsinos have allowed decay channels, such as $\tilde{\chi}_1^\pm \to \mathrm{W}^\pm\tilde{\chi}_1^0$, that do not lead to Higgs bosons. This type of mass hierarchy can arise in various scenarios, as discussed in refs. [77, 78]. Unlike in the TChiHH-G simplified model described above, where the heavier higgsino states were assumed to decay directly to the lightest one, here only the exclusive $\tilde{\chi}_2^0\tilde{\chi}_3^0$ higgsino production cross section contributes; we are not sensitive to the other higgsino production channels $\tilde{\chi}_1^\pm\tilde{\chi}_1^\mp$, $\tilde{\chi}_1^\pm\tilde{\chi}_3^0$, and $\tilde{\chi}_1^\pm\tilde{\chi}_2^0$. (The identical-particle combinations $\tilde{\chi}_2^0\tilde{\chi}_2^0$ and $\tilde{\chi}_3^0\tilde{\chi}_3^0$ are not produced because their couplings to the Z boson are suppressed [78].) The cross section for $\tilde{\chi}_2^0\tilde{\chi}_3^0$ alone is about 17% of that for the sum of all six higgsino cross sections [75, 76].

Some SUSY models [79, 80] predict production rates for energetic Higgs bosons that are greater in gluino cascade decays than in direct higgsino production, because of the much larger strong production cross section for gluinos. Figure 1 (right) corresponds to a model (T5HH) in which two gluinos are produced, each of which decays via a three-body process to a quark, an antiquark, and a $\tilde{\chi}_2^0$. The $\tilde{\chi}_2^0$ decays to a Higgs boson and a $\tilde{\chi}_1^0$, which is taken to be the LSP. The same signature also arises in a recently proposed model [81, 82], motivated by dark-matter considerations, where a bino-like $\tilde{\chi}_3^0$ becomes the NLSP, decaying via a Higgs boson to the $\tilde{\chi}_1^0$ LSP.

This paper is organized as follows. Section 2 provides an overview of the analysis strategy, while sections 3 and 4 describe the CMS detector and the simulated event samples, respectively. The event triggers and reconstruction of the data are presented in section 5, while event selection and the reconstruction of Higgs boson candidates are discussed

JHEP05(2022)014

in section 6. The background estimation is described in section 7, and the systematic uncertainties are discussed in section 8. Section 9 presents the results and interpretation, and section 10 gives a summary.

2 Analysis strategy

As discussed in section 1, the common signature of the SUSY processes targeted by this search is the appearance of two Higgs bosons, each decaying via $\mathrm{H} \to \mathrm{b}\overline{\mathrm{b}}$, and accompanied by $p_{\mathrm{T}}^{\mathrm{miss}} = |\vec{p}_{\mathrm{T}}^{\mathrm{miss}}|$. Additional jets can be present, either from initial-state radiation, or, as in the case of strong SUSY production, from additional particles in the decay chains. Experimentally, this signature can be manifested in a number of different jet configurations. The analysis is designed to address not only the simplest case, in which the b quarks from the Higgs boson decays appear as jets (b jets) that are individually resolved, but also the case in which b jets resulting from the decay of a high-momentum Higgs boson merge into a single wide jet. Furthermore, to provide sensitivity to a broad range of experimental b-tagging outcomes, including those arising from reconstruction inefficiencies and detector acceptance, we do not restrict the search to precisely the nominal four resolved b-tagged jets (for the resolved signature), or to the nominal two merged double b-tagged jets (for the boosted signature).

The momentum of the Higgs boson largely determines whether the resolved or boosted signature contributes more to the sensitivity; this momentum is in turn determined by the masses of the particles in the decay chain, especially the mass splitting between the higgsino and its daughter SUSY particle. For both types of signatures, the basic analysis procedure involves five steps:

1. Baseline event selection requirements are applied, narrowing the event sample to an *analysis region*, which includes signal, sideband, and control regions. These requirements include a veto of events containing isolated leptons (either electrons or muons). A loose $p_{\mathrm{T}}^{\mathrm{miss}}$ requirement is also applied for both signatures.

2. Higgs-boson candidates are identified, and their masses are reconstructed.

3. Binning is applied in certain analysis variables. This binning has two roles: first, to define the signal, sideband, and control regions within the analysis region for a robust, data-driven background estimation, and second, using additional variables (such as $p_{\mathrm{T}}^{\mathrm{miss}}$), to enhance the sensitivity to the different SUSY models across the large range of kinematically accessible SUSY particle masses.

4. *Control samples* are defined and used to validate the background estimation procedures and to estimate systematic uncertainties. These samples are selected with modifications of the baseline criteria (for example, by requiring one or more leptons) so that they do not overlap with the analysis region. These samples contain signal, sideband, and control regions paralleling those in the analysis region.

5. As a test of the null hypothesis (no signal), the background predictions based on yields in the sideband and control regions are compared with the observed yields in

JHEP05(2022)014

the signal regions. For each test of a specific SUSY model, a fit is performed that allows for the expected level of signal contamination across all parts of the overall analysis region.

The detailed event selection requirements and background estimation methods used are somewhat different for the resolved and boosted signatures, but they have certain basic features in common. The most important of these is the use of two key types of variables to define the signal, sideband, and control regions: (i) the number of single- or double-b-tagged jets and (ii) the measured masses of the Higgs-boson candidates.

The composition of the SM backgrounds in this analysis is relatively simple, with the dominant contribution arising from $t\bar{t}$ events that contain a single leptonic W boson decay, together with additional b-tagged jets from the misidentification of lighter-quark and gluon jets, or from gluon jets that split into b quark pairs. The leptonic W boson decay produces a neutrino that is the source of the observed $p_{\mathrm{T}}^{\mathrm{miss}}$. Most such events are vetoed by the baseline selection requirement that excludes events with a single isolated lepton. However, $t\bar{t}$ single-lepton events can sometimes escape this veto if the lepton is "lost" in some manner, or is a τ lepton that decays hadronically. Such events, which escape the isolated-lepton veto applied in the baseline selections, are referred to as *lost-lepton events*. Sub-dominant backgrounds arise from W+jets and Z+jets events, as well as from multijet events, produced by quantum chromodynamics (QCD) processes, in which $p_{\mathrm{T}}^{\mathrm{miss}}$ arises from jet mismeasurement. However, the QCD contribution is highly suppressed by requiring that the $\vec{p}_{\mathrm{T}}^{\mathrm{miss}}$ vector not be aligned with any of the highest transverse-momentum jets in the event.

3 The CMS detector

A detailed description of the CMS detector, along with a definition of the coordinate system and pertinent kinematic variables, is given in ref. [83]. Briefly, a cylindrical superconducting solenoid with an inner diameter of 6 m provides a 3.8 T axial magnetic field. Within the cylindrical volume are a silicon pixel and strip tracker, a lead tungstate crystal electromagnetic calorimeter (ECAL), and a brass and scintillator hadron calorimeter (HCAL). The tracking detectors cover the range $|\eta| < 2.5$, where η is the pseudorapidity. The ECAL and HCAL, each composed of a barrel and two endcap sections, cover $|\eta| < 3.0$. Forward calorimeters extend the coverage to $3.0 < |\eta| < 5.2$. Muons are measured within $|\eta| < 2.4$ by gas-ionization detectors embedded in the steel flux-return yoke outside the solenoid. The detector is nearly hermetic, permitting accurate measurements of $p_{\mathrm{T}}^{\mathrm{miss}}$.

Events of interest are selected using a two-tiered trigger system. The first level (L1), composed of custom hardware processors, uses information from the calorimeters and muon detectors to select events at a rate of around 100 kHz within a fixed latency of about 4 μs [84]. The second level, known as the high-level trigger (HLT), consists of a farm of processors running a version of the full event reconstruction software optimized for fast processing, and reduces the event rate to around 1 kHz before data storage [85].

In addition to the pp collision of interest selected by the trigger, the event record generally contains tracks and calorimeter energy deposits from a number of other collisions

JHEP05(2022)014

(pileup) occurring in the same bunch crossing, or in adjacent crossings within the time resolution of the data acquisition. The number of collisions varies with the instantaneous luminosity, averaging about 29 over the data set [86].

4 Simulated event samples

While the evaluation of the SM background, described in section 7, is based primarily on observed event yields in multiple control regions in data, Monte Carlo (MC) simulated event samples nevertheless play an important role in the analysis. Such samples are used to optimize the event selection requirements and background prediction methods without biasing the result; to evaluate correction factors, typically near unity, to the background predictions; and to evaluate the acceptance and efficiency for signal processes.

We use the MadGraph5_aMC@NLO 2.2.2 (2.4.2) [87, 88] event generator with leading order (LO) precision for simulation of the SM production of $\mathrm{t\bar{t}}$, W+jets, Z+jets, and QCD processes, for the 2016 (2017–2018) data taking periods. The $\mathrm{t\bar{t}}$ events are generated with up to three additional partons in the matrix element calculations. The W+jets and Z+jets events are generated with up to four additional partons. For the MadGraph LO samples, MLM parton matching is used [88]. Single top quark events produced through the s channel, diboson events such as those originating from WW, ZZ, or ZH production, and rare events such as those from $\mathrm{t\bar{t}W}$, $\mathrm{t\bar{t}Z}$, and WWZ production, are generated with MadGraph5_aMC@NLO at next-to-leading order (NLO), with FXFX matching [89], except that WW events in which both W bosons decay leptonically are generated using the POWHEG v2.0 [90–94] program at NLO. This same POWHEG generator is used to describe both tW production and t-channel production of single top quark events at NLO precision.

Samples of simulated signal events are generated at LO using MadGraph5_aMC@NLO 2.4.2, with up to two additional partons included in the matrix element calculations. The production cross sections for the electroweak models are computed at NLO plus next-to-leading-log (NLL) accuracy [75, 76], while those for strong production are determined with approximate next-to-NLO (NNLO) plus next-to-next-to-leading logarithmic (NNLL) accuracy [95–106]. For the TChiHH-G model, these samples are generated by performing a scan of $m(\widetilde{\chi}_1^0)$, with $m(\widetilde{\mathrm{G}}) = 1$ GeV. The TChiHH model is represented by a two-dimensional scan of $m(\widetilde{\chi}_1^0)$ and $m(\widetilde{\chi}_{2,3}^0)$. The TChiHH-G and TChiHH simulated samples are generated with both Higgs bosons constrained to decay via $\mathrm{H} \to \mathrm{b\bar{b}}$, and each event is weighted by the square of the standard model branching fraction. Auxiliary simulations show that inclusion of the non-$\mathrm{b\bar{b}}$ decay modes of the Higgs boson would slightly improve the sensitivity, mainly for the boosted signature, but these additional modes are not included here. Additional details on the simulation of electroweak production models are given in ref. [45]. Events with gluino pair production (T5HH) are generated for a range of $m(\widetilde{\mathrm{g}})$ values. The gluino decay is simulated with a three-body phase space model [107]. The mass of the intermediate $\widetilde{\chi}_2^0$ is set 50 GeV below $m(\widetilde{\mathrm{g}})$, ensuring that the daughter Higgs bosons have a large Lorentz boost, $m(\widetilde{\chi}_1^0)$ is set to 1 GeV, and all decay modes of the Higgs bosons are included.

All simulated samples make use of the PYTHIA 8.205 [108] program to describe parton showering and hadronization. The CUETP8M1 [109] (CP5 [110]) PYTHIA tune was used

JHEP05(2022)014

to produce the SM background samples for the analysis of the 2016 (2017 and 2018) data, with signal samples based on the CUETP8M1 tune for 2016 and on the CP2 tune [110] for 2017 and 2018. Simulated samples generated at LO (NLO) with the CUETP8M1 tune use the NNPDF3.0LO (NNPDF3.0NLO) [111] parton distribution functions (PDFs), while those using the CP2 or CP5 tune use the NNPDF3.1LO (NNPDF3.1NNLO) [112] PDFs.

The detector response is modeled with GEANT4 [113]. Normalization of the simulated background samples is performed using the most accurate cross section calculations available [87, 93, 94, 114–122], which generally correspond to NLO or NNLO precision. Because scans over numerous mass points are required for the signal models, the detector response for such events (except for those of the T5HH model) is described using the CMS fast simulation program [107, 123], which yields results that are generally consistent with those from the simulation based on GEANT4. Pileup pp interactions are superimposed on the generated events, with a number distribution that is adjusted to match the pileup distribution measured in data.

5 Triggers and event reconstruction

The data sample for the analysis region was obtained using triggers [84, 85] that require $p_{\mathrm{T,trig}}^{\mathrm{miss}}$ to exceed a threshold that varied between 90 and 140 GeV, depending on the LHC instantaneous luminosity. Single-lepton control samples, defined below, are collected with single-electron, single-muon, and $p_{\mathrm{T,trig}}^{\mathrm{miss}}$ triggers, while dilepton control samples are collected with single-electron and single-muon triggers. The value of $p_{\mathrm{T,trig}}^{\mathrm{miss}}$ is computed with trigger-level quantities and therefore has somewhat poorer resolution than $p_{\mathrm{T}}^{\mathrm{miss}}$. The trigger efficiency for the analysis sample is measured as a function of $p_{\mathrm{T}}^{\mathrm{miss}}$, and of H_{T}, the scalar sum of the transverse momentum (p_{T}) of jets, separately for each year of data taking. For the single-lepton control sample, it is measured as a function of $p_{\mathrm{T}}^{\mathrm{miss}}$, H_{T}, and lepton p_{T}, and for the dilepton control sample, as a function of the leading-lepton p_{T}. For the analysis sample, the efficiency at $p_{\mathrm{T}}^{\mathrm{miss}} = 150$ GeV is 30–70%, depending on the trigger thresholds (which varied with the instantaneous luminosity); the efficiency rises with $p_{\mathrm{T}}^{\mathrm{miss}}$ and is over 99% for $p_{\mathrm{T}}^{\mathrm{miss}} > 260$ GeV. The analysis of the boosted signature requires $p_{\mathrm{T}}^{\mathrm{miss}} > 300$ GeV and thus operates on the efficiency plateau; the resolved-signature analysis operates partly on the turn-on section of the efficiency curve, with a lower $p_{\mathrm{T}}^{\mathrm{miss}}$ threshold of 150 GeV. These measured efficiencies are applied as weights to the simulated SM and signal events, for the analysis region and the control samples.

The reconstruction of physics objects in an event proceeds from the candidate particles identified by the particle-flow (PF) algorithm [124], which uses information from the tracker, calorimeters, and muon systems to identify the candidates as charged or neutral hadrons, photons, electrons, or muons.

The primary pp interaction vertex is taken to be the reconstructed vertex with the largest value of summed physics-object p_{T}^2, as described in section 9.4.1 of ref. [125]. The physics objects for this purpose are the jets (reconstructed using the anti-k_{T} jet finding algorithm [126, 127] with the charged particle tracks assigned to the vertex), isolated tracks (including those identified as leptons), and the associated missing transverse momentum

JHEP05(2022)014

(computed as the negative vector sum of the $\vec{p}_{\mathrm{T}}$ values of those objects). Charged particle tracks associated with vertices other than the primary vertex are removed from further consideration. The primary vertex is required to lie within 24 cm of the center of the detector in the direction along the beam axis and within 2 cm in the plane transverse to that axis.

Jets from the primary pp interaction are formed from the charged PF candidates associated with the primary vertex, together with the neutral PF candidates, again using the anti-k_{T} algorithm [126], as implemented in the FastJet package [127]. The clustering is performed with distance parameter $R = 0.4$ (AK4 jets) when optimized for jets containing the fragmentation products of a single parton, and with distance parameter $R = 0.8$ (AK8 jets) for jets containing multiple partons. No removal of overlap jets between the AK4 and AK8 collections is applied. Jet quality criteria [128, 129] are imposed to select quark and gluon jets while rejecting those from spurious sources, such as electronics noise and detector malfunctions. The jet energies are corrected for the nonlinear response of the detector [130]. The estimated contribution to the jet p_{T} of neutral PF candidates from pileup is removed with a correction based on the area of the jet and the average energy density of the event [131], for AK4 jets, and with the PUPPI technique [132], for AK8 jets. Jets are required to have $|\eta| < 2.4$; AK4 and AK8 jets are required to have $p_{\mathrm{T}} > 30$ GeV and $p_{\mathrm{T}} > 300$ GeV, respectively. Finally, AK4 jets that have PF constituents matched to an isolated electron or muon are removed. To improve the consistency of the fast simulation description with respect to that based on Geant4, we apply a small correction, about 1%, to account for differences in the efficiency of the jet quality requirements [128, 129].

To improve the modeling of jets associated with initial-state radiation (ISR), the prediction of MadGraph5_aMC@NLO is compared with data in a control sample enriched in $\mathrm{t\bar{t}}$ events by the requirement of two light charged leptons (ee, μμ, or eμ) and two b-tagged jets. The number of all remaining jets in the event is denoted $N_{\mathrm{jet}}^{\mathrm{ISR}}$. A correction factor is applied to simulated $\mathrm{t\bar{t}}$ and strong-production signal events so that the $N_{\mathrm{jet}}^{\mathrm{ISR}}$ distribution agrees with that in data. The central value of the correction ranges from 0.92 for $N_{\mathrm{jet}}^{\mathrm{ISR}} = 1$ to 0.51 for $N_{\mathrm{jet}}^{\mathrm{ISR}} \geq 6$. The correction is found not to be necessary for $\mathrm{t\bar{t}}$ samples that are generated with the CP5 tune. For the electroweak signal samples, we account for the effect of ISR on the p_{T} distribution of the system of SUSY particles, $p_{\mathrm{T}}^{\mathrm{ISR}}$, by reweighting the distribution based on studies of the transverse momentum of Z+jets events [133]. The reweighting factors range between 1.18 at $p_{\mathrm{T}}^{\mathrm{ISR}} \sim 125$ GeV and 0.78 for $p_{\mathrm{T}}^{\mathrm{ISR}} > 600$ GeV.

The identification of jets originating from b quarks (b tagging) is integral to the reconstruction of Higgs bosons in the analysis and is performed separately for AK4 and AK8 jets. For AK4 jets we use a version of the combined secondary vertex algorithm based on deep neural networks (DeepCSV [134]), making use of Loose (L), Medium (M), and Tight (T) working points, as discussed in section 6. The detection efficiencies for true b quark jets, as well as the mistag rates for jets originating from up, down, or strange quarks or from gluons (light-parton jets), and for charm-quark jets, are measured with data samples enriched in, respectively, $\mathrm{t\bar{t}}$, QCD, and a combination of W+c and semileptonic $\mathrm{t\bar{t}}$ events [134]. Typical b jet efficiencies for the three DeepCSV working points are 85, 70, and 50%, with corresponding light-parton jet mistag rates of 10, 1, and 0.1%, and charm jet mistag rates of 40, 12, and 2.5%, for the L, M, and T working points, respectively. The

JHEP05(2022)014

numbers of observed b-tagged AK4 jets satisfying the L, M, and T requirements in an event are denoted $N_{\mathrm{b,L}}$, $N_{\mathrm{b,M}}$, and $N_{\mathrm{b,T}}$, respectively.

The identification of AK8 jets containing two b quarks, used in the analysis of the boosted signature, is performed with a deep-learning-based double-b tagging algorithm (DeepDoubleBvL, mass-decorrelated [135]) at its loose working point. The efficiencies for tagging AK8 jets from $\mathrm{H} \to \mathrm{b}\overline{\mathrm{b}}$ and for those that contain only light partons are 90 and 5%, respectively [135]. The efficiency of the double-b tagging is checked with a data sample enriched in $\mathrm{g} \to \mathrm{b}\overline{\mathrm{b}}$; the mistag rate is checked with data in a lower-$p_{\mathrm{T}}^{\mathrm{miss}}$ sideband ($200 < p_{\mathrm{T}}^{\mathrm{miss}} < 300\,\mathrm{GeV}$) of the baseline selection for the boosted signature. For both single and double b tagging, the simulation is reweighted to compensate for differences with respect to data based on measurements of the b tagging efficiency and mistag rate for each working point. Additional corrections are applied for differences in the flavor tagging efficiencies between the fast simulation and Geant4, where applicable.

The reconstructed $\vec{p}_{\mathrm{T}}^{\mathrm{miss}}$ is computed as the negative vector sum of the $\vec{p}_{\mathrm{T}}$ of all PF candidates, adjusted for known detector effects by taking into account the jet energy corrections described in ref. [136]. Filters are applied to reject events with well-defined anomalous sources of $p_{\mathrm{T}}^{\mathrm{miss}}$, such as calorimeter noise, nonfunctioning calorimeter cells, beam particles externally scattered into the detector, and other effects [136]. For data generated with the fast simulation, corrections of 0–12% are applied to account for differences in the modeling of $p_{\mathrm{T}}^{\mathrm{miss}}$.

Because the targeted signature is fully hadronic, we veto events with isolated charged lepton candidates as part of the definition of the analysis region. Conversely, we require isolated electrons and muons in the selection of certain control samples. Electrons are reconstructed from showers in the ECAL matched to tracks in the silicon detectors, taking into account the effects of bremsstrahlung in the material of the tracker. Additional criteria are imposed on the shower shape in the ECAL and on the ratio of energies associated with the electron candidate in the HCAL and ECAL [137]. We use the "cut-based veto" working point of the electron identification algorithm [137]. Muons are constructed from muon detector track segments matched to silicon detector tracks; we require candidates to satisfy the "medium" working point of the muon identification [138]. For both electrons and muons, the track is required to be consistent with the particle's origination at the primary vertex. Electron and muon candidates must also satisfy $|\eta| < 2.5$ and 2.4, respectively. Requirements on the lepton p_{T} are imposed that differ between veto leptons, where efficiency is prioritized, and control-sample leptons, where higher purity is desired; we require $p_{\mathrm{T}} > 10\,\mathrm{GeV}$ for veto leptons, and $p_{\mathrm{T}} > 30\,\mathrm{GeV}$ for those used to select events in the single-lepton control samples. For the dilepton control samples, the threshold p_{T} is 30 (20) GeV for the leading (subleading) lepton.

To select electrons and muons that originate in the decay of W and Z bosons, while suppressing those from the decays of hadrons and from particles misidentified as e or μ, both are required to be isolated from other PF candidates. The isolation criterion is based on the variable I, which is the scalar p_{T} sum of charged-hadron, neutral-hadron, and photon PF candidates within a cone of radius $\Delta R \equiv \sqrt{(\Delta\phi)^2 + (\Delta\eta)^2}$ around the lepton direction, after pileup subtraction, divided by the lepton p_{T}, where ϕ is the azimuthal angle. The

JHEP05(2022)014

radius of the cone depends on the lepton p_T: $\Delta R = 0.2$ for $p_T < 50$ GeV, $10\,\text{GeV}/p_T$ for $50 \leq p_T \leq 200$ GeV, and 0.05 for $p_T > 200$ GeV [139]. The isolation requirement is $I < 0.1$ (0.2) for electrons (muons).

The efficiency of electron and muon identification is measured with a tag-and-probe method applied to $Z \to \ell^+\ell^-$ samples in the data [137, 138]. Yields of these leptons in simulation are corrected to match the observations in data.

The efficiency of the charged lepton veto can be compromised if the charged lepton is lost, either because it is not reconstructed or fails the lepton selection requirements (including the isolation and p_T threshold requirements), or because it is a tau lepton that decays hadronically. To recover some of this veto efficiency, we also reject events with any additional isolated tracks corresponding to leptonic or hadronic PF candidates. To reduce the influence of tracks resulting from pileup, such isolated tracks are considered only if their distance of closest approach along the beam axis to a reconstructed vertex is smaller for the primary vertex than for any other vertex. The tracks are required to satisfy $|\eta| < 2.5$, as well as $p_T > 10$ GeV, or >5 GeV for a PF electron or muon. The isolation requirement is that the scalar p_T sum of all other charged particle tracks within a cone of radius 0.3 around the track direction, divided by the track p_T, must be less than 0.2 if the track is identified as a PF electron or muon, less than 0.1 otherwise. To limit the veto tracks to those likely to originate in W boson leptonic decays, we also restrict the transverse mass, requiring $m_T \equiv \sqrt{2 p_T p_T^{\text{miss}} (1 - \cos\Delta\phi)} < 100$ GeV. Here p_T is the transverse momentum of the particle and $\Delta\phi$ is the azimuthal angle between the particle momentum and $\vec{p}_T^{\,\text{miss}}$.

6 Event selection and reconstruction of Higgs boson candidates

In the first step of the analysis procedure, as outlined in section 2, baseline selection requirements are applied to define the analysis regions for both the resolved and boosted signatures. These baseline selection requirements are described below. Three of the baseline selection requirements are based on quantities that are in common to both signatures and are defined as follows:

1. A minimum requirement on p_T^{miss} is applied: $p_T^{\text{miss}} > 150$ GeV for the resolved signature and $p_T^{\text{miss}} > 300$ GeV for the boosted signature.

2. For both signatures, events are excluded if any veto leptons or isolated charged particle tracks are present. These veto objects are defined in section 5.

3. To suppress QCD background, events in either signature are rejected if any of the four highest p_T AK4 jets is approximately aligned with the missing momentum vector $\vec{p}_T^{\,\text{miss}}$. Such alignment is an indication that the observed $\vec{p}_T^{\,\text{miss}}$ in the event is a consequence of jet mismeasurement and is not genuine. This set of requirements, which we refer to collectively as the $\Delta\phi$ requirement, can only be imposed in the plane transverse to the beam axis. An event is vetoed if any of the azimuthal separations is small, specifically, if $\Delta\phi_{\vec{p}_T^{\,\text{miss}},\,\text{j}_i} < \{0.5, 0.5, 0.3, 0.3\}$ for the ith-highest p_T jet j_i.

The remaining baseline selection requirements depend on the individual details of the Higgs boson mass reconstruction and the counting of b jets, and we discuss these for the two signatures in turn.

JHEP05(2022)014

For the resolved signature, the following additional criteria are used to define the baseline requirements:

1. To control combinatorics in the Higgs boson reconstruction, events must contain either 4 or 5 AK4 jets. Besides the jets associated with the Higgs boson candidates, this requirement allows for one additional jet in the event, for example, from initial-state radiation.

2. Higgs boson reconstruction is performed as follows. The four jets with the highest b-tag discriminator values are selected and used to form two Higgs boson candidates, each one decaying into two b jets. There are three pairings among these four jets that could form the two Higgs boson candidates. To select one of them without biasing the mass distributions towards the true Higgs boson mass, we use the pair with the smallest absolute value of the mass difference, Δm_{bb}, between the two candidate masses $m(\mathrm{b}_i\mathrm{b}_j)$ and $m(\mathrm{b}_k\mathrm{b}_l)$, $\Delta m_{\mathrm{bb}} \equiv |m(\mathrm{b}_i\mathrm{b}_j) - m(\mathrm{b}_k\mathrm{b}_l)|$, and require $\Delta m_{\mathrm{bb}} < 40\,\mathrm{GeV}$. The average mass $\langle m_{\mathrm{bb}} \rangle$ of these two Higgs boson candidates is required to satisfy the loose baseline requirement $\langle m_{\mathrm{bb}} \rangle < 200\,\mathrm{GeV}$. This approach exploits the fact that signal events contain two particles of identical mass, without using the value of the Higgs boson mass itself. As such, it prevents the sculpting of an artificial peak in the background at $m(\mathrm{H})$, so that a peak observed at that mass would be meaningful, and the combinatorial background in the $\langle m_{\mathrm{bb}} \rangle$ spectrum can be investigated in the subsequent analysis.

3. To further suppress background from $\mathrm{t\bar{t}}$ lost-lepton events, we compute the angular separation, ΔR, between the b-tagged jets within each Higgs boson candidate. In $\mathrm{t\bar{t}}$ lost-lepton events, one of the t quark decays produces a W boson that decays leptonically. The b jet from that t quark decay is then usually paired with a mistagged jet from the other t quark decay in the event to form a Higgs boson candidate. The value of ΔR for that candidate will then typically be large. This background is therefore reduced by requiring $\Delta R_{\mathrm{max}} < 2.2$, where ΔR_{max} is the larger of the ΔR values associated with the two H boson candidates.

4. We define a b-counting variable, N_{b}, which is the number of b-tagged jets but using optimized selections based on tight, medium, and loose categories (see section 5) as follows:

   $N_{\mathrm{b}} = 2$: $N_{\mathrm{b,T}} = 2$ and $N_{\mathrm{b,M}} = 2$;

   $N_{\mathrm{b}} = 3$: $N_{\mathrm{b,T}} \geq 2$ and $N_{\mathrm{b,M}} = 3$ and $N_{\mathrm{b,L}} = 3$;

   $N_{\mathrm{b}} = 4$: $N_{\mathrm{b,T}} \geq 2$ and $N_{\mathrm{b,M}} \geq 3$ and $N_{\mathrm{b,L}} \geq 4$.

   We refer to these categories as 2b, 3b, and 4b, but it should be remembered that the b tagging thresholds on individual jets become looser as N_{b} increases. The baseline selection requires $N_{\mathrm{b}} \geq 2$.

Figure 2 shows the distributions in $p_{\mathrm{T}}^{\mathrm{miss}}$, Δm_{bb}, ΔR_{max}, N_{b}, and $\langle m_{\mathrm{bb}} \rangle$, for both data and simulation. The last two quantities shown, N_{b} and $\langle m_{\mathrm{bb}} \rangle$, are used as the basis for

JHEP05(2022)014

the background estimation, while additional binning is performed in the quantities $p_{\mathrm{T}}^{\mathrm{miss}}$ and ΔR_{max} to improve the sensitivity of the analysis. In each plot, the baseline selection is applied to all variables other than the one shown, and, for all distributions except N_{b}, an additional requirement $N_{\mathrm{b}} \geq 3$ is used to select the signal-like parts of the overall analysis region. To facilitate comparison of the distributions between data and simulation, the distributions from simulation are scaled to match the area of the data, using factors listed in the caption. The representative signals show the expected peaking in $\langle m_{\mathrm{bb}} \rangle$ near the H boson mass, as well as toward lower values of ΔR_{max}. The binning indicated by the vertical dotted lines is discussed in section 7. While these plots provide an overall picture of the background shapes and background composition in the analysis region, they do not give an accurate picture of the sensitivity of the analysis to the signal, because they do not yet reflect the final binning used to extract the signal.

The additional baseline criteria for the analysis of the boosted signature are as follows:

1. At least two AK8 jets, each with $p_{\mathrm{T}} > 300\,\mathrm{GeV}$. The p_{T} threshold results in a high probability that all daughter particles from the Higgs boson decay are contained within the jet. The kinematic merging of the Higgs boson decay products reduces the combinatorial challenge encountered in the resolved signature, and so the number of additional AK8 jets is unrestricted, as is the number of AK4 jets. Such additional jets can be produced in the signal processes involving strongly interacting particles, such as the T5HH model described in section 1. They can also arise from initial- or final-state radiation.

2. The mass m_{J} attributed to an AK8 jet is computed by the "soft drop" algorithm [140, 141], in which soft wide-angle radiation is recursively removed from a jet. For signal events, m_{J} is expected to show a peak near $m(\mathrm{H})$. For the baseline selection, the two highest p_{T} AK8 jets are required to satisfy the loose requirement $60 < m_{\mathrm{J}} < 260\,\mathrm{GeV}$.

3. We define the variable N_{H} as the number of AK8 jets passing the above criteria that are double-b tagged, that is, for which the value of the double-b tagging discriminator D_{bb} exceeds the loose working point threshold of 0.7. The value of N_{H}, 0, 1, or 2, is unrestricted in the baseline selection; it is used for the event classification discussed in section 7.

Figure 3 shows the distributions for data and simulated event samples with the boosted signature in $p_{\mathrm{T}}^{\mathrm{miss}}$, and in p_{T}, D_{bb}, and m_{J} for the two leading AK8 jets. The baseline requirements for the boosted signature are applied, except for those on the variable shown. The simulated SM background yields, scaled by the factor noted in the caption, are seen to describe the shape of the data well. Also shown are examples of SUSY models, which peak around the Higgs boson mass in m_{J}, and at high values of D_{bb}, for both jets.

In a small region of parameter space a candidate may be selected by both signatures. In this case it is assigned to the resolved selection. Slightly higher expected sensitivity is achieved with this choice than with the alternative. The efficiency of the combined resolved and boosted signatures for the targeted signal models ranges from 1 to 15%, depending on the values of the mass parameters in the models.

JHEP05(2022)014

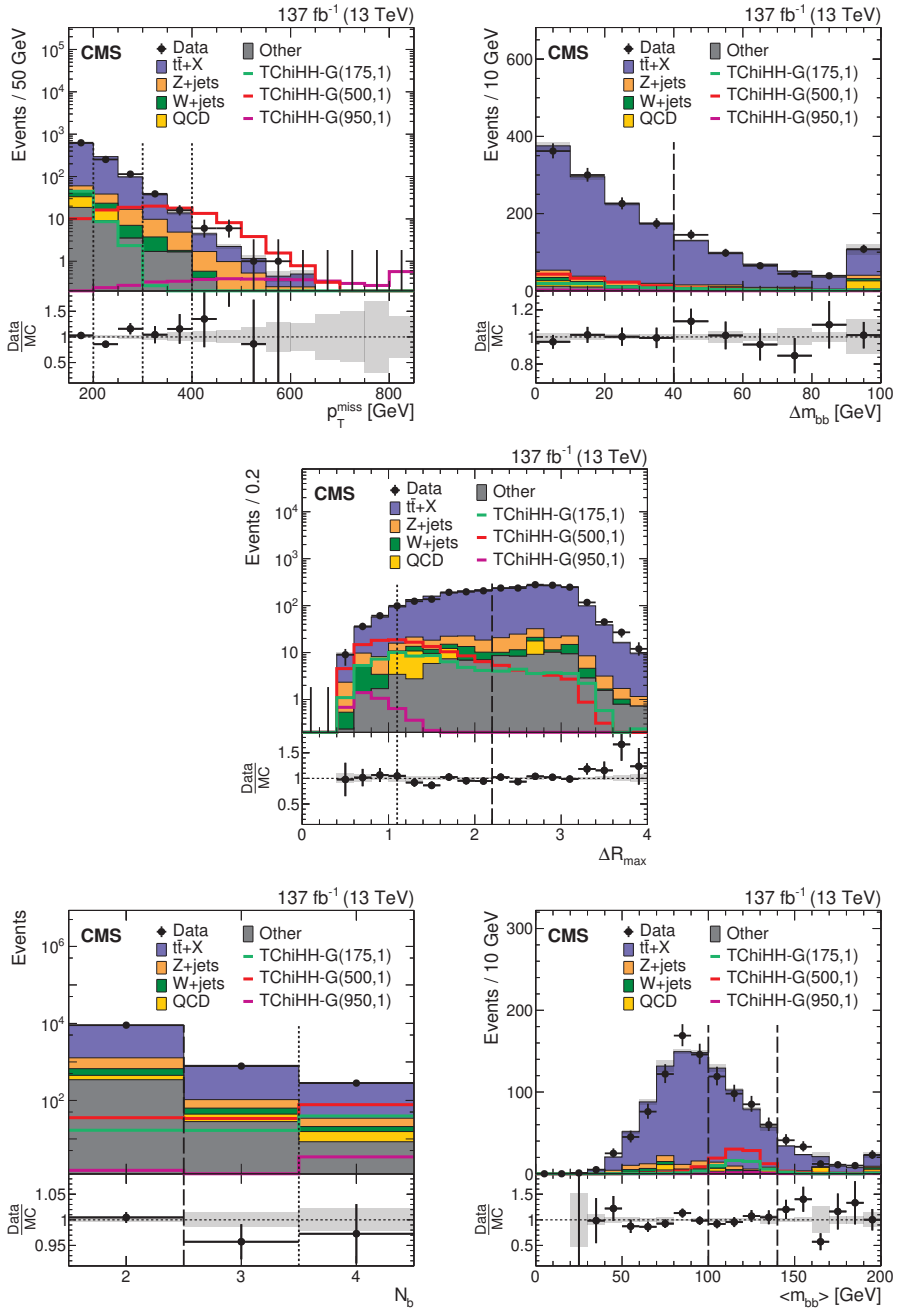

Figure 2. Distributions in key analysis variables of the resolved signature for events satisfying the baseline requirements and $N_b = 3$ or 4, except for those on the variable plotted: (upper left) p_T^{miss}, (upper right) Δm_{bb}, (middle) ΔR_{max}, (lower left) N_b, and (lower right) $\langle m_{bb} \rangle$. The rightmost bins include the overflow entries. The data are shown as black markers with error bars, simulated SM backgrounds by the stacked histograms (scaled by factors of 0.93–0.97 to match the total data yield in each plot), and simulations of signals TChiHH-G($m(\tilde{\chi}_1^0), m(\tilde{G})$ [GeV]) by the open colored histograms. Gray shading represents the statistical uncertainties of the simulation. Vertical lines indicate the boundaries for signal region selection (dashed), or for the signal region binning (dotted). The lower panels show the ratio of data to (scaled) simulation.

JHEP05(2022)014

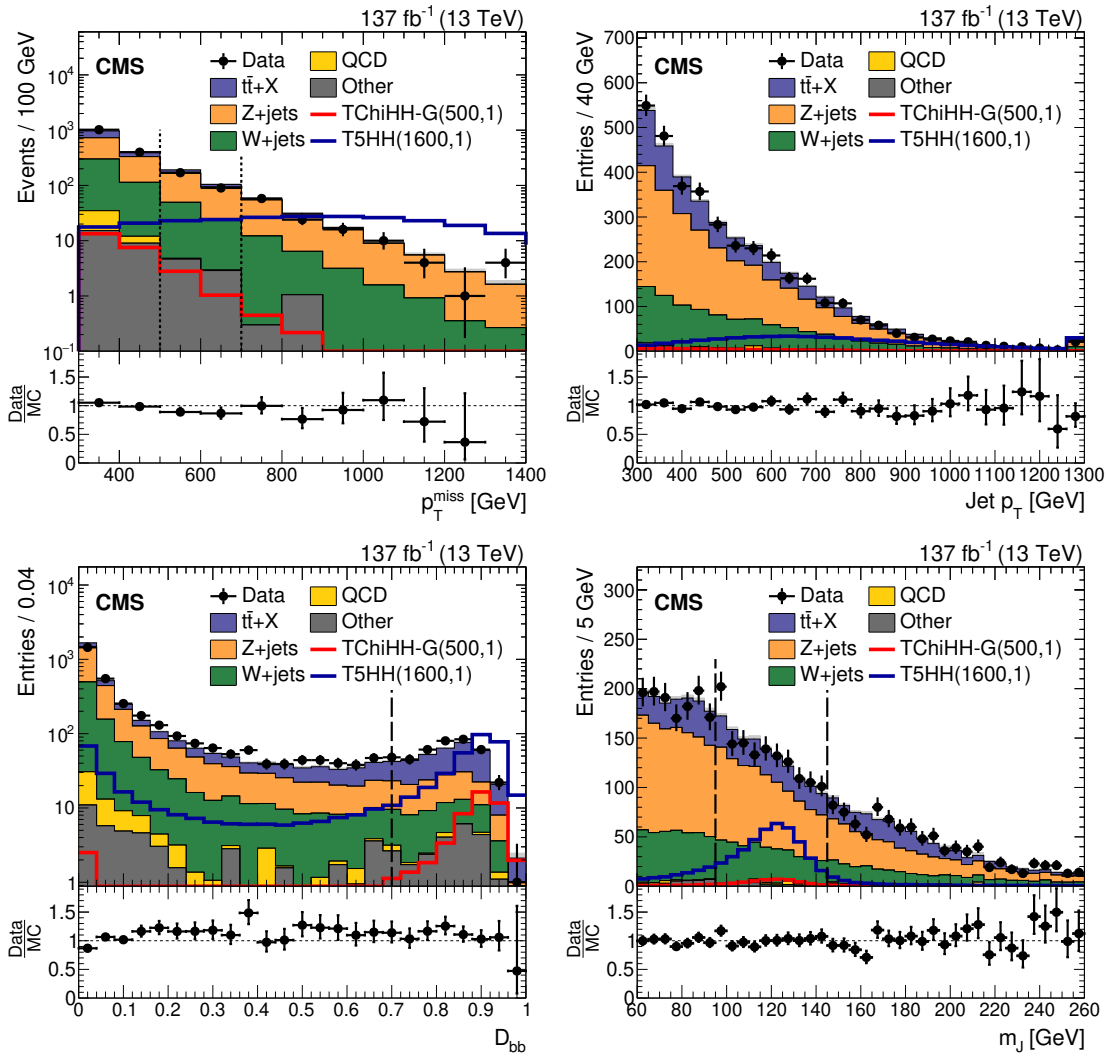

Figure 3. Distributions in key analysis variables after the baseline requirements for the boosted signature, except for those on the variable plotted: (upper left) $p_{\mathrm{T}}^{\mathrm{miss}}$, (upper right) jet p_{T}, (lower left) D_{bb}, and (lower right) m_{J}. Except for the $p_{\mathrm{T}}^{\mathrm{miss}}$ distribution, each plot contains two entries per event, for each of the two p_{T}-leading AK8 jets. The data are shown by the black markers with error bars, and SM backgrounds from simulation (scaled by 86% to match the data integral) by the filled histograms. Open colored histograms show simulations of the signals TChiHH-G$(m(\widetilde{\chi}_1^0), m(\widetilde{\mathrm{G}}))$ or T5HH$(m(\widetilde{\mathrm{g}}), m(\widetilde{\chi}_1^0)$ [GeV]). The vertical dashed lines show boundaries for the event classifications defined in section 7: (upper left) the $p_{\mathrm{T}}^{\mathrm{miss}}$ binning; (lower left) the D_{bb} threshold for identification of a jet as an $\mathrm{H} \to \mathrm{b}\overline{\mathrm{b}}$ candidate; (lower right) the boundaries of the H boson mass window. The lower panel in each plot shows the ratio of observed to (scaled) simulated yields.

JHEP05(2022)014

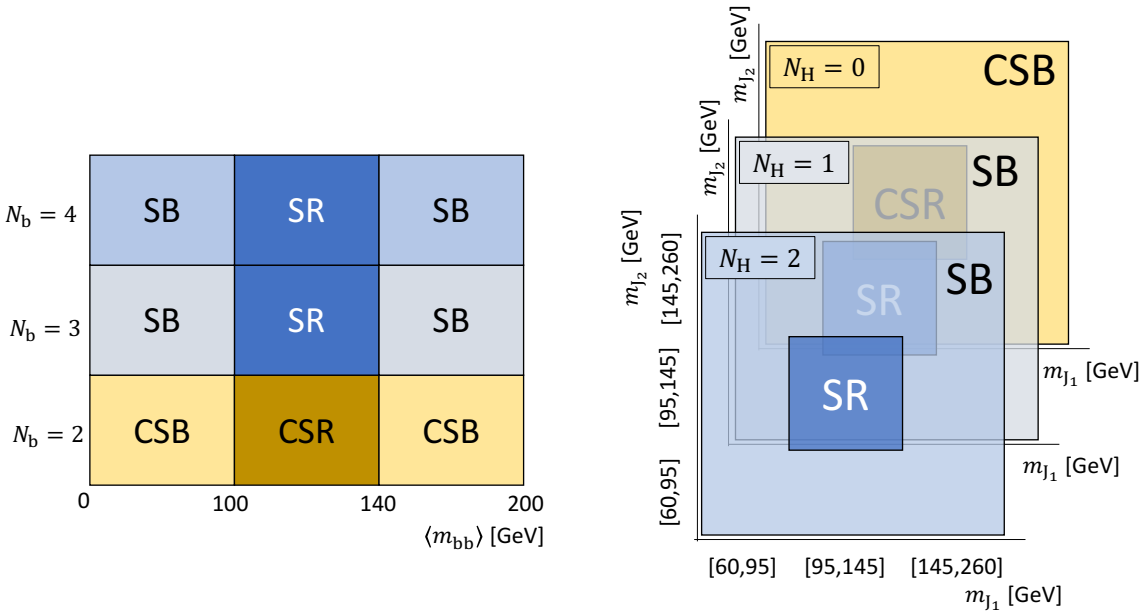

Figure 4. Configuration of the signal and control regions for the (left) resolved and (right) boosted signatures. The patterns shown are repeated in each of several bins in kinematic or topological variables for improved sensitivity, as discussed in the text.

7 Background estimation

After applying the baseline event selections for the resolved and boosted signatures described in section 6, we define the analysis regions shown in figure 4. The background in a given signal region (SR) is estimated using the event yields observed in three types of neighboring regions: the sideband regions (SB), the control sideband regions (CSB), and the control signal region (CSR). For both signatures, these regions are constructed using two types of discriminating variables:

1. Variable(s) characterizing the masses of the H boson candidates. The resolved signature uses a single variable, $\langle m_{bb} \rangle$, while the boosted signature uses both m_{J1} and m_{J2}, where J_1 and J_2 are the p_T-leading and subleading AK8 jets, respectively.

2. A b-counting variable derived from the jet flavor tagging. For the resolved signature, the variable is N_b, while for the boosted signature, it is N_H.

For the resolved signature, signal events primarily have four b-tagged jets, but they can also populate the region with three b-tagged jets, so the signal regions are defined by requiring $\langle m_{bb} \rangle$ to be in the Higgs boson mass window and either $N_b = 4$ or $N_b = 3$. For the boosted signature, signal events primarily have two identified double-b-tagged jets, but they can also populate the region with only one. The signal regions are therefore defined by requiring both m_{J1} and m_{J2} to be in the Higgs boson mass window and either $N_H = 1$ or $N_H = 2$.

The background event yield in a signal region is then estimated with the "ABCD method," which uses the measured event yields in three background-dominated regions to

JHEP05(2022)014

predict the background in a signal region. With the regions defined as shown in figure 4, the estimated background yield is

$$N_{\mathrm{SR}}^{\mathrm{pred}} = \kappa \frac{N_{\mathrm{CSR}}}{N_{\mathrm{CSB}}} N_{\mathrm{SB}}, \tag{7.1}$$

where N_{SB} is the observed event yield in the H boson mass sideband for events satisfying the same b-counting criteria as those applied in the SR, while N_{CSR} and N_{CSB} are, respectively, the event yields in regions corresponding to signal and sideband regions with respect to the Higgs candidate mass variable, but in the background regions with respect to the b-counting criterion. The coefficient κ is a correction factor, typically near unity, that takes into account a potential correlation between the two types of discriminating variables. It is taken from simulation but is validated with separate control regions in data, as discussed in section 8.

For the resolved signature, figure 4 (left), the variable N_{b} was defined in section 6, and the H boson mass window for the SR or CSR is given by $100 < \langle m_{\mathrm{bb}} \rangle < 140\,\mathrm{GeV}$, with the events both above and below this window constituting the SB or CSB. The SRs and SBs reside in b tagging regions $N_{\mathrm{b}} = 3$ and $N_{\mathrm{b}} = 4$, while the $N_{\mathrm{b}} = 2$ region contains the CSR and CSB. To increase the sensitivity to signal, these regions are further sorted into bins in two discriminating variables, ΔR_{max} (0–1.1 and 1.1–2.2) and $p_{\mathrm{T}}^{\mathrm{miss}}$ (150–200, 200–300, 300–400, and >400 GeV). The background determination by the ABCD method is performed separately for each of these eight bins, and for both the $N_{\mathrm{b}} = 3$ and $N_{\mathrm{b}} = 4$ SRs, for a total of 16 bins.

The corresponding ABCD regions for the boosted signature, figure 4 (right), are based on the number N_{H} of double-b-tagged jets (defined in section 6), with events sorted into regions 0H, 1H, and 2H having $N_{\mathrm{H}} = 0$, 1, and 2, respectively. The SRs and SBs lie within the 1H and 2H regions, and CSR and CSB in the 0H region. The events in the SR and CSR have $95 < m_{\mathrm{J}} < 145\,\mathrm{GeV}$ for both AK8 jets, while those in the SB and CSB have at least one of the jets lying outside that mass window, as illustrated in the right-hand plot of figure 4. The background yield $N_{\mathrm{SR,\,tot}}^{\mathrm{pred}}$ is determined for each of the 1H and 2H SRs by the ABCD approach, eq. (7.1). The events in these SRs are further sorted into three $p_{\mathrm{T}}^{\mathrm{miss}}$ bins (300–500, 500–700, and >700 GeV), for a total of six bins. The distribution of the predicted background yield among these $p_{\mathrm{T}}^{\mathrm{miss}}$ bins is discussed below.

The factors κ in eq. (7.1) can differ from unity if the H candidate mass variable is correlated with the b-counting variable, such that the $N_{\mathrm{SR}}/N_{\mathrm{SB}}$ and $N_{\mathrm{CSR}}/N_{\mathrm{CSB}}$ yield ratios differ. We thus evaluate κ as a double ratio

$$\kappa = \frac{N_{\mathrm{SR}}/N_{\mathrm{SB}}}{N_{\mathrm{CSR}}/N_{\mathrm{CSB}}}, \tag{7.2}$$

taking the yields in this case from simulation. A strength of this method is that many systematic uncertainties cancel in this double ratio. Figure 5 shows the values obtained for κ in each of the 16 analysis bins of the resolved signature. These corrections, with their uncertainties, are applied to the background yield predictions, as indicated in eq. (7.1). The determination of the values of κ for the boosted signature is illustrated in figure 6 (left), which shows the ratios from simulation $N_{\mathrm{CSR}}/N_{\mathrm{CSB}}$ for the 0H, and $N_{\mathrm{SR}}/N_{\mathrm{SB}}$ for the 1H

JHEP05(2022)014

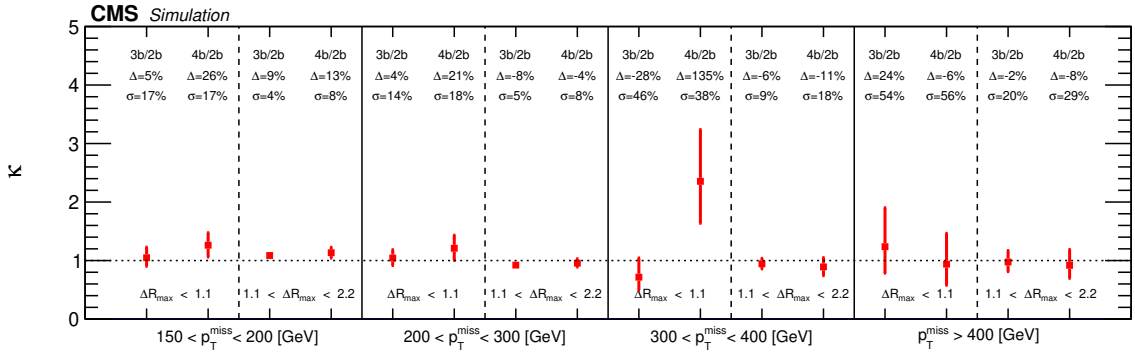

Figure 5. The double ratio $\kappa = (N_{\rm SR}/N_{\rm SB})/(N_{\rm CSR}/N_{\rm CSB})$ from the SM simulation for the $N_{\rm b} = 3$ and $N_{\rm b} = 4$ search samples for each $(p_{\rm T}^{\rm miss}, \Delta R_{\rm max})$ bin of the resolved signature. The value Δ gives the deviation of κ from unity, and σ its relative statistical uncertainty.

and 2H analysis regions. Dividing this ratio for the 1H (2H) region by the ratio for the 0H region we obtain the corresponding factor, with statistical uncertainties, $\kappa = 1.02 \pm 0.04$ (0.94 ± 0.17). As these are consistent with unity, we set $\kappa = 1$ in the calculation of the central values of the background yields, propagating the uncertainties in κ to these yields. For both signatures, systematic contributions to the κ uncertainties are evaluated as discussed in section 8.

For the boosted signature, the data yields are too small to permit a separate ABCD background calculation in each $p_{\rm T}^{\rm miss}$ bin. Instead we combine the $p_{\rm T}^{\rm miss}$-integrated estimate $N_{\rm SR,\,tot}^{\rm pred}$ for each of the 1H and 2H SRs with the binned $p_{\rm T}^{\rm miss}$ distribution $f_{\rm pTmiss}$ obtained from a separate data control region. This control region is a subset (0H+b) of the 0H region, comprising both the CSR and CSB regions but satisfying the further requirement of one tight b-tagged AK4 jet in addition to the two AK8 jets. The b tagging requirement serves to enrich this control region in $\rm t\bar{t}$ events, so as to approximate the SM content of the 1H and 2H regions. We thus have for the predicted yield, $N_{{\rm SR},i}^{\rm pred}$, in $p_{\rm T}^{\rm miss}$ bin i

$$N_{{\rm SR},i}^{\rm pred} = \kappa_i' \, f_{{\rm pTmiss},i} \, N_{\rm SR,\,tot}^{\rm pred}, \tag{7.3}$$

where $N_{\rm SR,\,tot}^{\rm pred}$ is the predicted background yield, as calculated from eq. (7.1) without any binning in $p_{\rm T}^{\rm miss}$, and $f_{{\rm pTmiss},i}$ is the fraction of events in the 0H+b region that fall in $p_{\rm T}^{\rm miss}$ bin i. Specifically,

$$f_{{\rm pTmiss},i} = \frac{N_{{\rm 0H+b},i}}{N_{\rm 0H+b,1} + N_{\rm 0H+b,2} + N_{\rm 0H+b,3}}, \tag{7.4}$$

and κ' is a correction factor obtained from simulation, as described below.

The yields $N_{\rm 0H+b,1,2,3}$ in the three $p_{\rm T}^{\rm miss}$ bins of the 0H+b region are included in the likelihood function described in section 9 so as to propagate the statistical uncertainties of $f_{\rm pTmiss}$ to the signal yield. We use the SM simulation to test the consistency of the $p_{\rm T}^{\rm miss}$ distribution in the 0H+b region with those of the 1H and 2H regions. This test is shown in figure 6 (right). The ratio distributions in the lower panel are seen to be uniform within the uncertainties of the simulation. We thus set the central values of the κ' factors

JHEP05(2022)014

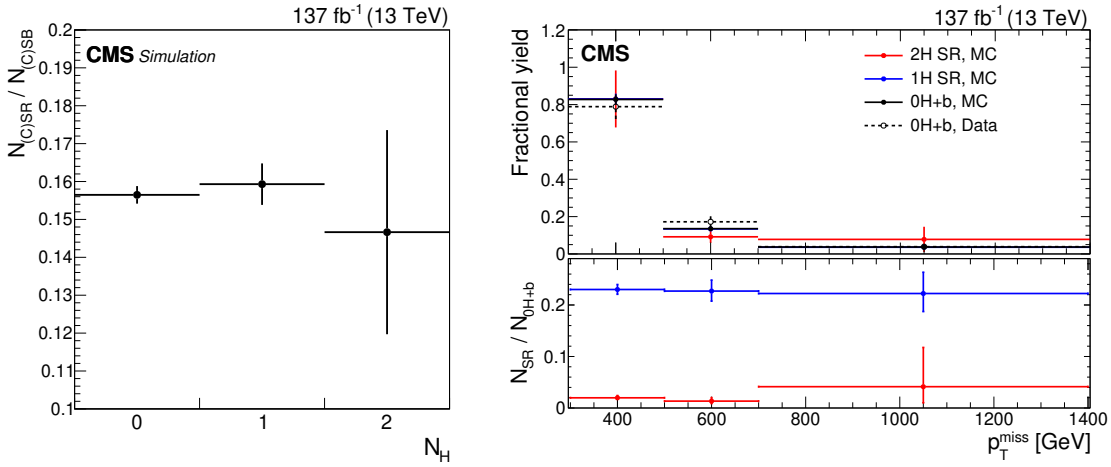

Figure 6. (left) The yield ratios $N_{\mathrm{CSR}}/N_{\mathrm{CSB}}$ for the 0H region, and $N_{\mathrm{SR}}/N_{\mathrm{SB}}$ for 1H and 2H regions of the boosted signature, from the SM simulation. (right) The $p_{\mathrm{T}}^{\mathrm{miss}}$ distributions of the 2H and 1H SR yields and the 0H+b control region yields, for SM simulation (MC, solid points), and for the control region in data (open black points). In the right-hand plot the upper panel shows the distributions normalized to unit area. The blue points, and in one bin the open point, are hidden under the solid black points. The lower panel shows the (unnormalized) ratios to the 0H+b yields of the 1H (blue) and 2H (red) SR yields, for the simulation. The error bars show the statistical uncertainties.

to unity, accounting for their uncertainties as described in section 8. The figure also shows agreement between the simulation and the fractional distribution f_{pTmiss} as measured in the data (open points).

8 Systematic uncertainties

Systematic uncertainties in the background estimates arise principally from the statistical uncertainties in control regions of the data, and from statistical and systematic uncertainties in the simulated samples used to measure κ and κ'. These quantities can be measured in SM-dominated control samples, providing a check on the procedure and estimates of the associated systematic uncertainties. Uncertainties in the simulation also affect the signal predictions. Sections 8.1 and 8.2 describe the evaluation of the background systematic uncertainties for the resolved and boosted signatures, respectively. Section 8.3 describes the systematic uncertainties in the signal model predictions.

8.1 Background systematic uncertainties (resolved signature)

We validate the κ factors described in section 7 and displayed in figure 5, and assign systematic uncertainties, by comparing their values obtained in simulation with those from three control samples, each of which is enriched in a specific class of SM background process. We compare the value of κ computed from the data with the one computed from the corresponding simulation. Since for each control sample we find the comparison to be consistent across $p_{\mathrm{T}}^{\mathrm{miss}}$ bins, we combine these bins, and take for the systematic uncertainty

JHEP05(2022)014

the larger of the data-simulation difference and the statistical uncertainty in the value obtained from simulation.

The $t\bar{t}$ systematic uncertainty is measured in a $t\bar{t}$-dominated single-lepton control sample selected by replacing the lepton and charged particle vetoes of the search sample with the requirement of one electron or muon with $p_T > 30\,\text{GeV}$, and no additional muons or electrons. The $\Delta\phi$ requirement is relaxed in the absence of QCD background, to improve the statistical precision, and a requirement $m_T < 100\,\text{GeV}$ is imposed to suppress signal contamination. We measure the relative systematic uncertainties in κ for the $t\bar{t}$ background in the $\Delta R_{max} < 1.1$ bins to be 13% and 19% for $N_b = 3$ and $N_b = 4$, respectively; the corresponding numbers for the $1.1 < \Delta R_{max} < 2.2$ bins are 2% and 8%.

The V+jets systematic uncertainty is measured in a Z+jets dominated dilepton control sample in which we select events with two electrons or muons of opposite sign, at least one of which has $p_T > 30\,\text{GeV}$, dilepton mass between 80 and 100 GeV, and $p_T^{miss} < 50\,\text{GeV}$. We then compute the p_T of the dilepton system, $p_T(Z)$, and treat this quantity as the true p_T^{miss}. That is, $p_T(Z)$ serves as a proxy for the p_T^{miss} that would be measured in an event with a $Z \to \nu\bar{\nu}$ decay. To increase the sample size, we relax the $\Delta\phi$ requirement and extend the range of $p_T(Z)$ down to zero. To reduce $t\bar{t}$ contamination, we take the CSR and CSB (SR and SB) regions to be defined by the b jet selection $N_{b,M} = 0\,(1)$. We measure the relative systematic uncertainties in κ for the V+jets background to be 16% and 5% for the $\Delta R_{max} < 1.1$ and $1.1 < \Delta R_{max} < 2.2$ bins, respectively.

The QCD multijet systematic uncertainty is measured in a QCD-enriched sample selected by inverting the $\Delta\phi$ requirement of the search sample. As with the dilepton control sample, the CSR and CSB (SR and SB) are defined by the b jet selection $N_{b,M} = 0\,(1)$. We measure the relative systematic uncertainties in κ for the QCD background to be 9% and 7% for the $\Delta R_{max} < 1.1$ and $1.1 < \Delta R_{max} < 2.2$ bins, respectively.

Finally, these results for each SM process are weighted by the fraction of total background arising from that process in each of the 16 analysis bins to obtain the uncertainties given in table 1. This direct in situ comparison with data of the simulation affecting κ covers all of the background-related uncertainties associated with MC modeling.

The effect of trigger efficiency modeling on κ has been evaluated and found to be negligible (<0.1%).

Table 1 gives a summary of the uncertainties in the κ factors for the resolved signature. These are propagated to the background prediction through eq. (7.1). The table shows that in most of the SRs the largest contribution to the systematic uncertainty in the background prediction is the statistical uncertainty in the simulation used to determine κ, which ranges from 4 to 56%.

8.2 Background systematic uncertainties (boosted signature)

Systematic uncertainties in the background yields are evaluated for each of the two steps (eq. (7.1) and eq. (7.3)) in the background determination for the boosted signature, and are summarized in table 2. For the first step, extraction of the p_T^{miss}-integrated yields $N^{pred}_{SR,\,tot}$ (eq. (7.3)), the systematic uncertainties are obtained by the method described above for the resolved signature. We construct a $t\bar{t}$ and W+jets dominated single-lepton control sample

JHEP05(2022)014

Source		Uncertainty [%]							
	p_T^{miss} [GeV]	150–200		200–300		300–400		>400	
	N_b	3	4	3	4	3	4	3	4
				$1.1 < \Delta R_{max} < 2.2$					
κ stat. unc.		4	8	5	8	9	18	20	29
	$t\bar{t}$	2	7	2	7	1	6	1	7
$\Delta\kappa$(data, MC)/κ	V+jets	<1	<1	1	<1	1	1	2	2
	QCD	<1	<1	<1	1	<1	<1	<1	1
κ total syst. unc.		2	7	2	7	1	6	2	7
				$\Delta R_{max} < 1.1$					
κ stat. unc.		17	17	14	18	46	38	54	56
	$t\bar{t}$	11	18	10	17	6	13	6	9
$\Delta\kappa$(data, MC)/κ	V+jets	1	1	4	5	10	6	6	10
	QCD	1	<1	<1	2	<1	<1	<1	<1
κ total syst. unc.		11	18	11	18	12	14	8	13

Table 1. Summary of the uncertainties in κ for the resolved signature. The sources are statistical uncertainties in the determination of κ and the systematic uncertainties $\Delta\kappa$(data, MC)/κ derived from the comparison of simulation with data in the single-lepton, dilepton, and low-$\Delta\phi$ control samples, each weighted by the fraction of background arising from the associated process in each search bin.

by applying the baseline selection for the boosted-signature analysis region, but releasing the lepton and isolated track vetoes and the $\Delta\phi$ requirement, and instead requiring exactly one electron or muon with $p_T > 30$ GeV and $m_T < 100$ GeV. Taking the larger of the data-simulation difference and the statistical uncertainty in that comparison, we find systematic uncertainties of 9 and 13% for the 1H and 2H SRs, respectively. The statistical uncertainty from the calculation of κ in simulation is assigned as a further systematic uncertainty.

The second step in the background prediction for the boosted signature is the application of the p_T^{miss} distribution f_{pTmiss} measured with the 0H+b control region. Systematic uncertainties arising from possible differences in the p_T^{miss} shape between the 0H+b control region and the SRs are contained in the correction factors κ' in eq. (7.3). These uncertainties are measured as the deviations, from the p_T^{miss}-averaged value, of a linear fit to the data in the lower panel of figure 6 (right); the values are 2, 3, and 9% (13, 19, and 63%) for the three p_T^{miss} bins in the 1H (2H) SR. We obtain an additional uncertainty in the p_T^{miss} distribution, attributable to the background composition of the simulation, by varying the Z+jets component by factors of two and one half. Taking the larger effect of these on κ' yields the uncertainties 3, 7, and 32%.

We assign a systematic uncertainty covering the effects of MC mismodeling in both $N^{pred}_{SR,\,tot}$ and f_{pTmiss} from the following sources: b and double-b tagging, jet energy scale, jet energy resolution, ISR corrections, and renormalization (μ_R) and factorization (μ_F) scales. The effect of each of these contributions ranges from 0 to 5%. The total systematic

JHEP05(2022)014

Source	p_T^{miss} [GeV]	Uncertainty [%]	
		1H	2H
SB, CSR, CSB statistics	>300	10	19
0H+b statistics	[300, 500]	8	
	[500, 700]	18	
	>700	38	
κ stat. unc.	>300	4	17
p_T^{miss} shape closure, κ'	[300, 500]	2	13
	[500, 700]	3	19
	>700	9	63
Δ(data, MC)	>300	9	13
Bkg. composition	[300, 500]	3	
	[500, 700]	7	
	>700	32	
MC modeling	>300	4	6
	[300, 500]	1	
	[500, 700]	2	
	>700	5	

Table 2. Summary of systematic uncertainties in the background prediction for the boosted signature. Values in cells spanning the 1H and 2H columns enter the yield calculations through the factor f_{pTmiss}, which is common to the 1H and 2H SRs. The values from the ABCD measurement with the p_T-integrated sample appear in the rows labeled $p_T^{miss} > 300$ GeV. The row labeled Δ(data, MC) gives the contribution derived from the comparison of simulation with data in the one-lepton control sample.

uncertainty is calculated by taking the largest uncertainty for each source, and adding those in quadrature. The individual sources are described in section 5 and their uncertainties in section 8.3.

As seen in table 2, the leading contributions are statistical uncertainties in the SB, CSR, CSB, and 0H+b yields in the data, and in those of the MC samples that are used to measure κ'.

8.3 Signal systematic uncertainties

Systematic uncertainties affecting the signal yields from simulation are listed in table 3. The systematic uncertainty in the ISR correction of the simulation of electroweak production models is evaluated by varying the correction factors described in section 5 (18–22%) by 100% of their nominal value. For strong production models, the systematic uncertainty is evaluated by varying the correction factors (4–26%) by 50% of their nominal value. To evaluate the uncertainty associated with μ_R and μ_F, we vary one or both by factors of 2.0 and 0.5 and take the combination (excluding the case of opposite variations of the two) that

JHEP05(2022)014

Source	Relative uncertainty [%]	
	Resolved	Boosted
MC sample size	0–18	1–15
ISR modeling	0–2	0–18
Renormalization and factorization scales μ_R and μ_F	0–2	0–7
Pileup corrections	0–3	0–9
Integrated luminosity	1.6	
Jet energy scale	0–7	0–12
Jet energy resolution	0–7	0–7
Isolated track veto	2–9	1–8
Trigger efficiency	1–12	0–4
m_J resolution	—	0–9
b tagging efficiency	2–6	—
b mistagging	0–1	—
bb tagging efficiency	—	6–15
Uncertainties attributable to the fast simulation		
Jet quality requirements	1	
p_T^{miss} modeling	0–14	0–12
m_J resolution	—	2–4
b tagging efficiency	0–1	—
b mistagging	0–1	—
bb tagging efficiency	—	0–1

Table 3. Sources of systematic uncertainties and their typical impact on the signal yields obtained from simulation. The range is reported as the median 68% confidence interval among all signal regions for every signal mass point considered. Entries reported as 0 correspond to values smaller than 0.5%.

gives the largest effect on the yield [142–144]. The uncertainty associated with the pileup reweighting is evaluated by varying the value of the total inelastic cross section by 5% [145]. The systematic uncertainty in the determination of the integrated luminosity varies between 1.2 and 2.5% [146–148], depending on the year of data collection; the total integrated luminosity for the three years has an uncertainty of 1.6%. The uncertainties related to the jet energy scale and jet energy resolution are calculated by varying jet properties in bins of p_T and η, according to the uncertainties in the jet energy corrections. The uncertainty in the m_J resolution is derived by comparing the mean and width of the W boson peak in the m_J spectrum between data and simulation in a $t\bar{t}$-enriched sample. The efficiency of the isolated-track veto for signal events, as measured in simulation, is greater than 90% except at the lowest NLSP masses. Differences with respect to simulation measured in data control samples lie in the range 20–30% of the inefficiency. We assign a systematic uncertainty of 50% of the inefficiency to account for the effect of this veto on the signal yields.

JHEP05(2022)014

The uncertainty in the trigger efficiency modeling is derived from the statistical uncertainty, and variations in the kinematic selections, for the trigger measurement sample, and from variation in the independent trigger used to measure the efficiency. This uncertainty is applied to each SR bin for each signal model based on its distribution in $p_{\mathrm{T}}^{\mathrm{miss}}$ and H_{T} in that bin. For the resolved signature, typical values range from 1–13%, though some bins have larger values. For $p_{\mathrm{T}}^{\mathrm{miss}} > 300\,\mathrm{GeV}$ the largest uncertainty is 4%.

Systematic uncertainties in the b tagging are obtained from the measurements in data of the b and double-b tagging efficiencies and mistag rates, described in section 5. These uncertainties lie in the ranges 2–7% for jets tagged as b quarks and 6–15% for the double-b-tagged jets.

Systematic uncertainties associated with use of the fast simulation are taken to be 100% of the differences with respect to the GEANT4 simulation. This amounts to 1% for the jet quality requirements, 2–4% for m_{J} resolution, and 1% for b and double-b tagging.

9 Results and interpretation

The observed distributions in the appropriate Higgs candidate mass quantity ($\langle m_{\mathrm{bb}} \rangle$ for the resolved signature and m_{J} for the boosted signature) are shown in figures 7–9. Figures 7 and 8 show the $\langle m_{\mathrm{bb}} \rangle$ distributions for the resolved signature in the SR+SB regions ($N_{\mathrm{b}} = 3$ and $N_{\mathrm{b}} = 4$) of the data, with the corresponding distributions for the CSR+CSB regions ($N_{\mathrm{b}} = 2$) overlaid. The latter distributions are reweighted event-by-event with the appropriate values of κ and are normalized to the same overall event yield as observed in the SR+SB region. The distributions are presented (i) in two slices of ΔR_{max} but integrated in $p_{\mathrm{T}}^{\mathrm{miss}}$ (figure 7) and (ii) in two slices of $p_{\mathrm{T}}^{\mathrm{miss}}$ but integrated over ΔR_{max} (figure 8). Overall, we observe that the shapes of the $\langle m_{\mathrm{bb}} \rangle$ distributions for $N_{\mathrm{b}} = 3$ and $N_{\mathrm{b}} = 4$ are highly similar to those for $N_{\mathrm{b}} = 2$, and we do not observe a large excess at the Higgs-boson mass. In figure 8, comparison of the $\langle m_{\mathrm{bb}} \rangle$ TChiHH-G distributions for $N_{\mathrm{b}} = 4$ at low and high values of $p_{\mathrm{T}}^{\mathrm{miss}}$ illustrates how the different $p_{\mathrm{T}}^{\mathrm{miss}}$ regions provide sensitivity to different parts of the model space. For the boosted signature, figure 9 shows the data distributions in m_{J}, and in $(m_{\mathrm{J1}}, m_{\mathrm{J2}})$, with simulation overlaid, for the 0H CSR+CSB and the 1H and 2H SR+SB regions, integrated in $p_{\mathrm{T}}^{\mathrm{miss}}$. Again, we do not observe a large excess in the data in the m_{J} distributions at the Higgs-boson mass. Systematic uncertainties are not included in these figures, as those uncertainties are computed only for the total yields in the analysis regions. The plots also show representative distributions for potential SUSY signals, with their clear peaks in the H boson mass window.

To extract the signal strength, μ, we perform maximum likelihood fits to the data using a probability density function for each bin that represents the SM yield plus the yield predicted by a specific model for the signal. The parameter μ is the ratio of the fitted to theoretical cross section. The likelihood function is a product of Poisson distributions, one for each of the SRs of the resolved and boosted signatures and their corresponding SB, CSR, and CSB regions. Additional Poisson variables represent the event yields in the three $p_{\mathrm{T}}^{\mathrm{miss}}$ bins of each of the 0H+b control regions used for the boosted signature. Equation (7.1), and eq. (7.3) for the boosted signature, are imposed as constraints on the background

JHEP05(2022)014

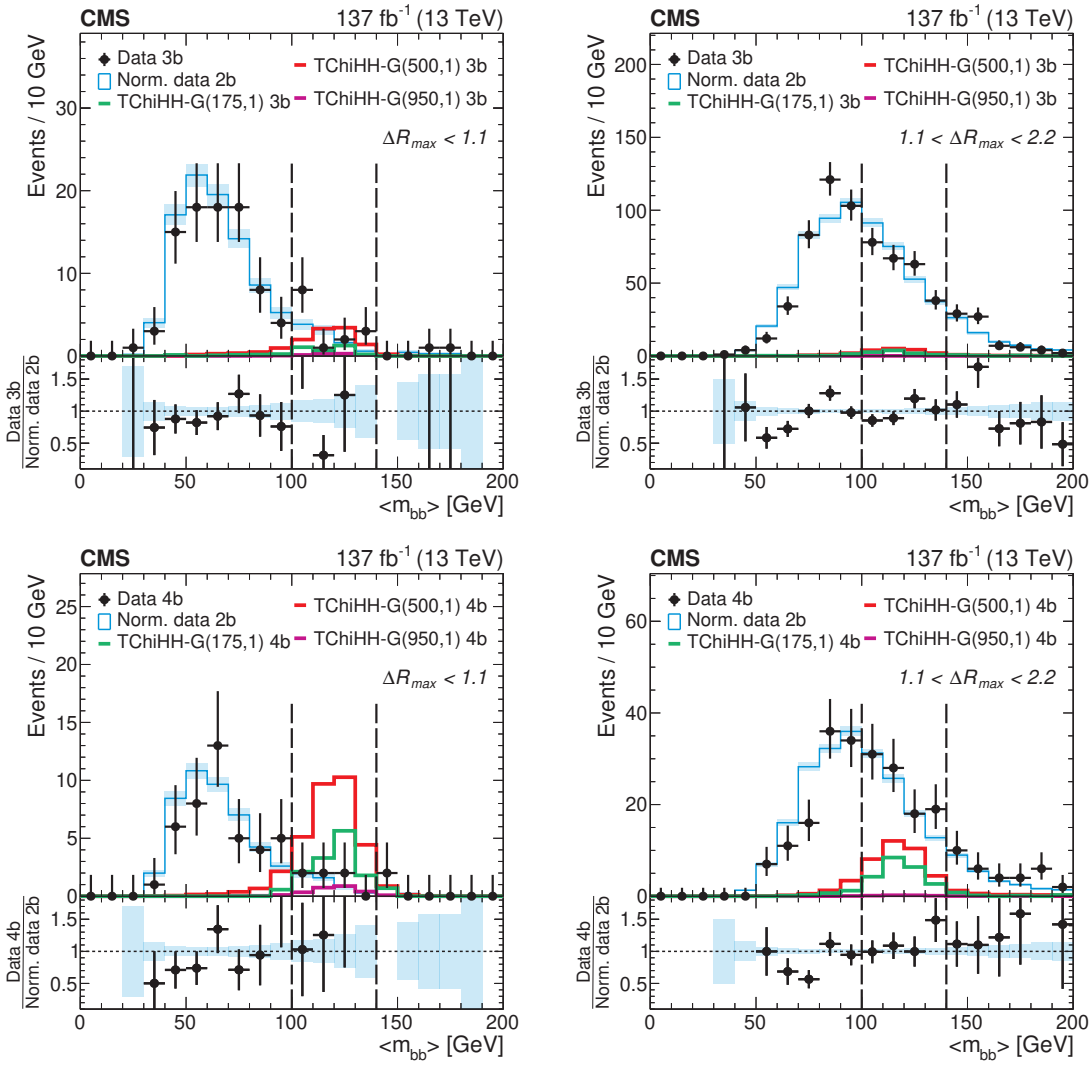

Figure 7. Distributions in $\langle m_{\mathrm{bb}} \rangle$ for the (upper row) $N_{\mathrm{b}} = 3$ and (lower row) $N_{\mathrm{b}} = 4$ data, denoted by black markers, with error bars indicating the statistical uncertainties. The left-hand set of plots corresponds to $\Delta R_{\mathrm{max}} < 1.1$, while the right-hand set corresponds to $1.1 < \Delta R_{\mathrm{max}} < 2.2$, in both cases integrated over $p_{\mathrm{T}}^{\mathrm{miss}}$. The overlaid cyan histograms show the corresponding distributions of the $N_{\mathrm{b}} = 2$ data, reweighted with the appropriate κ values and scaled in area to the $N_{\mathrm{b}} = 3$ or $N_{\mathrm{b}} = 4$ distribution and with statistical uncertainties indicated by the cyan shading (absent in the 140–150 bin because of a vanishing $N_{\mathrm{b}} = 2$ yield there). The ratio of these distributions appears in the lower panel. The red, green, and violet histograms show simulations of representative signals, denoted TChiHH-G($m(\widetilde{\chi}_1^0), m(\widetilde{\mathrm{G}})$ [GeV]) in the legends.

JHEP05(2022)014

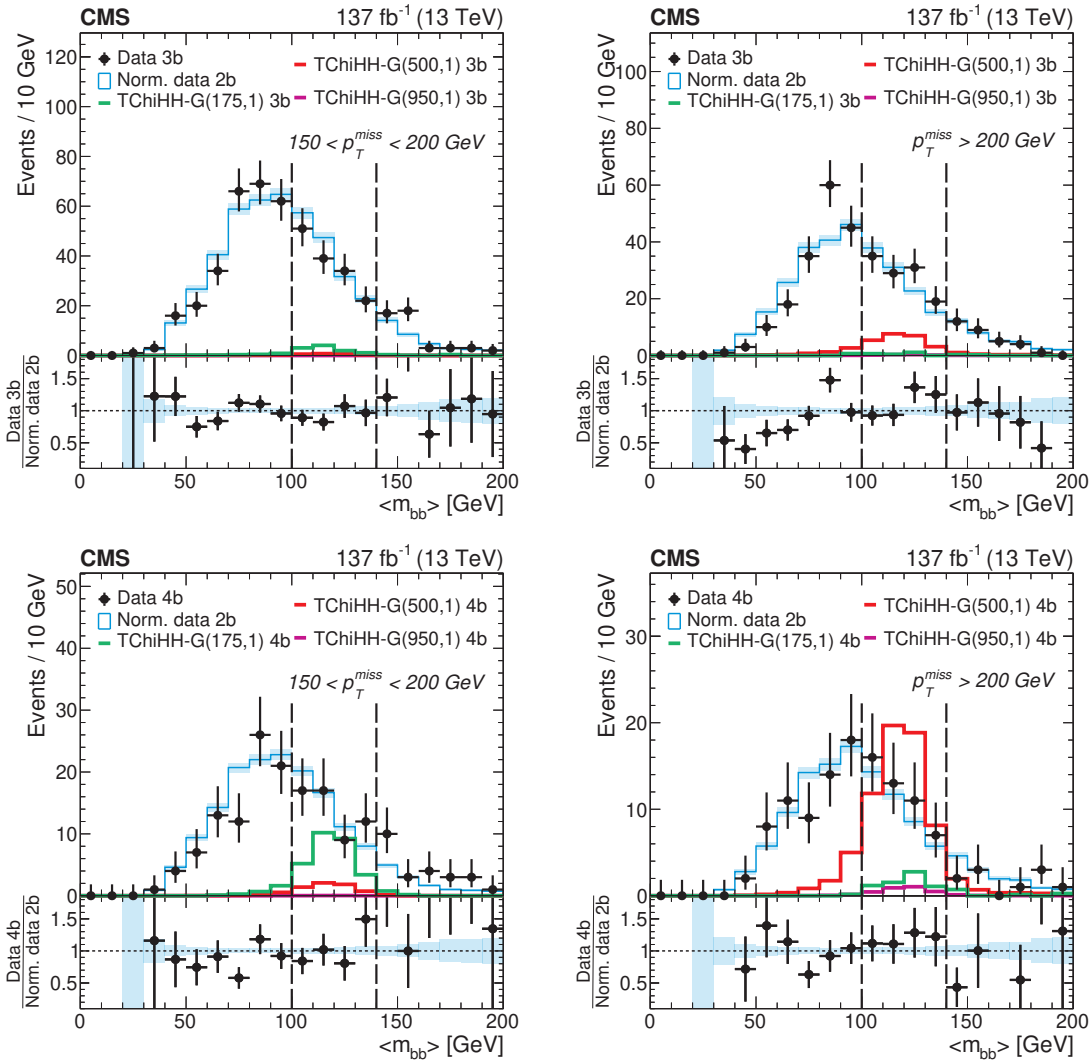

Figure 8. Distributions in $\langle m_{\mathrm{bb}} \rangle$ for the (upper row) $N_{\mathrm{b}} = 3$ and (lower row) $N_{\mathrm{b}} = 4$ data, denoted by black markers, with error bars indicating the statistical uncertainties. The left-hand set of plots corresponds to $150 < p_{\mathrm{T}}^{\mathrm{miss}} < 200$, while the right-hand set corresponds to $p_{\mathrm{T}}^{\mathrm{miss}} > 200\,\mathrm{GeV}$, in both cases integrated over ΔR_{max}. The overlaid cyan histograms show the corresponding distributions of the $N_{\mathrm{b}} = 2$ data, reweighted with the appropriate κ values and scaled in area to the $N_{\mathrm{b}} = 3$ or $N_{\mathrm{b}} = 4$ distribution and with statistical uncertainties indicated by the cyan shading. The ratio of these distributions appears in the lower panel. The red, green, and violet histograms show simulations of representative signals, denoted TChiHH-G$(m(\widetilde{\chi}_1^0), m(\widetilde{\mathrm{G}})\,[\mathrm{GeV}])$ in the legends.

JHEP05(2022)014

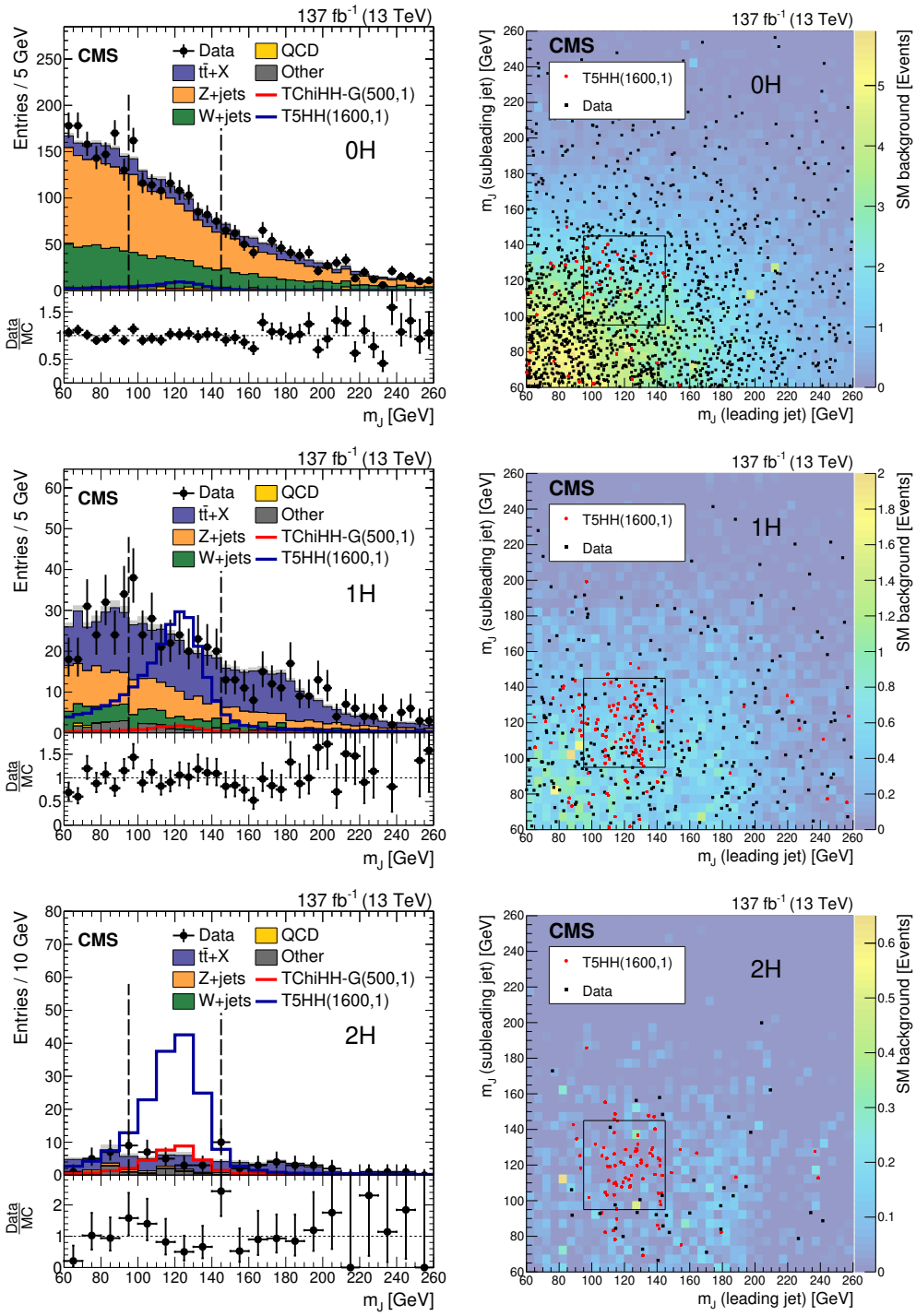

Figure 9. Distributions in m_{J} for the boosted signature, integrated in $p_{\mathrm{T}}^{\mathrm{miss}}$. The projections (left column) contain two entries per event, with statistical uncertainties in the data and simulation given by the vertical bars and gray shading, respectively. The SM yields are scaled to the data integral, by factors of 0.84, 0.92, and 1.13 in the 0H (upper), 1H (middle), and 2H (lower) plots, respectively. The data to simulation ratio appears in each lower panel. Simulated signals TChiHH-G($m(\widetilde{\chi}_1^0), m(\widetilde{\mathrm{G}})$) and T5HH($m(\widetilde{\mathrm{g}}), m(\widetilde{\chi}_1^0)$ [GeV]) are also shown. In the correlation plots (right column) the color scale represents the SM background, black dots the data, and red dots the expected signal. The dashed lines and boxes denote the boundaries of the SRs.

JHEP05(2022)014

Bin	$\Delta R_{\max}$	N_{b}	$p_{\mathrm{T}}^{\mathrm{miss}}$ [GeV]	κ	$N_{\mathrm{SR}}^{\mathrm{pred}}$	$N_{\mathrm{SR}}^{\mathrm{fit}}$	$N_{\mathrm{SR}}^{\mathrm{obs}}$
1	1.1–2.2	3	150–200	$1.09 \pm 0.04 \pm 0.02$	161^{+14}_{-13}	$149.7^{+8.9}_{-8.5}$	138
2			200–300	$0.92 \pm 0.04 \pm 0.02$	$90.4^{+9.7}_{-9.0}$	$91.5^{+6.9}_{-6.5}$	91
3			300–400	$0.94 \pm 0.09 \pm 0.01$	$11.5^{+3.4}_{-2.7}$	$12.8^{+2.6}_{-2.2}$	14
4			>400	$0.98^{+0.19}_{-0.16} \pm 0.02$	$2.8^{+2.3}_{-1.4}$	$2.8^{+1.4}_{-1.0}$	3
5		4	150–200	$1.13 \pm 0.09 \pm 0.08$	$53.5^{+8.8}_{-7.8}$	$54.1^{+5.6}_{-5.2}$	54
6			200–300	$0.96 \pm 0.07 \pm 0.07$	$28.3^{+5.6}_{-4.8}$	$33.2^{+4.2}_{-3.9}$	38
7			300–400	$0.89^{+0.16}_{-0.15} \pm 0.05$	$2.6^{+1.5}_{-1.1}$	$3.2^{+1.3}_{-1.0}$	4
8			>400	$0.92^{+0.27}_{-0.22} \pm 0.07$	$2.6^{+2.4}_{-1.4}$	$1.27^{+0.98}_{-0.63}$	0
9	<1.1	3	150–200	$1.05^{+0.18}_{-0.15} \pm 0.12$	$5.1^{+1.6}_{-1.3}$	$5.9^{+1.4}_{-1.2}$	8
10			200–300	$1.04^{+0.14}_{-0.13} \pm 0.11$	$2.17^{+0.79}_{-0.60}$	$2.31^{+0.73}_{-0.57}$	2
11			300–400	$0.72^{+0.33}_{-0.22} \pm 0.08$	$0.06^{+0.11}_{-0.04}$	$0.72^{+0.53}_{-0.33}$	4
12			>400	$1.24^{+0.67}_{-0.45} \pm 0.10$	$0.89^{+1.42}_{-0.60}$	$0.52^{+0.65}_{-0.35}$	0
13		4	150–200	$1.26^{+0.21}_{-0.20} \pm 0.23$	$2.68^{+1.06}_{-0.79}$	$2.58^{+0.85}_{-0.67}$	1
14			200–300	$1.21^{+0.22}_{-0.21} \pm 0.22$	$1.26^{+0.62}_{-0.44}$	$1.62^{+0.65}_{-0.48}$	3
15			300–400	$2.35^{+0.88}_{-0.72} \pm 0.34$	$0.42^{+0.61}_{-0.27}$	$1.16^{+0.87}_{-0.55}$	1
16			>400	$0.94^{+0.53}_{-0.36} \pm 0.13$	$0.67^{+1.10}_{-0.46}$	$0.78^{+0.76}_{-0.43}$	1

Table 4. For each SR of the resolved signature, the MC correction factor κ, predicted background yield $N_{\mathrm{SR}}^{\mathrm{pred}}$, yield from the background-only ($\mu = 0$) fit $N_{\mathrm{SR}}^{\mathrm{fit}}$, and observed yield $N_{\mathrm{SR}}^{\mathrm{obs}}$. The first and second uncertainties in the κ factors are statistical and systematic, respectively. The uncertainties in $N_{\mathrm{SR}}^{\mathrm{pred}}$ and $N_{\mathrm{SR}}^{\mathrm{fit}}$, extracted from the maximum likelihood fit, include both statistical and systematic contributions. The interpretation of the results in bin 11 is discussed in the text.

component of the Poisson means for each of these factors. The measured values of κ, with their statistical uncertainties, are introduced as Gaussian constraints. Other systematic uncertainties are implemented as additional free parameters with log-normal constraints. Correlations among signal bins are taken into account. Inclusion of the signal component in the functions for the Poisson means of the SB, CSR, CSB, and 0H+b regions accounts for potential signal contamination of these regions.

We determine confidence intervals for μ using the test statistic $q_\mu = -2\ln(\mathcal{L}_\mu/\mathcal{L}_{\max})$, where $\mathcal{L}_{\max}$ is the maximum likelihood determined by allowing all parameters including μ to vary, and $\mathcal{L}_\mu$ is the maximum likelihood for a fixed signal strength. Confidence ranges are set under the asymptotic approximation [149], with q_μ approximated with an Asimov data set [149] and used in conjunction with the $\mathrm{CL_s}$ criterion described in refs. [150, 151].

The observed yields, together with the predicted SM yields, are given in tables 4 and 5 for the resolved and boosted signatures, respectively, and are summarized in figure 10. For 15 of the 16 bins of the resolved signature, and the 6 bins of the boosted signature, the

JHEP05(2022)014

Bin	N_{H}	$p_{\mathrm{T}}^{\mathrm{miss}}$ [GeV]	$N_{\mathrm{SR,\,tot}}^{\mathrm{pred}}$	f_{pTmiss}	$N_{\mathrm{SR}}^{\mathrm{pred}}$	$N_{\mathrm{SR}}^{\mathrm{fit}}$	$N_{\mathrm{SR}}^{\mathrm{obs}}$
17		300–500		0.789 ± 0.030	$33.6^{+6.1}_{-5.2}$	$37.0^{+4.2}_{-4.0}$	42
18	1	500–700	42.6 ± 4.2	0.172 ± 0.028	$7.3^{+2.0}_{-1.6}$	$7.2^{+1.5}_{-1.3}$	6
19		>700		0.039 ± 0.014	$1.65^{+1.04}_{-0.66}$	$1.50^{+0.75}_{-0.53}$	1
20		300–500		0.789 ± 0.030	$4.0^{+1.5}_{-1.1}$	$4.0^{+1.2}_{-1.0}$	4
21	2	500–700	5.1 ± 1.0	0.172 ± 0.028	$0.88^{+0.40}_{-0.28}$	$0.74^{+0.29}_{-0.21}$	0
22		>700		0.039 ± 0.014	$0.20^{+0.21}_{-0.10}$	$0.14^{+0.13}_{-0.07}$	0

Table 5. For each N_{H} SR of the boosted signature, the total predicted background yield $N_{\mathrm{SR,\,tot}}^{\mathrm{pred}}$, and for each $p_{\mathrm{T}}^{\mathrm{miss}}$ bin the fraction f_{pTmiss}, both with their statistical uncertainties, the predicted background yield $N_{\mathrm{SR}}^{\mathrm{pred}}$, the yield from the background-only ($\mu = 0$) fit $N_{\mathrm{SR}}^{\mathrm{fit}}$, and the observed yield $N_{\mathrm{SR}}^{\mathrm{obs}}$. The values of $N_{\mathrm{SR}}^{\mathrm{pred}}$ and $N_{\mathrm{SR}}^{\mathrm{fit}}$ are extracted from the maximum likelihood fit, with uncertainties that include both statistical and systematic contributions.

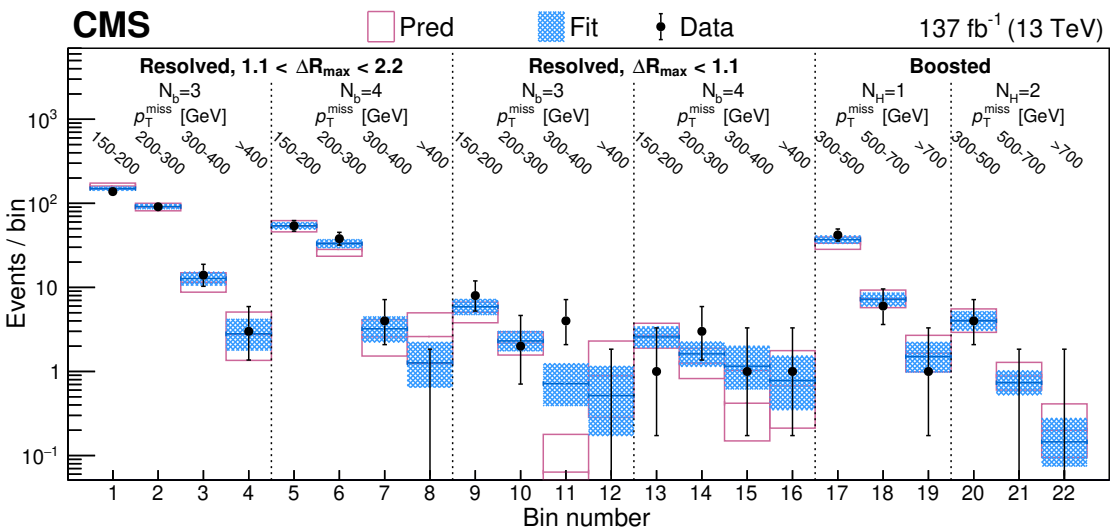

Figure 10. Observed and predicted yields in the search regions identified by the legend text. The points with error bars represent the observed yields, the magenta outline bands the predicted background yields ("Pred") with their total uncertainties derived as described in sections 7 and 8, and the blue shaded bands the values determined by the background-only fit ("Fit").

distribution of deviations of the observations with respect to SM predictions is consistent with statistical fluctuations. In the single bin 11, corresponding to $\Delta R_{\mathrm{max}} < 1.1$, $N_{\mathrm{b}} = 3$, $p_{\mathrm{T}}^{\mathrm{miss}} = 300$–$400\,\mathrm{GeV}$ of the resolved signature, the observed yield is 4 events while the prediction is $0.06^{+0.11}_{-0.04}$ (table 4). That prediction is based on small SB and CSR counts (2 events each), leading to highly asymmetric confidence bands. The probability of observing 4 or more events given this background estimate, as measured with a large sample of simulated pseudo-experiments, corresponds to 3.3 standard deviations (s.d.). The pseudo-experiments were generated with a null model based on the observed yields in the SB, CSR, and CSB regions and associated systematic uncertainties. When the observed SR yield is included in

JHEP05(2022)014

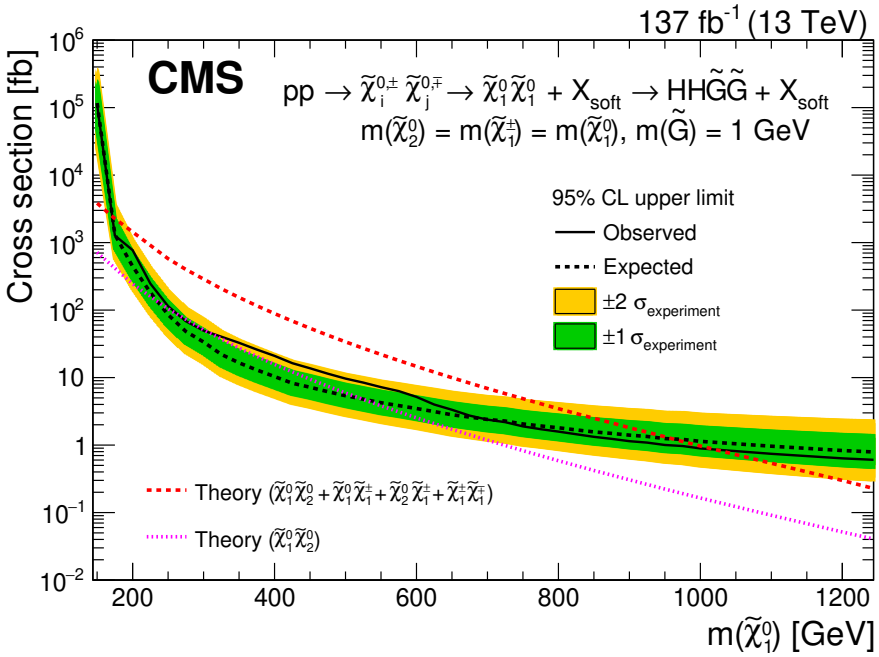

Figure 11. Observed and expected upper limits at 95% CL on the cross section for the GMSB-motivated simplified model TChiHH-G. The symbol X_{soft} in the legend represents low-energy particles emitted in the transitions to the $\tilde{\chi}_1^0$ NLSPs. The dashed black line with green and yellow bands shows the expected limit with its 1- and 2-s.d. uncertainties, while the solid black line shows the observed limit. The theoretical cross section is indicated by the dashed red line under the assumption that the decay chains leading to the $\tilde{\chi}_1^0\tilde{\chi}_1^0$ intermediate state include a degenerate set of all charginos and neutralinos, and by the dotted magenta line under the assumption that only the combination $\tilde{\chi}_1^0\tilde{\chi}_2^0$ contributes.

the background-only fit (column N_{SR}^{fit} in table 4) the background estimate becomes $0.72^{+0.53}_{-0.33}$. We have examined the four observed events in detail and find no exceptional features. The models we consider for potential contributions beyond the SM predict that events would be distributed over multiple bins, contrary to the observations here. To account for the look-elsewhere effect [152], we perform pseudo-experiments with all 16 bins of the resolved signature. We find that the probability of observing a 3.3 s.d. or larger excess in at least one bin corresponds to a global significance of 2.1 s.d.

We interpret the data in terms of the three models discussed in section 1. In each case, the data from both resolved and boosted signatures are included in the fit. Figure 11 shows the upper limit on the cross section at 95% CL for the TChiHH-G model of figure 1 (left). For the case of the production of the sum of all higgsino pairs, the data exclude masses of the $\tilde{\chi}_1^0$ in the range 175–1025 GeV. This represents the best limit to date on this model, extending previous ATLAS results [29], which exclude mass ranges 130–230 GeV and 290–880 GeV, and previous CMS results [45], which exclude 230–770 GeV. If instead only $\tilde{\chi}_1^0\tilde{\chi}_2^0$ production is included in the model, the excluded mass range is 265–305 GeV. Here the single-bin excess noted above leads to a limit less restrictive than the expected one. The separate contributions of the resolved and boosted signatures are displayed in

JHEP05(2022)014

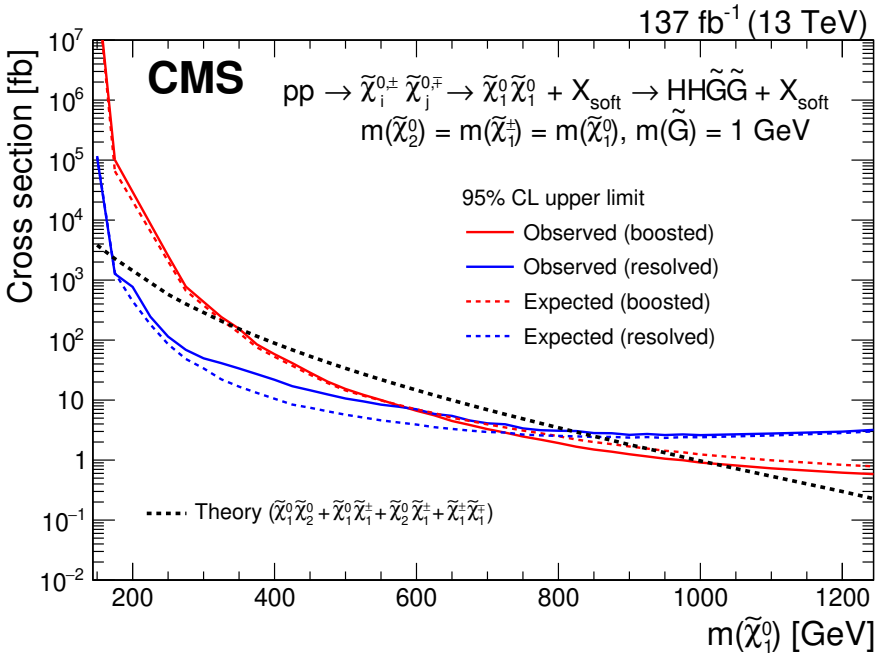

Figure 12. Separate resolved-signature (blue) and boosted-signature (red) contributions to the cross section limits for the GMSB-motivated simplified model TChiHH-G shown in figure 11. Here no overlapping events were removed. The symbol X_{soft} in the legend represents low-energy particles emitted in the transitions to the $\tilde{\chi}_1^0$ NLSPs. The solid and dashed lines, respectively, give the observed and expected upper limits at 95% CL. The dashed black line shows the theoretical cross section computed under the assumption that the decay chains leading to the $\tilde{\chi}_1^0\tilde{\chi}_1^0$ intermediate state include a degenerate set of all charginos and neutralinos.

figure 12. As expected, the resolved analysis provides most of the sensitivity at lower NLSP masses, where the energy available in the NLSP decay to LSP and H is limited. At higher NLSP masses the Higgs bosons receive a larger Lorentz boost, and the daughter b quarks tend to merge; the crossover where the boosted signature is more sensitive is about 800 GeV for the expected limits, and 600 GeV for the observed limits since the SRs of the boosted signature show no excess in the data.

For the TChiHH model (figure 1, center) the cross section limit is presented in figure 13 as a function of the independent masses $m(\tilde{\chi}_2^0)$ and $m(\tilde{\chi}_1^0)$. While the expected limit would exclude a substantial region of this plane, the observed exclusion is limited to a small region where $m(\tilde{\chi}_1^0)$ is less than 15 GeV, again because of the single-bin excess. For $m(\tilde{\chi}_1^0) = 1$ GeV the excluded range of $m(\tilde{\chi}_2^0)$ is 265–305 GeV.

Figure 14 shows the cross section upper limit as a function of $m(\tilde{g})$ for the T5HH model (figure 1, right) of gluino pair production with a $\tilde{\chi}_2^0$ NLSP slightly less massive than the gluino and a light LSP. Masses $m(\tilde{g}) < 2330$ GeV are excluded. This is the strongest mass limit for this model to date, extending a previous CMS result [51], which excluded $m(\tilde{g}) < 2010$ GeV. Most of the sensitivity to this model is provided by the boosted signature. This reflects the choice of large NLSP mass, which leads to energetic H boson daughters.

JHEP05(2022)014

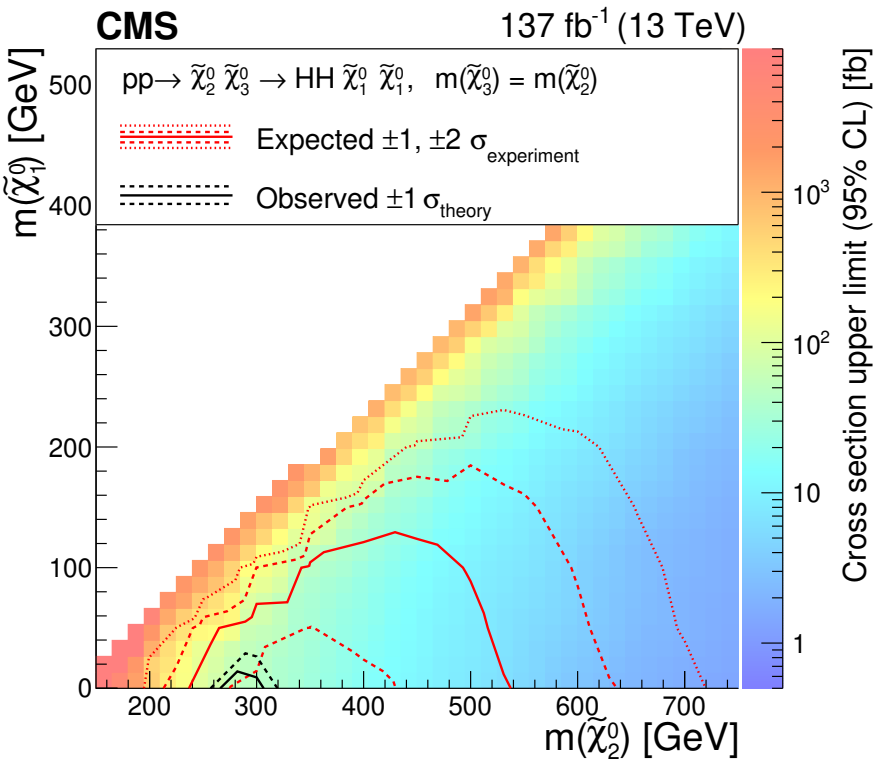

Figure 13. Limits at 95% CL on the cross section for the TChiHH signal model in which production of the intermediate state $\tilde{\chi}^0_2\tilde{\chi}^0_3$ (assumed mass degenerate) is followed by the decay of each to $\tilde{\chi}^0_1$H. The color scale gives the cross section limit as a function of $(m(\tilde{\chi}^0_2), m(\tilde{\chi}^0_1))$. The black solid and dashed curves show the observed excluded region and its 1-s.d. uncertainty. The red solid and dashed (dotted) contours show the expected excluded region with its 1 (2)-s.d. uncertainty.

10 Summary

A search has been presented for physics beyond the standard model in channels leading to pairs of Higgs bosons and an imbalance of transverse momentum, produced in proton-proton collisions at $\sqrt{s} = 13$ TeV. The data sample, collected by the CMS experiment at the LHC, corresponds to an integrated luminosity of 137 fb^{-1}. The Higgs bosons are reconstructed via their decay to a pair of b quarks, observed either as distinct b quark jets (resolved signature), or as wide-angle jets that each contain the pair of b quarks (boosted signature). The observed event yields in 15 of the 16 analysis bins of the resolved signature, and all 6 bins of the boosted signature, are consistent with the background predictions based on SM processes. In one bin of the resolved signature, an excess is observed, for which the global significance is 2.1 standard deviations when all 16 bins are considered. A narrow, single-bin effect is not typical of the supersymmetry (SUSY) models under consideration.

These results are used to set limits on the cross sections for the production of particles predicted by SUSY, considering both the direct production of neutralinos and their production through intermediate states with gluinos. For the electroweak production of nearly-degenerate higgsinos, each of whose decay cascades yields a $\tilde{\chi}^0_1$ that in turn decays

JHEP05(2022)014

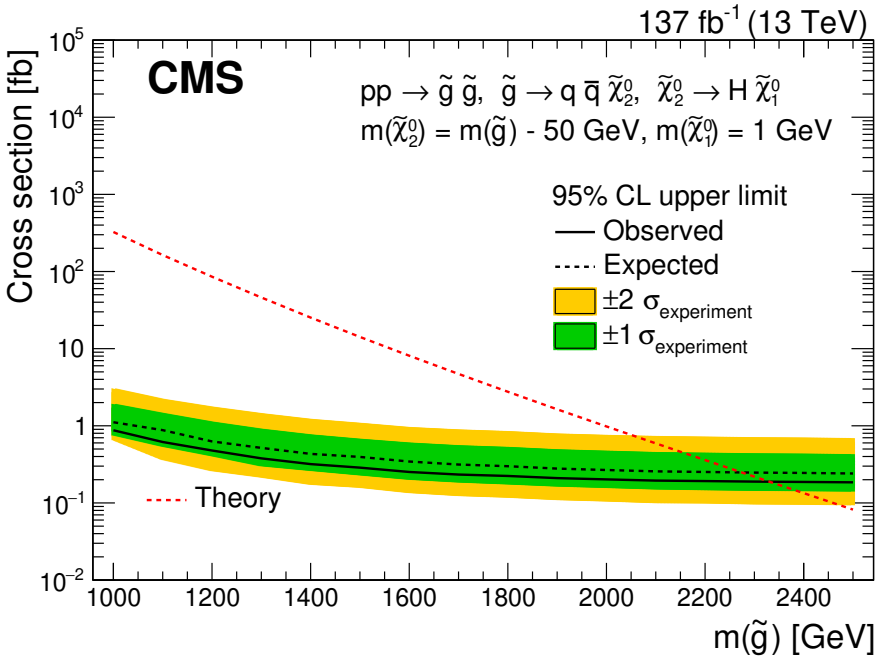

Figure 14. Observed and expected upper limits at 95% CL on the cross section for the simplified model T5HH, the strong production of a pair of gluinos each of which decays via a three-body process to quarks and a $\tilde{\chi}^0_2$ NLSP, which subsequently decays to a Higgs boson and a $\tilde{\chi}^0_1$ LSP. The dashed black line with green and yellow bands shows the expected limit with its 1- and 2-s.d. uncertainties; the solid black line shows the observed limit, and the dashed red line the theoretical cross section.

through a Higgs boson to the lightest SUSY particle (LSP), a massless goldstino, $\tilde{\chi}^0_1$ masses in the range 175–1025 GeV are excluded at 95% confidence level. For a model with a mass splitting between the directly produced, degenerate higgsinos $\tilde{\chi}^0_2\tilde{\chi}^0_3$, and a bino LSP, a small region where $m(\tilde{\chi}^0_1)$ is less than 15 GeV is excluded; for $m(\tilde{\chi}^0_1) = 1$ GeV the excluded range of $m(\tilde{\chi}^0_2)$ is 265–305 GeV. For the strong production of gluino pairs decaying via a slightly lighter $\tilde{\chi}^0_2$ to a Higgs boson and a light $\tilde{\chi}^0_1$ LSP, gluino masses below 2330 GeV are excluded. The bounds on masses found here extend previous limits for these models by about 150 and 320 GeV for the $\tilde{\chi}^0_1$ and gluino, respectively.

Acknowledgments

We congratulate our colleagues in the CERN accelerator departments for the excellent performance of the LHC and thank the technical and administrative staffs at CERN and at other CMS institutes for their contributions to the success of the CMS effort. In addition, we gratefully acknowledge the computing center s and personnel of the Worldwide LHC Computing Grid and other center s for delivering so effectively the computing infrastructure essential to our analyses. Finally, we acknowledge the enduring support for the construction and operation of the LHC, the CMS detector, and the supporting computing infrastructure provided by the following funding agencies: BMBWF and FWF (Austria); FNRS and FWO

JHEP05(2022)014

(Belgium); CNPq, CAPES, FAPERJ, FAPERGS, and FAPESP (Brazil); MES and BNSF (Bulgaria); CERN; CAS, MoST, and NSFC (China); MINCIENCIAS (Colombia); MSES and CSF (Croatia); RIF (Cyprus); SENESCYT (Ecuador); MoER, ERC PUT and ERDF (Estonia); Academy of Finland, MEC, and HIP (Finland); CEA and CNRS/IN2P3 (France); BMBF, DFG, and HGF (Germany); GSRI (Greece); NKFIA (Hungary); DAE and DST (India); IPM (Iran); SFI (Ireland); INFN (Italy); MSIP and NRF (Republic of Korea); MES (Latvia); LAS (Lithuania); MOE and UM (Malaysia); BUAP, CINVESTAV, CONACYT, LNS, SEP, and UASLP-FAI (Mexico); MOS (Montenegro); MBIE (New Zealand); PAEC (Pakistan); MSHE and NSC (Poland); FCT (Portugal); JINR (Dubna); MON, RosAtom, RAS, RFBR, and NRC KI (Russia); MESTD (Serbia); MCIN/AEI and PCTI (Spain); MOSTR (Sri Lanka); Swiss Funding Agencies (Switzerland); MST (Taipei); ThEPCenter, IPST, STAR, and NSTDA (Thailand); TUBITAK and TAEK (Turkey); NASU (Ukraine); STFC (United Kingdom); DOE and NSF (U.S.A.).

Individuals have received support from the Marie-Curie program and the European Research Council and Horizon 2020 Grant, contract Nos. 675440, 724704, 752730, 758316, 765710, 824093, 884104, and COST Action CA16108 (European Union); the Leventis Foundation; the Alfred P. Sloan Foundation; the Alexander von Humboldt Foundation; the Belgian Federal Science Policy Office; the Fonds pour la Formation à la Recherche dans l'Industrie et dans l'Agriculture (FRIA-Belgium); the Agentschap voor Innovatie door Wetenschap en Technologie (IWT-Belgium); the F.R.S.-FNRS and FWO (Belgium) under the "Excellence of Science — EOS" — be.h project n. 30820817; the Beijing Municipal Science & Technology Commission, No. Z191100007219010; the Ministry of Education, Youth and Sports (MEYS) of the Czech Republic; the Deutsche Forschungsgemeinschaft (DFG), under Germany's Excellence Strategy — EXC 2121 "Quantum Universe" — 390833306, and under project number 400140256-GRK2497; the Lendület ("Momentum") Program and the János Bolyai Research Scholarship of the Hungarian Academy of Sciences, the New National Excellence Program ÚNKP, the NKFIA research grants 123842, 123959, 124845, 124850, 125105, 128713, 128786, and 129058 (Hungary); the Council of Science and Industrial Research, India; the Latvian Council of Science; the Ministry of Science and Higher Education and the National Science Center, contracts Opus 2014/15/B/ST2/03998 and 2015/19/B/ST2/02861 (Poland); the Fundação para a Ciência e a Tecnologia, grant CEECIND/01334/2018 (Portugal); the National Priorities Research Program by Qatar National Research Fund; the Ministry of Science and Higher Education, projects no. 0723-2020-0041 and no. FSWW-2020-0008, and the Russian Foundation for Basic Research, project No. 19-42-703014 (Russia); MCIN/AEI/10.13039/501100011033, ERDF "a way of making Europe", and the Programa Estatal de Fomento de la Investigación Científica y Técnica de Excelencia María de Maeztu, grant MDM-2017-0765 and Programa Severo Ochoa del Principado de Asturias (Spain); the Stavros Niarchos Foundation (Greece); the Rachadapisek Sompot Fund for Postdoctoral Fellowship, Chulalongkorn University and the Chulalongkorn Academic into Its 2nd Century Project Advancement Project (Thailand); the Kavli Foundation; the Nvidia Corporation; the SuperMicro Corporation; the Welch Foundation, contract C-1845; and the Weston Havens Foundation (U.S.A.).

JHEP05(2022)014

Open Access. This article is distributed under the terms of the Creative Commons Attribution License (CC-BY 4.0), which permits any use, distribution and reproduction in any medium, provided the original author(s) and source are credited.

References

[1] ATLAS collaboration, *Observation of a new particle in the search for the Standard Model Higgs boson with the ATLAS detector at the LHC*, *Phys. Lett. B* **716** (2012) 1 [arXiv:1207.7214] [INSPIRE].

[2] CMS collaboration, *Observation of a new boson at a mass of* 125 *GeV with the CMS experiment at the LHC*, *Phys. Lett. B* **716** (2012) 30 [arXiv:1207.7235] [INSPIRE].

[3] CMS collaboration, *Observation of a new boson with mass near* 125 *GeV in pp collisions at* $\sqrt{s} = 7$ *and* 8 *TeV*, *JHEP* **06** (2013) 081 [arXiv:1303.4571] [INSPIRE].

[4] ATLAS and CMS collaborations, *Combined measurement of the Higgs boson mass in pp collisions at* $\sqrt{s} = 7$ *and* 8 *TeV with the ATLAS and CMS experiments*, *Phys. Rev. Lett.* **114** (2015) 191803 [arXiv:1503.07589] [INSPIRE].

[5] P. Ramond, *Dual theory for free fermions*, *Phys. Rev. D* **3** (1971) 2415 [INSPIRE].

[6] Y.A. Golfand and E.P. Likhtman, *Extension of the algebra of Poincaré group generators and violation of P invariance*, *JETP Lett.* **13** (1971) 323 [INSPIRE].

[7] A. Neveu and J.H. Schwarz, *Factorizable dual model of pions*, *Nucl. Phys. B* **31** (1971) 86 [INSPIRE].

[8] D.V. Volkov and V.P. Akulov, *Possible universal neutrino interaction*, *JETP Lett.* **16** (1972) 438 [INSPIRE].

[9] J. Wess and B. Zumino, *A Lagrangian model invariant under supergauge transformations*, *Phys. Lett. B* **49** (1974) 52 [INSPIRE].

[10] J. Wess and B. Zumino, *Supergauge transformations in four dimensions*, *Nucl. Phys. B* **70** (1974) 39 [INSPIRE].

[11] P. Fayet, *Supergauge invariant extension of the Higgs mechanism and a model for the electron and its neutrino*, *Nucl. Phys. B* **90** (1975) 104 [INSPIRE].

[12] P. Fayet and S. Ferrara, *Supersymmetry*, *Phys. Rept.* **32** (1977) 249 [INSPIRE].

[13] H.P. Nilles, *Supersymmetry, supergravity and particle physics*, *Phys. Rept.* **110** (1984) 1 [INSPIRE].

[14] S.P. Martin, *A supersymmetry primer*, *Adv. Ser. Direct. High Energy Phys.* **18** (1998) 1 [hep-ph/9709356] [INSPIRE].

[15] S. Dimopoulos and G.F. Giudice, *Naturalness constraints in supersymmetric theories with nonuniversal soft terms*, *Phys. Lett. B* **357** (1995) 573 [hep-ph/9507282] [INSPIRE].

[16] R. Barbieri and D. Pappadopulo, *S-particles at their naturalness limits*, *JHEP* **10** (2009) 061 [arXiv:0906.4546] [INSPIRE].

[17] M. Papucci, J.T. Ruderman and A. Weiler, *Natural SUSY endures*, *JHEP* **09** (2012) 035 [arXiv:1110.6926] [INSPIRE].

[18] LHC Higgs Cross Section Working Group collaboration, *Handbook of LHC Higgs cross sections: 4. Deciphering the nature of the Higgs sector*, CYRM-2017-002 [arXiv:1610.07922] [INSPIRE].

JHEP05(2022)014

[19] ATLAS collaboration, *Search for supersymmetry in events with photons, bottom quarks, and missing transverse momentum in proton-proton collisions at a centre-of-mass energy of* 7 *TeV with the ATLAS detector*, *Phys. Lett. B* **719** (2013) 261 [arXiv:1211.1167] [INSPIRE].

[20] ATLAS collaboration, *Search for direct pair production of a chargino and a neutralino decaying to the* 125 *GeV Higgs boson in* $\sqrt{s} = 8$ *TeV pp collisions with the ATLAS detector*, *Eur. Phys. J. C* **75** (2015) 208 [arXiv:1501.07110] [INSPIRE].

[21] ATLAS collaboration, *Search for supersymmetry in final states with two same-sign or three leptons and jets using* 36 fb^{-1} *of* $\sqrt{s} = 13$ *TeV pp collision data with the ATLAS detector*, *JHEP* **09** (2017) 084 [*Erratum ibid.* **08** (2019) 121] [arXiv:1706.03731] [INSPIRE].

[22] ATLAS collaboration, *Search for new phenomena with large jet multiplicities and missing transverse momentum using large-radius jets and flavour-tagging at ATLAS in* 13 *TeV pp collisions*, *JHEP* **12** (2017) 034 [arXiv:1708.02794] [INSPIRE].

[23] ATLAS collaboration, *Search for squarks and gluinos in events with an isolated lepton, jets, and missing transverse momentum at* $\sqrt{s} = 13$ *TeV with the ATLAS detector*, *Phys. Rev. D* **96** (2017) 112010 [arXiv:1708.08232] [INSPIRE].

[24] ATLAS collaboration, *Search for squarks and gluinos in final states with jets and missing transverse momentum using* 36 fb^{-1} *of* $\sqrt{s} = 13$ *TeV pp collision data with the ATLAS detector*, *Phys. Rev. D* **97** (2018) 112001 [arXiv:1712.02332] [INSPIRE].

[25] ATLAS collaboration, *Search for electroweak production of supersymmetric states in scenarios with compressed mass spectra at* $\sqrt{s} = 13$ *TeV with the ATLAS detector*, *Phys. Rev. D* **97** (2018) 052010 [arXiv:1712.08119] [INSPIRE].

[26] ATLAS collaboration, *Search for photonic signatures of gauge-mediated supersymmetry in* 13 *TeV pp collisions with the ATLAS detector*, *Phys. Rev. D* **97** (2018) 092006 [arXiv:1802.03158] [INSPIRE].

[27] ATLAS collaboration, *Search for electroweak production of supersymmetric particles in final states with two or three leptons at* $\sqrt{s} = 13$ *TeV with the ATLAS detector*, *Eur. Phys. J. C* **78** (2018) 995 [arXiv:1803.02762] [INSPIRE].

[28] ATLAS collaboration, *Search for chargino-neutralino production using recursive jigsaw reconstruction in final states with two or three charged leptons in proton-proton collisions at* $\sqrt{s} = 13$ *TeV with the ATLAS detector*, *Phys. Rev. D* **98** (2018) 092012 [arXiv:1806.02293] [INSPIRE].

[29] ATLAS collaboration, *Search for pair production of higgsinos in final states with at least three b-tagged jets in* $\sqrt{s} = 13$ *TeV pp collisions using the ATLAS detector*, *Phys. Rev. D* **98** (2018) 092002 [arXiv:1806.04030] [INSPIRE].

[30] ATLAS collaboration, *Search for chargino and neutralino production in final states with a Higgs boson and missing transverse momentum at* $\sqrt{s} = 13$ *TeV with the ATLAS detector*, *Phys. Rev. D* **100** (2019) 012006 [arXiv:1812.09432] [INSPIRE].

[31] ATLAS collaboration, *Search for electroweak production of charginos and sleptons decaying into final states with two leptons and missing transverse momentum in* $\sqrt{s} = 13$ *TeV pp collisions using the ATLAS detector*, *Eur. Phys. J. C* **80** (2020) 123 [arXiv:1908.08215] [INSPIRE].

[32] ATLAS collaboration, *Search for direct production of electroweakinos in final states with one lepton, missing transverse momentum and a Higgs boson decaying into two b-jets in pp collisions at* $\sqrt{s} = 13$ *TeV with the ATLAS detector*, *Eur. Phys. J. C* **80** (2020) 691 [arXiv:1909.09226] [INSPIRE].

JHEP05(2022)014

[33] ATLAS collaboration, *Searches for electroweak production of supersymmetric particles with compressed mass spectra in $\sqrt{s} = 13$ TeV pp collisions with the ATLAS detector*, Phys. Rev. D **101** (2020) 052005 [arXiv:1911.12606] [INSPIRE].

[34] ATLAS collaboration, *Search for chargino-neutralino production with mass splittings near the electroweak scale in three-lepton final states in $\sqrt{s} = 13$ TeV pp collisions with the ATLAS detector*, Phys. Rev. D **101** (2020) 072001 [arXiv:1912.08479] [INSPIRE].

[35] ATLAS collaboration, *Search for direct production of electroweakinos in final states with missing transverse momentum and a Higgs boson decaying into photons in pp collisions at $\sqrt{s} = 13$ TeV with the ATLAS detector*, JHEP **10** (2020) 005 [arXiv:2004.10894] [INSPIRE].

[36] ATLAS collaboration, *Search for supersymmetry in events with four or more charged leptons in 139 fb^{-1} of $\sqrt{s} = 13$ TeV pp collisions with the ATLAS detector*, JHEP **07** (2021) 167 [arXiv:2103.11684] [INSPIRE].

[37] ATLAS collaboration, *Search for charginos and neutralinos in final states with two boosted hadronically decaying bosons and missing transverse momentum in pp collisions at $\sqrt{s} = 13$ TeV with the ATLAS detector*, Phys. Rev. D **104** (2021) 112010 [arXiv:2108.07586] [INSPIRE].

[38] CMS collaboration, *Searches for electroweak production of charginos, neutralinos, and sleptons decaying to leptons and W, Z, and Higgs bosons in pp collisions at 8 TeV*, Eur. Phys. J. C **74** (2014) 3036 [arXiv:1405.7570] [INSPIRE].

[39] CMS collaboration, *Search for top squark and higgsino production using diphoton Higgs boson decays*, Phys. Rev. Lett. **112** (2014) 161802 [arXiv:1312.3310] [INSPIRE].

[40] CMS collaboration, *Searches for electroweak neutralino and chargino production in channels with Higgs, Z, and W bosons in pp collisions at 8 TeV*, Phys. Rev. D **90** (2014) 092007 [arXiv:1409.3168] [INSPIRE].

[41] CMS collaboration, *Search for physics beyond the standard model in events with two leptons of same sign, missing transverse momentum, and jets in proton-proton collisions at $\sqrt{s} = 13$ TeV*, Eur. Phys. J. C **77** (2017) 578 [arXiv:1704.07323] [INSPIRE].

[42] CMS collaboration, *Search for electroweak production of charginos and neutralinos in WH events in proton-proton collisions at $\sqrt{s} = 13$ TeV*, JHEP **11** (2017) 029 [arXiv:1706.09933] [INSPIRE].

[43] CMS collaboration, *Search for supersymmetry in events with at least one photon, missing transverse momentum, and large transverse event activity in proton-proton collisions at $\sqrt{s} = 13$ TeV*, JHEP **12** (2017) 142 [arXiv:1707.06193] [INSPIRE].

[44] CMS collaboration, *Search for supersymmetry with Higgs boson to diphoton decays using the razor variables at $\sqrt{s} = 13$ TeV*, Phys. Lett. B **779** (2018) 166 [arXiv:1709.00384] [INSPIRE].

[45] CMS collaboration, *Search for Higgsino pair production in pp collisions at $\sqrt{s} = 13$ TeV in final states with large missing transverse momentum and two Higgs bosons decaying via $H \to b\bar{b}$*, Phys. Rev. D **97** (2018) 032007 [arXiv:1709.04896] [INSPIRE].

[46] CMS collaboration, *Combined search for electroweak production of charginos and neutralinos in proton-proton collisions at $\sqrt{s} = 13$ TeV*, JHEP **03** (2018) 160 [arXiv:1801.03957] [INSPIRE].

[47] CMS collaboration, *Search for new phenomena in final states with two opposite-charge, same-flavor leptons, jets, and missing transverse momentum in pp collisions at $\sqrt{s} = 13$ TeV*, JHEP **03** (2018) 076 [arXiv:1709.08908] [INSPIRE].

JHEP05(2022)014

[48] CMS collaboration, *Search for supersymmetry in events with one lepton and multiple jets exploiting the angular correlation between the lepton and the missing transverse momentum in proton-proton collisions at* $\sqrt{s} = 13$ *TeV*, *Phys. Lett. B* **780** (2018) 384 [arXiv:1709.09814] [INSPIRE].

[49] CMS collaboration, *Search for supersymmetry in events with at least three electrons or muons, jets, and missing transverse momentum in proton-proton collisions at* $\sqrt{s} = 13$ *TeV*, *JHEP* **02** (2018) 067 [arXiv:1710.09154] [INSPIRE].

[50] CMS collaboration, *Search for gauge-mediated supersymmetry in events with at least one photon and missing transverse momentum in pp collisions at* $\sqrt{s} = 13$ *TeV*, *Phys. Lett. B* **780** (2018) 118 [arXiv:1711.08008] [INSPIRE].

[51] CMS collaboration, *Search for physics beyond the standard model in events with high-momentum Higgs bosons and missing transverse momentum in proton-proton collisions at* 13 *TeV*, *Phys. Rev. Lett.* **120** (2018) 241801 [arXiv:1712.08501] [INSPIRE].

[52] CMS collaboration, *Search for new physics in events with two soft oppositely charged leptons and missing transverse momentum in proton-proton collisions at* $\sqrt{s} = 13$ *TeV*, *Phys. Lett. B* **782** (2018) 440 [arXiv:1801.01846] [INSPIRE].

[53] CMS collaboration, *Searches for pair production of charginos and top squarks in final states with two oppositely charged leptons in proton-proton collisions at* $\sqrt{s} = 13$ *TeV*, *JHEP* **11** (2018) 079 [arXiv:1807.07799] [INSPIRE].

[54] CMS collaboration, *Search for supersymmetry in events with a photon, a lepton, and missing transverse momentum in proton-proton collisions at* $\sqrt{s} = 13$ *TeV*, *JHEP* **01** (2019) 154 [arXiv:1812.04066] [INSPIRE].

[55] CMS collaboration, *Search for supersymmetry in events with a photon, jets, b-jets, and missing transverse momentum in proton-proton collisions at* 13 *TeV*, *Eur. Phys. J. C* **79** (2019) 444 [arXiv:1901.06726] [INSPIRE].

[56] CMS collaboration, *Search for supersymmetry in final states with photons and missing transverse momentum in proton-proton collisions at* 13 *TeV*, *JHEP* **06** (2019) 143 [arXiv:1903.07070] [INSPIRE].

[57] CMS collaboration, *Combined search for supersymmetry with photons in proton-proton collisions at* $\sqrt{s} = 13$ *TeV*, *Phys. Lett. B* **801** (2020) 135183 [arXiv:1907.00857] [INSPIRE].

[58] CMS collaboration, *Search for supersymmetry using Higgs boson to diphoton decays at* $\sqrt{s} = 13$ *TeV*, *JHEP* **11** (2019) 109 [arXiv:1908.08500] [INSPIRE].

[59] CMS collaboration, *Searches for physics beyond the standard model with the* M_{T2} *variable in hadronic final states with and without disappearing tracks in proton-proton collisions at* $\sqrt{s} = 13$ *TeV*, *Eur. Phys. J. C* **80** (2020) 3 [arXiv:1909.03460] [INSPIRE].

[60] CMS collaboration, *Search for physics beyond the standard model in events with jets and two same-sign or at least three charged leptons in proton-proton collisions at* $\sqrt{s} = 13$ *TeV*, *Eur. Phys. J. C* **80** (2020) 752 [arXiv:2001.10086] [INSPIRE].

[61] CMS collaboration, *Search for supersymmetry in proton-proton collisions at* $\sqrt{s} = 13$ *TeV in events with high-momentum Z bosons and missing transverse momentum*, *JHEP* **09** (2020) 149 [arXiv:2008.04422] [INSPIRE].

[62] CMS collaboration, *Search for supersymmetry in final states with two oppositely charged same-flavor leptons and missing transverse momentum in proton-proton collisions at* $\sqrt{s} = 13$ *TeV*, *JHEP* **04** (2021) 123 [arXiv:2012.08600] [INSPIRE].

JHEP05(2022)014

[63] CMS collaboration, *Search for electroweak production of charginos and neutralinos in proton-proton collisions at* $\sqrt{s} = 13$ *TeV*, *JHEP* **04** (2022) 147 [arXiv:2106.14246] [INSPIRE].

[64] CMS collaboration, *Search for chargino-neutralino production in events with Higgs and W bosons using* $137\,fb^{-1}$ *of proton-proton collisions at* $\sqrt{s} = 13$ *TeV*, *JHEP* **10** (2021) 045 [arXiv:2107.12553] [INSPIRE].

[65] CMS collaboration, *Search for higgsinos decaying to two Higgs bosons and missing transverse momentum in proton-proton collisions at* $\sqrt{s} = 13$ *TeV*, 10.17182/hepdata.114414 (2021).

[66] Particle Data Group collaboration, *Review of particle physics*, *PTEP* **2020** (2020) 083C01 [INSPIRE].

[67] G.R. Farrar and P. Fayet, *Phenomenology of the production, decay, and detection of new hadronic states associated with supersymmetry*, *Phys. Lett. B* **76** (1978) 575 [INSPIRE].

[68] N. Arkani-Hamed et al., *MARMOSET: The path from LHC data to the new standard model via on-shell effective theories*, hep-ph/0703088 [INSPIRE].

[69] J. Alwall, P. Schuster and N. Toro, *Simplified models for a first characterization of new physics at the LHC*, *Phys. Rev. D* **79** (2009) 075020 [arXiv:0810.3921] [INSPIRE].

[70] J. Alwall, M.-P. Le, M. Lisanti and J.G. Wacker, *Model-independent jets plus missing energy searches*, *Phys. Rev. D* **79** (2009) 015005 [arXiv:0809.3264] [INSPIRE].

[71] LHC New Physics Working Group collaboration, *Simplified models for LHC new physics searches*, *J. Phys. G* **39** (2012) 105005 [arXiv:1105.2838] [INSPIRE].

[72] S. Dimopoulos, M. Dine, S. Raby and S.D. Thomas, *Experimental signatures of low-energy gauge mediated supersymmetry breaking*, *Phys. Rev. Lett.* **76** (1996) 3494 [hep-ph/9601367] [INSPIRE].

[73] K.T. Matchev and S.D. Thomas, *Higgs and Z boson signatures of supersymmetry*, *Phys. Rev. D* **62** (2000) 077702 [hep-ph/9908482] [INSPIRE].

[74] J.T. Ruderman and D. Shih, *General neutralino NLSPs at the early LHC*, *JHEP* **08** (2012) 159 [arXiv:1103.6083] [INSPIRE].

[75] B. Fuks, M. Klasen, D.R. Lamprea and M. Rothering, *Gaugino production in proton-proton collisions at a center-of-mass energy of* 8 *TeV*, *JHEP* **10** (2012) 081 [arXiv:1207.2159] [INSPIRE].

[76] B. Fuks, M. Klasen, D.R. Lamprea and M. Rothering, *Precision predictions for electroweak superpartner production at hadron colliders with* resummino, *Eur. Phys. J. C* **73** (2013) 2480 [arXiv:1304.0790] [INSPIRE].

[77] H. Baer, V. Barger, P. Huang, D. Mickelson, M. Padeffke-Kirkland and X. Tata, *Natural SUSY with a bino- or wino-like LSP*, *Phys. Rev. D* **91** (2015) 075005 [arXiv:1501.06357] [INSPIRE].

[78] Z. Kang, P. Ko and J. Li, *New physics opportunities in the boosted di-Higgs-boson plus missing transverse energy signature*, *Phys. Rev. Lett.* **116** (2016) 131801 [arXiv:1504.04128] [INSPIRE].

[79] G.D. Kribs, A. Martin, T.S. Roy and M. Spannowsky, *Discovering Higgs bosons of the MSSM using jet substructure*, *Phys. Rev. D* **82** (2010) 095012 [arXiv:1006.1656] [INSPIRE].

[80] S. Gori, P. Schwaller and C.E.M. Wagner, *Search for Higgs bosons in SUSY cascade decays and neutralino dark matter*, *Phys. Rev. D* **83** (2011) 115022 [arXiv:1103.4138] [INSPIRE].

JHEP05(2022)014

[81] E. Arganda, A. Delgado, R.A. Morales and M. Quirós, *Novel Higgsino dark matter signal interpretation at the LHC*, *Phys. Rev. D* **104** (2021) 055003 [arXiv:2104.13827] [INSPIRE].

[82] A. Delgado and M. Quirós, *Higgsino Dark Matter in the MSSM*, *Phys. Rev. D* **103** (2021) 015024 [arXiv:2008.00954] [INSPIRE].

[83] CMS collaboration, *The CMS experiment at the CERN LHC*, 2008 *JINST* **3** S08004 [INSPIRE].

[84] CMS collaboration, *Performance of the CMS Level-1 trigger in proton-proton collisions at* $\sqrt{s} = 13$ *TeV*, 2020 *JINST* **15** P10017 [arXiv:2006.10165] [INSPIRE].

[85] CMS collaboration, *The CMS trigger system*, 2017 *JINST* **12** P01020 [arXiv:1609.02366] [INSPIRE].

[86] CMS collaboration, *Pileup mitigation at CMS in* 13 *TeV data*, 2020 *JINST* **15** P09018 [arXiv:2003.00503] [INSPIRE].

[87] J. Alwall et al., *The automated computation of tree-level and next-to-leading order differential cross sections, and their matching to parton shower simulations*, *JHEP* **07** (2014) 079 [arXiv:1405.0301] [INSPIRE].

[88] J. Alwall et al., *Comparative study of various algorithms for the merging of parton showers and matrix elements in hadronic collisions*, *Eur. Phys. J. C* **53** (2008) 473 [arXiv:0706.2569] [INSPIRE].

[89] R. Frederix and S. Frixione, *Merging meets matching in MC@NLO*, *JHEP* **12** (2012) 061 [arXiv:1209.6215] [INSPIRE].

[90] P. Nason, *A new method for combining NLO QCD with shower Monte Carlo algorithms*, *JHEP* **11** (2004) 040 [hep-ph/0409146] [INSPIRE].

[91] S. Frixione, P. Nason and C. Oleari, *Matching NLO QCD computations with parton shower simulations: the POWHEG method*, *JHEP* **11** (2007) 070 [arXiv:0709.2092] [INSPIRE].

[92] S. Alioli, P. Nason, C. Oleari and E. Re, *A general framework for implementing NLO calculations in shower Monte Carlo programs: the POWHEG BOX*, *JHEP* **06** (2010) 043 [arXiv:1002.2581] [INSPIRE].

[93] S. Alioli, P. Nason, C. Oleari and E. Re, *NLO single-top production matched with shower in POWHEG: s- and t-channel contributions*, *JHEP* **09** (2009) 111 [*Erratum ibid.* **02** (2010) 011] [arXiv:0907.4076] [INSPIRE].

[94] E. Re, *Single-top Wt-channel production matched with parton showers using the POWHEG method*, *Eur. Phys. J. C* **71** (2011) 1547 [arXiv:1009.2450] [INSPIRE].

[95] W. Beenakker, R. Hopker, M. Spira and P.M. Zerwas, *Squark and gluino production at hadron colliders*, *Nucl. Phys. B* **492** (1997) 51 [hep-ph/9610490] [INSPIRE].

[96] A. Kulesza and L. Motyka, *Threshold resummation for squark-antisquark and gluino-pair production at the LHC*, *Phys. Rev. Lett.* **102** (2009) 111802 [arXiv:0807.2405] [INSPIRE].

[97] A. Kulesza and L. Motyka, *Soft gluon resummation for the production of gluino-gluino and squark-antisquark pairs at the LHC*, *Phys. Rev. D* **80** (2009) 095004 [arXiv:0905.4749] [INSPIRE].

[98] W. Beenakker, S. Brensing, M. Krämer, A. Kulesza, E. Laenen and I. Niessen, *Soft-gluon resummation for squark and gluino hadroproduction*, *JHEP* **12** (2009) 041 [arXiv:0909.4418] [INSPIRE].

[99] W. Beenakker et al., *Squark and gluino hadroproduction*, *Int. J. Mod. Phys. A* **26** (2011) 2637 [arXiv:1105.1110] [INSPIRE].

JHEP05(2022)014

[100] W. Beenakker, C. Borschensky, M. Krämer, A. Kulesza and E. Laenen, *NNLL-fast: predictions for coloured supersymmetric particle production at the LHC with threshold and Coulomb resummation*, *JHEP* **12** (2016) 133 [arXiv:1607.07741] [INSPIRE].

[101] W. Beenakker, S. Brensing, M. Krämer, A. Kulesza, E. Laenen and I. Niessen, *NNLL resummation for squark-antisquark pair production at the LHC*, *JHEP* **01** (2012) 076 [arXiv:1110.2446] [INSPIRE].

[102] W. Beenakker et al., *Towards NNLL resummation: hard matching coefficients for squark and gluino hadroproduction*, *JHEP* **10** (2013) 120 [arXiv:1304.6354] [INSPIRE].

[103] W. Beenakker et al., *NNLL resummation for squark and gluino production at the LHC*, *JHEP* **12** (2014) 023 [arXiv:1404.3134] [INSPIRE].

[104] W. Beenakker, M. Krämer, T. Plehn, M. Spira and P.M. Zerwas, *Stop production at hadron colliders*, *Nucl. Phys. B* **515** (1998) 3 [hep-ph/9710451] [INSPIRE].

[105] W. Beenakker, S. Brensing, M. Krämer, A. Kulesza, E. Laenen and I. Niessen, *Supersymmetric top and bottom squark production at hadron colliders*, *JHEP* **08** (2010) 098 [arXiv:1006.4771] [INSPIRE].

[106] W. Beenakker, C. Borschensky, R. Heger, M. Krämer, A. Kulesza and E. Laenen, *NNLL resummation for stop pair-production at the LHC*, *JHEP* **05** (2016) 153 [arXiv:1601.02954] [INSPIRE].

[107] CMS collaboration, *The fast simulation of the CMS detector at LHC*, *J. Phys. Conf. Ser.* **331** (2011) 032049 [INSPIRE].

[108] T. Sjöstrand et al., *An introduction to PYTHIA 8.2*, *Comput. Phys. Commun.* **191** (2015) 159 [arXiv:1410.3012] [INSPIRE].

[109] CMS collaboration, *Event generator tunes obtained from underlying event and multiparton scattering measurements*, *Eur. Phys. J. C* **76** (2016) 155 [arXiv:1512.00815] [INSPIRE].

[110] CMS collaboration, *Extraction and validation of a new set of CMS PYTHIA8 tunes from underlying-event measurements*, *Eur. Phys. J. C* **80** (2020) 4 [arXiv:1903.12179] [INSPIRE].

[111] NNPDF collaboration, *Parton distributions with QED corrections*, *Nucl. Phys. B* **877** (2013) 290 [arXiv:1308.0598] [INSPIRE].

[112] NNPDF collaboration, *Parton distributions from high-precision collider data*, *Eur. Phys. J. C* **77** (2017) 663 [arXiv:1706.00428] [INSPIRE].

[113] GEANT4 collaboration, GEANT4 — *a simulation toolkit*, *Nucl. Instrum. Meth. A* **506** (2003) 250 [INSPIRE].

[114] T. Melia, P. Nason, R. Rontsch and G. Zanderighi, *W^+W^-, WZ and ZZ production in the POWHEG BOX*, *JHEP* **11** (2011) 078 [arXiv:1107.5051] [INSPIRE].

[115] M. Beneke, P. Falgari, S. Klein and C. Schwinn, *Hadronic top-quark pair production with NNLL threshold resummation*, *Nucl. Phys. B* **855** (2012) 695 [arXiv:1109.1536] [INSPIRE].

[116] M. Cacciari, M. Czakon, M. Mangano, A. Mitov and P. Nason, *Top-pair production at hadron colliders with next-to-next-to-leading logarithmic soft-gluon resummation*, *Phys. Lett. B* **710** (2012) 612 [arXiv:1111.5869] [INSPIRE].

[117] P. Bärnreuther, M. Czakon and A. Mitov, *Percent level precision physics at the Tevatron: first genuine NNLO QCD corrections to $q\bar{q} \to t\bar{t} + X$*, *Phys. Rev. Lett.* **109** (2012) 132001 [arXiv:1204.5201] [INSPIRE].

[118] M. Czakon and A. Mitov, *NNLO corrections to top-pair production at hadron colliders: the all-fermionic scattering channels*, *JHEP* **12** (2012) 054 [arXiv:1207.0236] [INSPIRE].

JHEP05(2022)014

[119] M. Czakon and A. Mitov, *NNLO corrections to top pair production at hadron colliders: the quark-gluon reaction*, *JHEP* **01** (2013) 080 [arXiv:1210.6832] [INSPIRE].

[120] M. Czakon, P. Fiedler and A. Mitov, *Total top-quark pair-production cross section at hadron colliders through* $O(\alpha_S^4)$, *Phys. Rev. Lett.* **110** (2013) 252004 [arXiv:1303.6254] [INSPIRE].

[121] R. Gavin, Y. Li, F. Petriello and S. Quackenbush, *W physics at the LHC with FEWZ 2.1*, *Comput. Phys. Commun.* **184** (2013) 208 [arXiv:1201.5896] [INSPIRE].

[122] R. Gavin, Y. Li, F. Petriello and S. Quackenbush, *FEWZ 2.0: A code for hadronic Z production at next-to-next-to-leading order*, *Comput. Phys. Commun.* **182** (2011) 2388 [arXiv:1011.3540] [INSPIRE].

[123] A. Giammanco, *The fast simulation of the CMS experiment*, *J. Phys. Conf. Ser.* **513** (2014) 022012 [INSPIRE].

[124] CMS collaboration, *Particle-flow reconstruction and global event description with the CMS detector*, 2017 *JINST* **12** P10003 [arXiv:1706.04965] [INSPIRE].

[125] D. Contardo, M. Klute, J. Mans, L. Silvestris and J. Butler, *Technical Proposal for the Phase-II Upgrade of the CMS Detector*, CERN-LHCC-2015-010, LHCC-P-008, CMS-TDR-15-02 (2015).

[126] M. Cacciari, G.P. Salam and G. Soyez, *The anti-*k_t *jet clustering algorithm*, *JHEP* **04** (2008) 063 [arXiv:0802.1189] [INSPIRE].

[127] M. Cacciari, G.P. Salam and G. Soyez, *FastJet user manual*, *Eur. Phys. J. C* **72** (2012) 1896 [arXiv:1111.6097] [INSPIRE].

[128] CMS collaboration, *Jet performance in pp collisions at* $\sqrt{s} = 7$ *TeV*,, CMS-PAS-JME-10-003 (2010).

[129] CMS collaboration, *Jet algorithms performance in* 13 *TeV data*, CMS-PAS-JME-16-003 (2017).

[130] CMS collaboration, *Jet energy scale and resolution in the CMS experiment in pp collisions at* 8 *TeV*, 2017 *JINST* **12** P02014 [arXiv:1607.03663] [INSPIRE].

[131] M. Cacciari and G.P. Salam, *Pileup subtraction using jet areas*, *Phys. Lett. B* **659** (2008) 119 [arXiv:0707.1378] [INSPIRE].

[132] D. Bertolini, P. Harris, M. Low and N. Tran, *Pileup per particle identification*, *JHEP* **10** (2014) 059 [arXiv:1407.6013] [INSPIRE].

[133] CMS collaboration, *Search for top-squark pair production in the single-lepton final state in pp collisions at* $\sqrt{s} = 8$ *TeV*, *Eur. Phys. J. C* **73** (2013) 2677 [arXiv:1308.1586] [INSPIRE].

[134] CMS collaboration, *Identification of heavy-flavour jets with the CMS detector in pp collisions at* 13 *TeV*, 2018 *JINST* **13** P05011 [arXiv:1712.07158] [INSPIRE].

[135] CMS collaboration, *Performance of deep tagging algorithms for boosted double quark jet topology in proton-proton collisions at* 13 *TeV with the Phase-0 CMS detector*, CMS-DP-2018-046 (2018).

[136] CMS collaboration, *Performance of missing transverse momentum reconstruction in proton-proton collisions at* $\sqrt{s} = 13$ *TeV using the CMS detector*, 2019 *JINST* **14** P07004 [arXiv:1903.06078] [INSPIRE].

[137] CMS collaboration, *Electron and photon reconstruction and identification with the CMS experiment at the CERN LHC*, 2021 *JINST* **16** P05014 [arXiv:2012.06888] [INSPIRE].

JHEP05(2022)014

[138] CMS collaboration, *Performance of the CMS muon detector and muon reconstruction with proton-proton collisions at* $\sqrt{s} = 13$ *TeV*, 2018 *JINST* **13** P06015 [arXiv:1804.04528] [INSPIRE].

[139] K. Rehermann and B. Tweedie, *Efficient identification of boosted semileptonic top quarks at the LHC*, *JHEP* **03** (2011) 059 [arXiv:1007.2221] [INSPIRE].

[140] A.J. Larkoski, S. Marzani, G. Soyez and J. Thaler, *Soft drop*, *JHEP* **05** (2014) 146 [arXiv:1402.2657] [INSPIRE].

[141] M. Dasgupta, A. Fregoso, S. Marzani and G.P. Salam, *Towards an understanding of jet substructure*, *JHEP* **09** (2013) 029 [arXiv:1307.0007] [INSPIRE].

[142] A. Kalogeropoulos and J. Alwall, *The SysCalc code: A tool to derive theoretical systematic uncertainties*, arXiv:1801.08401 [INSPIRE].

[143] S. Catani, D. de Florian, M. Grazzini and P. Nason, *Soft gluon resummation for Higgs boson production at hadron colliders*, *JHEP* **07** (2003) 028 [hep-ph/0306211] [INSPIRE].

[144] M. Cacciari, S. Frixione, M.L. Mangano, P. Nason and G. Ridolfi, *The* $t\bar{t}$ *cross-section at* 1.8 *TeV and* 1.96 *TeV: a study of the systematics due to parton densities and scale dependence*, *JHEP* **04** (2004) 068 [hep-ph/0303085] [INSPIRE].

[145] CMS collaboration, *Measurement of the inelastic proton-proton cross section at* $\sqrt{s} = 13$ *TeV*, *JHEP* **07** (2018) 161 [arXiv:1802.02613] [INSPIRE].

[146] CMS collaboration, *Precision luminosity measurement in proton-proton collisions at* $\sqrt{s} = 13$ *TeV in 2015 and 2016 at CMS*, *Eur. Phys. J. C* **81** (2021) 800 [arXiv:2104.01927] [INSPIRE].

[147] CMS collaboration, *CMS luminosity measurement for the 2017 data-taking period at* $\sqrt{s} = 13$ *TeV*, CMS-PAS-LUM-17-004 (2018).

[148] CMS collaboration, *CMS luminosity measurement for the 2018 data-taking period at* $\sqrt{s} = 13$ *TeV*, CMS-PAS-LUM-18-002 (2019).

[149] G. Cowan, K. Cranmer, E. Gross and O. Vitells, *Asymptotic formulae for likelihood-based tests of new physics*, *Eur. Phys. J. C* **71** (2011) 1554 [*Erratum ibid.* **73** (2013) 2501] [arXiv:1007.1727] [INSPIRE].

[150] T. Junk, *Confidence level computation for combining searches with small statistics*, *Nucl. Instrum. Meth. A* **434** (1999) 435 [hep-ex/9902006] [INSPIRE].

[151] A.L. Read, *Presentation of search results: the* CL_s *technique*, *J. Phys. G* **28** (2002) 2693 [INSPIRE].

[152] G. Cowan, *Statistics for searches at the LHC*, in *LHC Phenomenology*, E. Gardi, N. Glover and R. Aidan eds., Scottish Graduate Series, Springer, Cham (2015) [DOI] [arXiv:1307.2487] [INSPIRE].

JHEP05(2022)014

The CMS collaboration

Yerevan Physics Institute, Yerevan, Armenia

A. Tumasyan

Institut für Hochenergiephysik, Vienna, Austria

W. Adam, J.W. Andrejkovic, T. Bergauer, S. Chatterjee, K. Damanakis, M. Dragicevic, A. Escalante Del Valle, R. Frühwirth[1], M. Jeitler[1], N. Krammer, L. Lechner, D. Liko, I. Mikulec, P. Paulitsch, F.M. Pitters, J. Schieck[1], R. Schöfbeck, D. Schwarz, S. Templ, W. Waltenberger, C.-E. Wulz[1]

Institute for Nuclear Problems, Minsk, Belarus

V. Chekhovsky, A. Litomin, V. Makarenko

Universiteit Antwerpen, Antwerpen, Belgium

M.R. Darwish[2], E.A. De Wolf, T. Janssen, T. Kello[3], A. Lelek, H. Rejeb Sfar, P. Van Mechelen, S. Van Putte, N. Van Remortel

Vrije Universiteit Brussel, Brussel, Belgium

F. Blekman, E.S. Bols, J. D'Hondt, M. Delcourt, H. El Faham, S. Lowette, S. Moortgat, A. Morton, D. Müller, A.R. Sahasransu, S. Tavernier, W. Van Doninck

Université Libre de Bruxelles, Bruxelles, Belgium

D. Beghin, B. Bilin, B. Clerbaux, G. De Lentdecker, L. Favart, A.K. Kalsi, K. Lee, M. Mahdavikhorrami, I. Makarenko, L. Moureaux, L. Pétré, A. Popov, N. Postiau, E. Starling, L. Thomas, M. Vanden Bemden, C. Vander Velde, P. Vanlaer

Ghent University, Ghent, Belgium

T. Cornelis, D. Dobur, J. Knolle, L. Lambrecht, G. Mestdach, M. Niedziela, C. Roskas, A. Samalan, K. Skovpen, M. Tytgat, B. Vermassen, L. Wezenbeek

Université Catholique de Louvain, Louvain-la-Neuve, Belgium

A. Benecke, A. Bethani, G. Bruno, F. Bury, C. Caputo, P. David, C. Delaere, I.S. Donertas, A. Giammanco, K. Jaffel, Sa. Jain, V. Lemaitre, K. Mondal, J. Prisciandaro, A. Taliercio, M. Teklishyn, T.T. Tran, P. Vischia, S. Wertz

Centro Brasileiro de Pesquisas Fisicas, Rio de Janeiro, Brazil

G.A. Alves, C. Hensel, A. Moraes, P. Rebello Teles

Universidade do Estado do Rio de Janeiro, Rio de Janeiro, Brazil

W.L. Aldá Júnior, M. Alves Gallo Pereira, M. Barroso Ferreira Filho, H. Brandao Malbouisson, W. Carvalho, J. Chinellato[4], E.M. Da Costa, G.G. Da Silveira[5], D. De Jesus Damiao, V. Dos Santos Sousa, S. Fonseca De Souza, C. Mora Herrera, K. Mota Amarilo, L. Mundim, H. Nogima, A. Santoro, S.M. Silva Do Amaral, A. Sznajder, M. Thiel, F. Torres Da Silva De Araujo[6], A. Vilela Pereira

JHEP05(2022)014

Universidade Estadual Paulista (a), Universidade Federal do ABC (b), São Paulo, Brazil

C.A. Bernardes[5], L. Calligaris, T.R. Fernandez Perez Tomei, E.M. Gregores, D.S. Lemos, P.G. Mercadante, S.F. Novaes, Sandra S. Padula

Institute for Nuclear Research and Nuclear Energy, Bulgarian Academy of Sciences, Sofia, Bulgaria

A. Aleksandrov, G. Antchev, R. Hadjiiska, P. Iaydjiev, M. Misheva, M. Rodozov, M. Shopova, G. Sultanov

University of Sofia, Sofia, Bulgaria

A. Dimitrov, T. Ivanov, L. Litov, B. Pavlov, P. Petkov, A. Petrov

Beihang University, Beijing, China

T. Cheng, T. Javaid[7], M. Mittal, L. Yuan

Department of Physics, Tsinghua University, Beijing, China

M. Ahmad, G. Bauer, C. Dozen[8], Z. Hu, J. Martins[9], Y. Wang, K. Yi[10,11]

Institute of High Energy Physics, Beijing, China

E. Chapon, G.M. Chen[7], H.S. Chen[7], M. Chen, F. Iemmi, A. Kapoor, D. Leggat, H. Liao, Z.-A. Liu[7], V. Milosevic, F. Monti, R. Sharma, J. Tao, J. Thomas-Wilsker, J. Wang, H. Zhang, J. Zhao

State Key Laboratory of Nuclear Physics and Technology, Peking University, Beijing, China

A. Agapitos, Y. An, Y. Ban, C. Chen, A. Levin, Q. Li, X. Lyu, Y. Mao, S.J. Qian, D. Wang, J. Xiao

Sun Yat-Sen University, Guangzhou, China

M. Lu, Z. You

Institute of Modern Physics and Key Laboratory of Nuclear Physics and Ion-beam Application (MOE) — Fudan University, Shanghai, China

X. Gao[3], H. Okawa, Y. Zhang

Zhejiang University, Hangzhou, China, Zhejiang, China

Z. Lin, M. Xiao

Universidad de Los Andes, Bogota, Colombia

C. Avila, A. Cabrera, C. Florez, J. Fraga

Universidad de Antioquia, Medellin, Colombia

J. Mejia Guisao, F. Ramirez, J.D. Ruiz Alvarez, C.A. Salazar González

University of Split, Faculty of Electrical Engineering, Mechanical Engineering and Naval Architecture, Split, Croatia

D. Giljanovic, N. Godinovic, D. Lelas, I. Puljak

JHEP05(2022)014

University of Split, Faculty of Science, Split, Croatia

Z. Antunovic, M. Kovac, T. Sculac

Institute Rudjer Boskovic, Zagreb, Croatia

V. Brigljevic, D. Ferencek, D. Majumder, M. Roguljic, A. Starodumov[12], T. Susa

University of Cyprus, Nicosia, Cyprus

A. Attikis, K. Christoforou, A. Ioannou, G. Kole, M. Kolosova, S. Konstantinou, J. Mousa, C. Nicolaou, F. Ptochos, P.A. Razis, H. Rykaczewski, H. Saka

Charles University, Prague, Czech Republic

M. Finger[13], M. Finger Jr.[13], A. Kveton

Escuela Politecnica Nacional, Quito, Ecuador

E. Ayala

Universidad San Francisco de Quito, Quito, Ecuador

E. Carrera Jarrin

Academy of Scientific Research and Technology of the Arab Republic of Egypt, Egyptian Network of High Energy Physics, Cairo, Egypt

S. Elgammal[14], S. Khalil[15]

Center for High Energy Physics (CHEP-FU), Fayoum University, El-Fayoum, Egypt

M.A. Mahmoud, Y. Mohammed

National Institute of Chemical Physics and Biophysics, Tallinn, Estonia

S. Bhowmik, R.K. Dewanjee, K. Ehataht, M. Kadastik, S. Nandan, C. Nielsen, J. Pata, M. Raidal, L. Tani, C. Veelken

Department of Physics, University of Helsinki, Helsinki, Finland

P. Eerola, L. Forthomme, H. Kirschenmann, K. Osterberg, M. Voutilainen

Helsinki Institute of Physics, Helsinki, Finland

S. Bharthuar, E. Brücken, F. Garcia, J. Havukainen, M.S. Kim, R. Kinnunen, T. Lampén, K. Lassila-Perini, S. Lehti, T. Lindén, M. Lotti, L. Martikainen, M. Myllymäki, J. Ott, H. Siikonen, E. Tuominen, J. Tuominiemi

Lappeenranta University of Technology, Lappeenranta, Finland

P. Luukka, H. Petrow, T. Tuuva

IRFU, CEA, Université Paris-Saclay, Gif-sur-Yvette, France

C. Amendola, M. Besancon, F. Couderc, M. Dejardin, D. Denegri, J.L. Faure, F. Ferri, S. Ganjour, P. Gras, G. Hamel de Monchenault, P. Jarry, B. Lenzi, E. Locci, J. Malcles, J. Rander, A. Rosowsky, M.Ö. Sahin, A. Savoy-Navarro[16], M. Titov, G.B. Yu

JHEP05(2022)014

Laboratoire Leprince-Ringuet, CNRS/IN2P3, Ecole Polytechnique, Institut Polytechnique de Paris, Palaiseau, France
S. Ahuja, F. Beaudette, M. Bonanomi, A. Buchot Perraguin, P. Busson, A. Cappati, C. Charlot, O. Davignon, B. Diab, G. Falmagne, S. Ghosh, R. Granier de Cassagnac, A. Hakimi, I. Kucher, J. Motta, M. Nguyen, C. Ochando, P. Paganini, J. Rembser, R. Salerno, U. Sarkar, J.B. Sauvan, Y. Sirois, A. Tarabini, A. Zabi, A. Zghiche

Université de Strasbourg, CNRS, IPHC UMR 7178, Strasbourg, France
J.-L. Agram[17], J. Andrea, D. Apparu, D. Bloch, G. Bourgatte, J.-M. Brom, E.C. Chabert, C. Collard, D. Darej, J.-C. Fontaine[17], U. Goerlach, C. Grimault, A.-C. Le Bihan, E. Nibigira, P. Van Hove

Institut de Physique des 2 Infinis de Lyon (IP2I), Villeurbanne, France
E. Asilar, S. Beauceron, C. Bernet, G. Boudoul, C. Camen, A. Carle, N. Chanon, D. Contardo, P. Depasse, H. El Mamouni, J. Fay, S. Gascon, M. Gouzevitch, B. Ille, I.B. Laktineh, H. Lattaud, A. Lesauvage, M. Lethuillier, L. Mirabito, S. Perries, K. Shchablo, V. Sordini, L. Torterotot, G. Touquet, M. Vander Donckt, S. Viret

Georgian Technical University, Tbilisi, Georgia
I. Lomidze, T. Toriashvili[18], Z. Tsamalaidze[13]

RWTH Aachen University, I. Physikalisches Institut, Aachen, Germany
V. Botta, L. Feld, K. Klein, M. Lipinski, D. Meuser, A. Pauls, N. Röwert, J. Schulz, M. Teroerde

RWTH Aachen University, III. Physikalisches Institut A, Aachen, Germany
A. Dodonova, D. Eliseev, M. Erdmann, P. Fackeldey, B. Fischer, S. Ghosh, T. Hebbeker, K. Hoepfner, F. Ivone, L. Mastrolorenzo, M. Merschmeyer, A. Meyer, G. Mocellin, S. Mondal, S. Mukherjee, D. Noll, A. Novak, T. Pook, A. Pozdnyakov, Y. Rath, H. Reithler, J. Roemer, A. Schmidt, S.C. Schuler, A. Sharma, L. Vigilante, S. Wiedenbeck, S. Zaleski

RWTH Aachen University, III. Physikalisches Institut B, Aachen, Germany
C. Dziwok, G. Flügge, W. Haj Ahmad[19], O. Hlushchenko, T. Kress, A. Nowack, O. Pooth, D. Roy, A. Stahl[20], T. Ziemons, A. Zotz

Deutsches Elektronen-Synchrotron, Hamburg, Germany
H. Aarup Petersen, M. Aldaya Martin, P. Asmuss, S. Baxter, M. Bayatmakou, O. Behnke, A. Bermúdez Martínez, S. Bhattacharya, A.A. Bin Anuar, K. Borras[21], D. Brunner, A. Campbell, A. Cardini, C. Cheng, F. Colombina, S. Consuegra Rodríguez, G. Correia Silva, V. Danilov, M. De Silva, L. Didukh, G. Eckerlin, D. Eckstein, L.I. Estevez Banos, O. Filatov, E. Gallo[22], A. Geiser, A. Giraldi, A. Grohsjean, M. Guthoff, A. Jafari[23], N.Z. Jomhari, H. Jung, A. Kasem[21], M. Kasemann, H. Kaveh, C. Kleinwort, R. Kogler, D. Krücker, W. Lange, J. Lidrych, K. Lipka, W. Lohmann[24], R. Mankel, I.-A. Melzer-Pellmann, M. Mendizabal Morentin, J. Metwally, A.B. Meyer, M. Meyer, J. Mnich, A. Mussgiller, Y. Otarid, D. Pérez Adán, D. Pitzl, A. Raspereza, B. Ribeiro Lopes, J. Rübenach, A. Saggio, A. Saibel, M. Savitskyi,

JHEP05(2022)014

M. Scham[25], V. Scheurer, S. Schnake, P. Schütze, C. Schwanenberger[22], M. Shchedrolosiev, R.E. Sosa Ricardo, D. Stafford, N. Tonon, M. Van De Klundert, R. Walsh, D. Walter, Q. Wang, Y. Wen, K. Wichmann, L. Wiens, C. Wissing, S. Wuchterl

University of Hamburg, Hamburg, Germany

R. Aggleton, S. Albrecht, S. Bein, L. Benato, P. Connor, K. De Leo, M. Eich, F. Feindt, A. Fröhlich, C. Garbers, E. Garutti, P. Gunnellini, M. Hajheidari, J. Haller, A. Hinzmann, G. Kasieczka, R. Klanner, T. Kramer, V. Kutzner, J. Lange, T. Lange, A. Lobanov, A. Malara, A. Nigamova, K.J. Pena Rodriguez, M. Rieger, O. Rieger, P. Schleper, M. Schröder, J. Schwandt, J. Sonneveld, H. Stadie, G. Steinbrück, A. Tews, I. Zoi

Karlsruher Institut fuer Technologie, Karlsruhe, Germany

J. Bechtel, S. Brommer, M. Burkart, E. Butz, R. Caspart, T. Chwalek, W. De Boer[†], A. Dierlamm, A. Droll, K. El Morabit, N. Faltermann, M. Giffels, J.O. Gosewisch, A. Gottmann, F. Hartmann[20], C. Heidecker, U. Husemann, P. Keicher, R. Koppenhöfer, S. Maier, M. Metzler, S. Mitra, Th. Müller, M. Neukum, A. Nürnberg, G. Quast, K. Rabbertz, J. Rauser, D. Savoiu, M. Schnepf, D. Seith, I. Shvetsov, H.J. Simonis, R. Ulrich, J. Van Der Linden, R.F. Von Cube, M. Wassmer, M. Weber, S. Wieland, R. Wolf, S. Wozniewski, S. Wunsch

Institute of Nuclear and Particle Physics (INPP), NCSR Demokritos, Aghia Paraskevi, Greece

G. Anagnostou, G. Daskalakis, T. Geralis, A. Kyriakis, D. Loukas, A. Stakia

National and Kapodistrian University of Athens, Athens, Greece

M. Diamantopoulou, D. Karasavvas, G. Karathanasis, P. Kontaxakis, C.K. Koraka, A. Manousakis-Katsikakis, A. Panagiotou, I. Papavergou, N. Saoulidou, K. Theofilatos, E. Tziaferi, K. Vellidis, E. Vourliotis

National Technical University of Athens, Athens, Greece

G. Bakas, K. Kousouris, I. Papakrivopoulos, G. Tsipolitis, A. Zacharopoulou

University of Ioánnina, Ioánnina, Greece

K. Adamidis, I. Bestintzanos, I. Evangelou, C. Foudas, P. Gianneios, P. Katsoulis, P. Kokkas, N. Manthos, I. Papadopoulos, J. Strologas

MTA-ELTE Lendület CMS Particle and Nuclear Physics Group, Eötvös Loránd University, Budapest, Hungary

M. Csanad, K. Farkas, M.M.A. Gadallah[26], S. Lökös[27], P. Major, K. Mandal, A. Mehta, G. Pasztor, A.J. Rádl, O. Surányi, G.I. Veres

Wigner Research Centre for Physics, Budapest, Hungary

M. Bartók[28], G. Bencze, C. Hajdu, D. Horvath[29], F. Sikler, V. Veszpremi

Institute of Nuclear Research ATOMKI, Debrecen, Hungary

S. Czellar, D. Fasanella, J. Karancsi[28], J. Molnar, Z. Szillasi, D. Teyssier

JHEP05(2022)014

Institute of Physics, University of Debrecen, Debrecen, Hungary
P. Raics, Z.L. Trocsanyi[30], B. Ujvari

Karoly Robert Campus, MATE Institute of Technology, Gyongyos, Hungary
T. Csorgo[31], F. Nemes[31], T. Novak

Indian Institute of Science (IISc), Bangalore, India
S. Choudhury, J.R. Komaragiri, D. Kumar, L. Panwar, P.C. Tiwari

National Institute of Science Education and Research, HBNI, Bhubaneswar, India
S. Bahinipati[32], C. Kar, P. Mal, T. Mishra, V.K. Muraleedharan Nair Bindhu[33], A. Nayak[33], P. Saha, N. Sur, S.K. Swain, D. Vats[33]

Panjab University, Chandigarh, India
S. Bansal, S.B. Beri, V. Bhatnagar, G. Chaudhary, S. Chauhan, N. Dhingra[34], R. Gupta, A. Kaur, M. Kaur, P. Kumari, M. Meena, K. Sandeep, J.B. Singh, A.K. Virdi

University of Delhi, Delhi, India
A. Ahmed, A. Bhardwaj, B.C. Choudhary, M. Gola, S. Keshri, A. Kumar, M. Naimuddin, P. Priyanka, K. Ranjan, A. Shah

Saha Institute of Nuclear Physics, HBNI, Kolkata, India
M. Bharti[35], R. Bhattacharya, S. Bhattacharya, D. Bhowmik, S. Dutta, S. Dutta, B. Gomber[36], M. Maity[37], P. Palit, P.K. Rout, G. Saha, B. Sahu, S. Sarkar, M. Sharan, S. Thakur[35]

Indian Institute of Technology Madras, Madras, India
P.K. Behera, S.C. Behera, P. Kalbhor, A. Muhammad, R. Pradhan, P.R. Pujahari, A. Sharma, A.K. Sikdar

Bhabha Atomic Research Centre, Mumbai, India
D. Dutta, V. Jha, V. Kumar, D.K. Mishra, K. Naskar[38], P.K. Netrakanti, L.M. Pant, P. Shukla

Tata Institute of Fundamental Research-A, Mumbai, India
T. Aziz, S. Dugad, M. Kumar

Tata Institute of Fundamental Research-B, Mumbai, India
S. Banerjee, R. Chudasama, M. Guchait, S. Karmakar, S. Kumar, G. Majumder, K. Mazumdar, S. Mukherjee

Indian Institute of Science Education and Research (IISER), Pune, India
K. Alpana, S. Dube, B. Kansal, A. Laha, S. Pandey, A. Rastogi, S. Sharma

Isfahan University of Technology, Isfahan, Iran
H. Bakhshiansohi[39], E. Khazaie, M. Zeinali[40]

JHEP05(2022)014

Institute for Research in Fundamental Sciences (IPM), Tehran, Iran
S. Chenarani[41], S.M. Etesami, M. Khakzad, M. Mohammadi Najafabadi

University College Dublin, Dublin, Ireland
M. Grunewald

INFN Sezione di Bari [a], Bari, Italy, Università di Bari [b], Bari, Italy, Politecnico di Bari [c], Bari, Italy
M. Abbrescia[a,b], R. Aly[a,b,42], C. Aruta[a,b], A. Colaleo[a], D. Creanza[a,c], N. De Filippis[a,c], M. De Palma[a,b], A. Di Florio[a,b], A. Di Pilato[a,b], W. Elmetenawee[a,b], L. Fiore[a], A. Gelmi[a,b], M. Gul[a], G. Iaselli[a,c], M. Ince[a,b], S. Lezki[a,b], G. Maggi[a,c], M. Maggi[a], I. Margjeka[a,b], V. Mastrapasqua[a,b], S. My[a,b], S. Nuzzo[a,b], A. Pellecchia[a,b], A. Pompili[a,b], G. Pugliese[a,c], D. Ramos[a], A. Ranieri[a], G. Selvaggi[a,b], L. Silvestris[a], F.M. Simone[a,b], Ü. Sözbilir[a], R. Venditti[a], P. Verwilligen[a]

INFN Sezione di Bologna [a], Bologna, Italy, Università di Bologna [b], Bologna, Italy
G. Abbiendi[a], C. Battilana[a,b], D. Bonacorsi[a,b], L. Borgonovi[a], L. Brigliadori[a], R. Campanini[a,b], P. Capiluppi[a,b], A. Castro[a,b], F.R. Cavallo[a], M. Cuffiani[a,b], G.M. Dallavalle[a], T. Diotalevi[a,b], F. Fabbri[a], A. Fanfani[a,b], P. Giacomelli[a], L. Giommi[a,b], C. Grandi[a], L. Guiducci[a,b], S. Lo Meo[a,43], L. Lunerti[a,b], S. Marcellini[a], G. Masetti[a], F.L. Navarria[a,b], A. Perrotta[a], F. Primavera[a,b], A.M. Rossi[a,b], T. Rovelli[a,b], G.P. Siroli[a,b]

INFN Sezione di Catania [a], Catania, Italy, Università di Catania [b], Catania, Italy
S. Albergo[a,b,44], S. Costa[a,b,44], A. Di Mattia[a], R. Potenza[a,b], A. Tricomi[a,b,44], C. Tuve[a,b]

INFN Sezione di Firenze [a], Firenze, Italy, Università di Firenze [b], Firenze, Italy
G. Barbagli[a], A. Cassese[a], R. Ceccarelli[a,b], V. Ciulli[a,b], C. Civinini[a], R. D'Alessandro[a,b], E. Focardi[a,b], G. Latino[a,b], P. Lenzi[a,b], M. Lizzo[a,b], M. Meschini[a], S. Paoletti[a], R. Seidita[a,b], G. Sguazzoni[a], L. Viliani[a]

INFN Laboratori Nazionali di Frascati, Frascati, Italy
L. Benussi, S. Bianco, D. Piccolo

INFN Sezione di Genova [a], Genova, Italy, Università di Genova [b], Genova, Italy
M. Bozzo[a,b], F. Ferro[a], R. Mulargia[a,b], E. Robutti[a], S. Tosi[a,b]

INFN Sezione di Milano-Bicocca [a], Milano, Italy, Università di Milano-Bicocca [b], Milano, Italy
A. Benaglia[a], G. Boldrini, F. Brivio[a,b], F. Cetorelli[a,b], F. De Guio[a,b], M.E. Dinardo[a,b], P. Dini[a], S. Gennai[a], A. Ghezzi[a,b], P. Govoni[a,b], L. Guzzi[a,b],

JHEP05(2022)014

M.T. Lucchini[a,b], M. Malberti[a], S. Malvezzi[a], A. Massironi[a], D. Menasce[a], L. Moroni[a], M. Paganoni[a,b], D. Pedrini[a], B.S. Pinolini, S. Ragazzi[a,b], N. Redaelli[a], T. Tabarelli de Fatis[a,b], D. Valsecchi[a,b,20], D. Zuolo[a,b]

INFN Sezione di Napoli [a], Napoli, Italy, Università di Napoli 'Federico II' [b], Napoli, Italy, Università della Basilicata [c], Potenza, Italy, Università G. Marconi [d], Roma, Italy

S. Buontempo[a], F. Carnevali[a,b], N. Cavallo[a,c], A. De Iorio[a,b], F. Fabozzi[a,c], A.O.M. Iorio[a,b], L. Lista[a,b,45], S. Meola[a,d,20], P. Paolucci[a,20], B. Rossi[a], C. Sciacca[a,b]

INFN Sezione di Padova [a], Padova, Italy, Università di Padova [b], Padova, Italy, Università di Trento [c], Trento, Italy

P. Azzi[a], N. Bacchetta[a], D. Bisello[a,b], P. Bortignon[a], A. Bragagnolo[a,b], R. Carlin[a,b], P. Checchia[a], T. Dorigo[a], U. Dosselli[a], F. Gasparini[a,b], U. Gasparini[a,b], G. Grosso, S.Y. Hoh[a,b], L. Layer[a,46], E. Lusiani, M. Margoni[a,b], A.T. Meneguzzo[a,b], J. Pazzini[a,b], P. Ronchese[a,b], R. Rossin[a,b], F. Simonetto[a,b], G. Strong[a], M. Tosi[a,b], H. Yarar[a,b], M. Zanetti[a,b], P. Zotto[a,b], A. Zucchetta[a,b], G. Zumerle[a,b]

INFN Sezione di Pavia [a], Pavia, Italy, Università di Pavia [b], Pavia, Italy

C. Aimè[a,b], A. Braghieri[a], S. Calzaferri[a,b], D. Fiorina[a,b], P. Montagna[a,b], S.P. Ratti[a,b], V. Re[a], C. Riccardi[a,b], P. Salvini[a], I. Vai[a], P. Vitulo[a,b]

INFN Sezione di Perugia [a], Perugia, Italy, Università di Perugia [b], Perugia, Italy

P. Asenov[a,47], G.M. Bilei[a], D. Ciangottini[a,b], L. Fanò[a,b], M. Magherini[b], G. Mantovani[a,b], V. Mariani[a,b], M. Menichelli[a], F. Moscatelli[a,47], A. Piccinelli[a,b], M. Presilla[a,b], A. Rossi[a,b], A. Santocchia[a,b], D. Spiga[a], T. Tedeschi[a,b]

INFN Sezione di Pisa [a], Pisa, Italy, Università di Pisa [b], Pisa, Italy, Scuola Normale Superiore di Pisa [c], Pisa, Italy, Università di Siena [d], Siena, Italy

P. Azzurri[a], G. Bagliesi[a], V. Bertacchi[a,c], L. Bianchini[a], T. Boccali[a], E. Bossini[a,b], R. Castaldi[a], M.A. Ciocci[a,b], V. D'Amante[a,d], R. Dell'Orso[a], M.R. Di Domenico[a,d], S. Donato[a], A. Giassi[a], F. Ligabue[a,c], E. Manca[a,c], G. Mandorli[a,c], D. Matos Figueiredo, A. Messineo[a,b], F. Palla[a], S. Parolia[a,b], G. Ramirez-Sanchez[a,c], A. Rizzi[a,b], G. Rolandi[a,c], S. Roy Chowdhury[a,c], A. Scribano[a], N. Shafiei[a,b], P. Spagnolo[a], R. Tenchini[a], G. Tonelli[a,b], N. Turini[a,d], A. Venturi[a], P.G. Verdini[a]

INFN Sezione di Roma [a], Rome, Italy, Sapienza Università di Roma [b], Rome, Italy

P. Barria[a], M. Campana[a,b], F. Cavallari[a], D. Del Re[a,b], E. Di Marco[a], M. Diemoz[a], E. Longo[a,b], P. Meridiani[a], G. Organtini[a,b], F. Pandolfi[a], R. Paramatti[a,b], C. Quaranta[a,b], S. Rahatlou[a,b], C. Rovelli[a], F. Santanastasio[a,b], L. Soffi[a], R. Tramontano[a,b]

JHEP05(2022)014

INFN Sezione di Torino [a], Torino, Italy, Università di Torino [b], Torino, Italy, Università del Piemonte Orientale [c], Novara, Italy

N. Amapane[a,b], R. Arcidiacono[a,c], S. Argiro[a,b], M. Arneodo[a,c], N. Bartosik[a], R. Bellan[a,b], A. Bellora[a,b], J. Berenguer Antequera[a,b], C. Biino[a], N. Cartiglia[a], M. Costa[a,b], R. Covarelli[a,b], N. Demaria[a], B. Kiani[a,b], F. Legger[a], C. Mariotti[a], S. Maselli[a], E. Migliore[a,b], E. Monteil[a,b], M. Monteno[a], M.M. Obertino[a,b], G. Ortona[a], L. Pacher[a,b], N. Pastrone[a], M. Pelliccioni[a], M. Ruspa[a,c], K. Shchelina[a], F. Siviero[a,b], V. Sola[a], A. Solano[a,b], D. Soldi[a,b], A. Staiano[a], M. Tornago[a,b], D. Trocino[a], A. Vagnerini[a,b]

INFN Sezione di Trieste [a], Trieste, Italy, Università di Trieste [b], Trieste, Italy

S. Belforte[a], V. Candelise[a,b], M. Casarsa[a], F. Cossutti[a], A. Da Rold[a,b], G. Della Ricca[a,b], G. Sorrentino[a,b], F. Vazzoler[a,b]

Kyungpook National University, Daegu, Korea

S. Dogra, C. Huh, B. Kim, D.H. Kim, G.N. Kim, J. Kim, J. Lee, S.W. Lee, C.S. Moon, Y.D. Oh, S.I. Pak, S. Sekmen, Y.C. Yang

Chonnam National University, Institute for Universe and Elementary Particles, Kwangju, Korea

H. Kim, D.H. Moon

Hanyang University, Seoul, Korea

B. Francois, T.J. Kim, J. Park

Korea University, Seoul, Korea

S. Cho, S. Choi, B. Hong, K. Lee, K.S. Lee, J. Lim, J. Park, S.K. Park, J. Yoo

Kyung Hee University, Department of Physics, Seoul, Republic of Korea, Seoul, Korea

J. Goh, A. Gurtu

Sejong University, Seoul, Korea

H.S. Kim, Y. Kim

Seoul National University, Seoul, Korea

J. Almond, J.H. Bhyun, J. Choi, S. Jeon, J. Kim, J.S. Kim, S. Ko, H. Kwon, H. Lee, S. Lee, B.H. Oh, M. Oh, S.B. Oh, H. Seo, U.K. Yang, I. Yoon

University of Seoul, Seoul, Korea

W. Jang, D.Y. Kang, Y. Kang, S. Kim, B. Ko, J.S.H. Lee, Y. Lee, J.A. Merlin, I.C. Park, Y. Roh, M.S. Ryu, D. Song, I.J. Watson, S. Yang

Yonsei University, Department of Physics, Seoul, Korea

S. Ha, H.D. Yoo

Sungkyunkwan University, Suwon, Korea

M. Choi, H. Lee, Y. Lee, I. Yu

JHEP05(2022)014

College of Engineering and Technology, American University of the Middle East (AUM), Egaila, Kuwait, Dasman, Kuwait

T. Beyrouthy, Y. Maghrbi

Riga Technical University, Riga, Latvia

K. Dreimanis, V. Veckalns[48]

Vilnius University, Vilnius, Lithuania

M. Ambrozas, A. Carvalho Antunes De Oliveira, A. Juodagalvis, A. Rinkevicius, G. Tamulaitis

National Centre for Particle Physics, Universiti Malaya, Kuala Lumpur, Malaysia

N. Bin Norjoharuddeen, W.A.T. Wan Abdullah, M.N. Yusli, Z. Zolkapli

Universidad de Sonora (UNISON), Hermosillo, Mexico

J.F. Benitez, A. Castaneda Hernandez, M. León Coello, J.A. Murillo Quijada, A. Sehrawat, L. Valencia Palomo

Centro de Investigacion y de Estudios Avanzados del IPN, Mexico City, Mexico

G. Ayala, H. Castilla-Valdez, E. De La Cruz-Burelo, I. Heredia-De La Cruz[49], R. Lopez-Fernandez, C.A. Mondragon Herrera, D.A. Perez Navarro, A. Sánchez Hernández

Universidad Iberoamericana, Mexico City, Mexico

S. Carrillo Moreno, C. Oropeza Barrera, F. Vazquez Valencia

Benemerita Universidad Autonoma de Puebla, Puebla, Mexico

I. Pedraza, H.A. Salazar Ibarguen, C. Uribe Estrada

University of Montenegro, Podgorica, Montenegro

J. Mijuskovic[50], N. Raicevic

University of Auckland, Auckland, New Zealand

D. Krofcheck

University of Canterbury, Christchurch, New Zealand

P.H. Butler

National Centre for Physics, Quaid-I-Azam University, Islamabad, Pakistan

A. Ahmad, M.I. Asghar, A. Awais, M.I.M. Awan, H.R. Hoorani, W.A. Khan, M.A. Shah, M. Shoaib, M. Waqas

AGH University of Science and Technology Faculty of Computer Science, Electronics and Telecommunications, Krakow, Poland

V. Avati, L. Grzanka, M. Malawski

National Centre for Nuclear Research, Swierk, Poland

H. Bialkowska, M. Bluj, B. Boimska, M. Górski, M. Kazana, M. Szleper, P. Zalewski

JHEP05(2022)014

Institute of Experimental Physics, Faculty of Physics, University of Warsaw, Warsaw, Poland

K. Bunkowski, K. Doroba, A. Kalinowski, M. Konecki, J. Krolikowski

Laboratório de Instrumentação e Física Experimental de Partículas, Lisboa, Portugal

M. Araujo, P. Bargassa, D. Bastos, A. Boletti, P. Faccioli, M. Gallinaro, J. Hollar, N. Leonardo, T. Niknejad, M. Pisano, J. Seixas, O. Toldaiev, J. Varela

Joint Institute for Nuclear Research, Dubna, Russia

S. Afanasiev, D. Budkouski, I. Golutvin, I. Gorbunov, V. Karjavine, V. Korenkov, A. Lanev, A. Malakhov, V. Matveev[51,52], V. Palichik, V. Perelygin, M. Savina, D. Seitova, V. Shalaev, S. Shmatov, S. Shulha, V. Smirnov, O. Teryaev, N. Voytishin, B.S. Yuldashev[53], A. Zarubin, I. Zhizhin

Petersburg Nuclear Physics Institute, Gatchina (St. Petersburg), Russia

G. Gavrilov, V. Golovtcov, Y. Ivanov, V. Kim[54], E. Kuznetsova[55], V. Murzin, V. Oreshkin, I. Smirnov, D. Sosnov, V. Sulimov, L. Uvarov, S. Volkov, A. Vorobyev

Institute for Nuclear Research, Moscow, Russia

Yu. Andreev, A. Dermenev, S. Gninenko, N. Golubev, A. Karneyeu, D. Kirpichnikov, M. Kirsanov, N. Krasnikov, A. Pashenkov, G. Pivovarov, A. Toropin

Institute for Theoretical and Experimental Physics named by A.I. Alikhanov of NRC 'Kurchatov Institute', Moscow, Russia

V. Epshteyn, V. Gavrilov, N. Lychkovskaya, A. Nikitenko[56], V. Popov, A. Stepennov, M. Toms, E. Vlasov, A. Zhokin

Moscow Institute of Physics and Technology, Moscow, Russia

T. Aushev

National Research Nuclear University 'Moscow Engineering Physics Institute' (MEPhI), Moscow, Russia

M. Chadeeva[57], A. Oskin, P. Parygin, E. Popova, V. Rusinov, D. Selivanova

P.N. Lebedev Physical Institute, Moscow, Russia

V. Andreev, M. Azarkin, I. Dremin, M. Kirakosyan, A. Terkulov

Skobeltsyn Institute of Nuclear Physics, Lomonosov Moscow State University, Moscow, Russia

A. Belyaev, E. Boos, V. Bunichev, M. Dubinin[58], L. Dudko, A. Ershov, A. Gribushin, V. Klyukhin, O. Kodolova, I. Lokhtin, S. Obraztsov, S. Petrushanko, V. Savrin

Novosibirsk State University (NSU), Novosibirsk, Russia

V. Blinov[59], T. Dimova[59], L. Kardapoltsev[59], A. Kozyrev[59], I. Ovtin[59], O. Radchenko[59], Y. Skovpen[59]

JHEP05(2022)014

Institute for High Energy Physics of National Research Centre 'Kurchatov Institute', Protvino, Russia

I. Azhgirey, I. Bayshev, D. Elumakhov, V. Kachanov, D. Konstantinov, P. Mandrik, V. Petrov, R. Ryutin, S. Slabospitskii, A. Sobol, S. Troshin, N. Tyurin, A. Uzunian, A. Volkov

National Research Tomsk Polytechnic University, Tomsk, Russia

A. Babaev, V. Okhotnikov

Tomsk State University, Tomsk, Russia

V. Borshch, V. Ivanchenko, E. Tcherniaev

University of Belgrade: Faculty of Physics and VINCA Institute of Nuclear Sciences, Belgrade, Serbia

P. Adzic[60], M. Dordevic, P. Milenovic, J. Milosevic

Centro de Investigaciones Energéticas Medioambientales y Tecnológicas (CIEMAT), Madrid, Spain

M. Aguilar-Benitez, J. Alcaraz Maestre, A. Álvarez Fernández, I. Bachiller, M. Barrio Luna, Cristina F. Bedoya, C.A. Carrillo Montoya, M. Cepeda, M. Cerrada, N. Colino, B. De La Cruz, A. Delgado Peris, J.P. Fernández Ramos, J. Flix, M.C. Fouz, O. Gonzalez Lopez, S. Goy Lopez, J.M. Hernandez, M.I. Josa, J. León Holgado, D. Moran, Á. Navarro Tobar, C. Perez Dengra, A. Pérez-Calero Yzquierdo, J. Puerta Pelayo, I. Redondo, L. Romero, S. Sánchez Navas, L. Urda Gómez, C. Willmott

Universidad Autónoma de Madrid, Madrid, Spain

J.F. de Trocóniz, R. Reyes-Almanza

Universidad de Oviedo, Instituto Universitario de Ciencias y Tecnologías Espaciales de Asturias (ICTEA), Oviedo, Spain

B. Alvarez Gonzalez, J. Cuevas, C. Erice, J. Fernandez Menendez, S. Folgueras, I. Gonzalez Caballero, J.R. González Fernández, E. Palencia Cortezon, C. Ramón Álvarez, V. Rodríguez Bouza, A. Soto Rodríguez, A. Trapote, N. Trevisani, C. Vico Villalba

Instituto de Física de Cantabria (IFCA), CSIC-Universidad de Cantabria, Santander, Spain

J.A. Brochero Cifuentes, I.J. Cabrillo, A. Calderon, J. Duarte Campderros, M. Fernandez, C. Fernandez Madrazo, P.J. Fernández Manteca, A. García Alonso, G. Gomez, C. Martinez Rivero, P. Martinez Ruiz del Arbol, F. Matorras, P. Matorras Cuevas, J. Piedra Gomez, C. Prieels, A. Ruiz-Jimeno, L. Scodellaro, I. Vila, J.M. Vizan Garcia

University of Colombo, Colombo, Sri Lanka

M.K. Jayananda, B. Kailasapathy[61], D.U.J. Sonnadara, D.D.C. Wickramarathna

JHEP05(2022)014

University of Ruhuna, Department of Physics, Matara, Sri Lanka

W.G.D. Dharmaratna, K. Liyanage, N. Perera, N. Wickramage

CERN, European Organization for Nuclear Research, Geneva, Switzerland

T.K. Aarrestad, D. Abbaneo, J. Alimena, E. Auffray, G. Auzinger, J. Baechler, P. Baillon[†], D. Barney, J. Bendavid, M. Bianco, A. Bocci, T. Camporesi, M. Capeans Garrido, G. Cerminara, N. Chernyavskaya, S.S. Chhibra, M. Cipriani, L. Cristella, D. d'Enterria, A. Dabrowski, A. David, A. De Roeck, M.M. Defranchis, M. Deile, M. Dobson, M. Dünser, N. Dupont, A. Elliott-Peisert, N. Emriskova, F. Fallavollita[62], A. Florent, G. Franzoni, W. Funk, S. Giani, D. Gigi, K. Gill, F. Glege, L. Gouskos, M. Haranko, J. Hegeman, V. Innocente, T. James, P. Janot, J. Kaspar, J. Kieseler, M. Komm, N. Kratochwil, C. Lange, S. Laurila, P. Lecoq, A. Lintuluoto, K. Long, C. Lourenço, B. Maier, L. Malgeri, S. Mallios, M. Mannelli, A.C. Marini, F. Meijers, S. Mersi, E. Meschi, F. Moortgat, M. Mulders, S. Orfanelli, L. Orsini, F. Pantaleo, E. Perez, M. Peruzzi, A. Petrilli, G. Petrucciani, A. Pfeiffer, M. Pierini, D. Piparo, M. Pitt, H. Qu, T. Quast, D. Rabady, A. Racz, G. Reales Gutiérrez, M. Rovere, H. Sakulin, J. Salfeld-Nebgen, S. Scarfi, C. Schäfer, C. Schwick, M. Selvaggi, A. Sharma, P. Silva, W. Snoeys, P. Sphicas[63], S. Summers, K. Tatar, V.R. Tavolaro, D. Treille, P. Tropea, A. Tsirou, G.P. Van Onsem, J. Wanczyk[64], K.A. Wozniak, W.D. Zeuner

Paul Scherrer Institut, Villigen, Switzerland

L. Caminada[65], A. Ebrahimi, W. Erdmann, R. Horisberger, Q. Ingram, H.C. Kaestli, D. Kotlinski, U. Langenegger, M. Missiroli[65], L. Noehte[65], T. Rohe

ETH Zurich — Institute for Particle Physics and Astrophysics (IPA), Zurich, Switzerland

K. Androsov[64], M. Backhaus, P. Berger, A. Calandri, A. De Cosa, G. Dissertori, M. Dittmar, M. Donegà, C. Dorfer, F. Eble, K. Gedia, F. Glessgen, T.A. Gómez Espinosa, C. Grab, D. Hits, W. Lustermann, A.-M. Lyon, R.A. Manzoni, L. Marchese, C. Martin Perez, M.T. Meinhard, F. Nessi-Tedaldi, J. Niedziela, F. Pauss, V. Perovic, S. Pigazzini, M.G. Ratti, M. Reichmann, C. Reissel, T. Reitenspiess, B. Ristic, D. Ruini, D.A. Sanz Becerra, V. Stampf, J. Steggemann[64], R. Wallny, D.H. Zhu

Universität Zürich, Zurich, Switzerland

C. Amsler[66], P. Bärtschi, C. Botta, D. Brzhechko, M.F. Canelli, K. Cormier, A. De Wit, R. Del Burgo, J.K. Heikkilä, M. Huwiler, W. Jin, A. Jofrehei, B. Kilminster, S. Leontsinis, S.P. Liechti, A. Macchiolo, P. Meiring, V.M. Mikuni, U. Molinatti, I. Neutelings, A. Reimers, P. Robmann, S. Sanchez Cruz, K. Schweiger, M. Senger, Y. Takahashi

National Central University, Chung-Li, Taiwan

C. Adloff[67], C.M. Kuo, W. Lin, A. Roy, T. Sarkar[37], S.S. Yu

JHEP05(2022)014

National Taiwan University (NTU), Taipei, Taiwan

L. Ceard, Y. Chao, K.F. Chen, P.H. Chen, P.s. Chen, H. Cheng, W.-S. Hou, Y.y. Li, R.-S. Lu, E. Paganis, A. Psallidas, A. Steen, H.y. Wu, E. Yazgan, P.r. Yu

Chulalongkorn University, Faculty of Science, Department of Physics, Bangkok, Thailand

B. Asavapibhop, C. Asawatangtrakuldee, N. Srimanobhas

Çukurova University, Physics Department, Science and Art Faculty, Adana, Turkey

F. Boran, S. Damarseckin[68], Z.S. Demiroglu, F. Dolek, I. Dumanoglu[69], E. Eskut, Y. Guler[70], E. Gurpinar Guler[70], C. Isik, O. Kara, A. Kayis Topaksu, U. Kiminsu, G. Onengut, K. Ozdemir[71], A. Polatoz, A.E. Simsek, B. Tali[72], U.G. Tok, S. Turkcapar, I.S. Zorbakir

Middle East Technical University, Physics Department, Ankara, Turkey

B. Isildak[73], G. Karapinar, K. Ocalan[74], M. Yalvac[75]

Bogazici University, Istanbul, Turkey

B. Akgun, I.O. Atakisi, E. Gülmez, M. Kaya[76], O. Kaya[77], Ö. Özçelik, S. Tekten[78], E.A. Yetkin[79]

Istanbul Technical University, Istanbul, Turkey

A. Cakir, K. Cankocak[69], Y. Komurcu, S. Sen[80]

Istanbul University, Istanbul, Turkey

S. Cerci[72], I. Hos[81], B. Kaynak, S. Ozkorucuklu, H. Sert, D. Sunar Cerci[72], C. Zorbilmez

Institute for Scintillation Materials of National Academy of Science of Ukraine, Kharkov, Ukraine

B. Grynyov

National Scientific Center, Kharkov Institute of Physics and Technology, Kharkov, Ukraine

L. Levchuk

University of Bristol, Bristol, United Kingdom

D. Anthony, E. Bhal, S. Bologna, J.J. Brooke, A. Bundock, E. Clement, D. Cussans, H. Flacher, J. Goldstein, G.P. Heath, H.F. Heath, L. Kreczko, B. Krikler, S. Paramesvaran, S. Seif El Nasr-Storey, V.J. Smith, N. Stylianou[82], K. Walkingshaw Pass, R. White

Rutherford Appleton Laboratory, Didcot, United Kingdom

K.W. Bell, A. Belyaev[83], C. Brew, R.M. Brown, D.J.A. Cockerill, C. Cooke, K.V. Ellis, K. Harder, S. Harper, M.-L. Holmberg[84], J. Linacre, K. Manolopoulos, D.M. Newbold, E. Olaiya, D. Petyt, T. Reis, T. Schuh, C.H. Shepherd-Themistocleous, I.R. Tomalin, T. Williams

JHEP05(2022)014

Imperial College, London, United Kingdom

R. Bainbridge, P. Bloch, S. Bonomally, J. Borg, S. Breeze, O. Buchmuller, V. Cepaitis, G.S. Chahal[85], D. Colling, P. Dauncey, G. Davies, M. Della Negra, S. Fayer, G. Fedi, G. Hall, M.H. Hassanshahi, G. Iles, J. Langford, L. Lyons, A.-M. Magnan, S. Malik, A. Martelli, D.G. Monk, J. Nash[86], M. Pesaresi, B.C. Radburn-Smith, D.M. Raymond, A. Richards, A. Rose, E. Scott, C. Seez, A. Shtipliyski, A. Tapper, K. Uchida, T. Virdee[20], M. Vojinovic, N. Wardle, S.N. Webb, D. Winterbottom

Brunel University, Uxbridge, United Kingdom

K. Coldham, J.E. Cole, A. Khan, P. Kyberd, I.D. Reid, L. Teodorescu, S. Zahid

Baylor University, Waco, Texas, U.S.A.

S. Abdullin, A. Brinkerhoff, B. Caraway, J. Dittmann, K. Hatakeyama, A.R. Kanuganti, B. McMaster, N. Pastika, M. Saunders, S. Sawant, C. Sutantawibul, J. Wilson

Catholic University of America, Washington, DC, U.S.A.

R. Bartek, A. Dominguez, R. Uniyal, A.M. Vargas Hernandez

The University of Alabama, Tuscaloosa, Alabama, U.S.A.

A. Buccilli, S.I. Cooper, D. Di Croce, S.V. Gleyzer, C. Henderson, C.U. Perez, P. Rumerio[87], C. West

Boston University, Boston, Massachusetts, U.S.A.

A. Akpinar, A. Albert, D. Arcaro, C. Cosby, Z. Demiragli, E. Fontanesi, D. Gastler, S. May, J. Rohlf, K. Salyer, D. Sperka, D. Spitzbart, I. Suarez, A. Tsatsos, S. Yuan, D. Zou

Brown University, Providence, Rhode Island, U.S.A.

G. Benelli, B. Burkle, X. Coubez[21], D. Cutts, M. Hadley, U. Heintz, J.M. Hogan[88], T. KWON, G. Landsberg, K.T. Lau, D. Li, M. Lukasik, J. Luo, M. Narain, N. Pervan, S. Sagir[89], F. Simpson, E. Usai, W.Y. Wong, X. Yan, D. Yu, W. Zhang

University of California, Davis, Davis, California, U.S.A.

J. Bonilla, C. Brainerd, R. Breedon, M. Calderon De La Barca Sanchez, M. Chertok, J. Conway, P.T. Cox, R. Erbacher, G. Haza, F. Jensen, O. Kukral, R. Lander, M. Mulhearn, D. Pellett, B. Regnery, D. Taylor, Y. Yao, F. Zhang

University of California, Los Angeles, California, U.S.A.

M. Bachtis, R. Cousins, A. Datta, D. Hamilton, J. Hauser, M. Ignatenko, M.A. Iqbal, T. Lam, W.A. Nash, S. Regnard, D. Saltzberg, B. Stone, V. Valuev

University of California, Riverside, Riverside, California, U.S.A.

K. Burt, Y. Chen, R. Clare, J.W. Gary, M. Gordon, G. Hanson, G. Karapostoli, O.R. Long, N. Manganelli, M. Olmedo Negrete, W. Si, S. Wimpenny, Y. Zhang

JHEP05(2022)014

University of California, San Diego, La Jolla, California, U.S.A.
J.G. Branson, P. Chang, S. Cittolin, S. Cooperstein, N. Deelen, D. Diaz, J. Duarte, R. Gerosa, L. Giannini, J. Guiang, R. Kansal, V. Krutelyov, R. Lee, J. Letts, M. Masciovecchio, F. Mokhtar, M. Pieri, B.V. Sathia Narayanan, V. Sharma, M. Tadel, A. Vartak, F. Würthwein, Y. Xiang, A. Yagil

University of California, Santa Barbara — Department of Physics, Santa Barbara, California, U.S.A.
N. Amin, C. Campagnari, M. Citron, A. Dorsett, V. Dutta, J. Incandela, M. Kilpatrick, J. Kim, B. Marsh, H. Mei, M. Oshiro, M. Quinnan, J. Richman, U. Sarica, F. Setti, J. Sheplock, P. Siddireddy, D. Stuart, S. Wang

California Institute of Technology, Pasadena, California, U.S.A.
A. Bornheim, O. Cerri, I. Dutta, J.M. Lawhorn, N. Lu, J. Mao, H.B. Newman, T.Q. Nguyen, M. Spiropulu, J.R. Vlimant, C. Wang, S. Xie, Z. Zhang, R.Y. Zhu

Carnegie Mellon University, Pittsburgh, Pennsylvania, U.S.A.
J. Alison, S. An, M.B. Andrews, P. Bryant, T. Ferguson, A. Harilal, C. Liu, T. Mudholkar, M. Paulini, A. Sanchez, W. Terrill

University of Colorado Boulder, Boulder, Colorado, U.S.A.
J.P. Cumalat, W.T. Ford, A. Hassani, E. MacDonald, R. Patel, A. Perloff, C. Savard, K. Stenson, K.A. Ulmer, S.R. Wagner, N. Zipper

Cornell University, Ithaca, New York, U.S.A.
J. Alexander, S. Bright-Thonney, X. Chen, Y. Cheng, D.J. Cranshaw, S. Hogan, J. Monroy, J.R. Patterson, D. Quach, J. Reichert, M. Reid, A. Ryd, W. Sun, J. Thom, P. Wittich, R. Zou

Fermi National Accelerator Laboratory, Batavia, Illinois, U.S.A.
M. Albrow, M. Alyari, G. Apollinari, A. Apresyan, A. Apyan, S. Banerjee, L.A.T. Bauerdick, D. Berry, J. Berryhill, P.C. Bhat, K. Burkett, J.N. Butler, A. Canepa, G.B. Cerati, H.W.K. Cheung, F. Chlebana, K.F. Di Petrillo, V.D. Elvira, Y. Feng, J. Freeman, Z. Gecse, L. Gray, D. Green, S. Grünendahl, O. Gutsche, R.M. Harris, R. Heller, T.C. Herwig, J. Hirschauer, B. Jayatilaka, S. Jindariani, M. Johnson, U. Joshi, T. Klijnsma, B. Klima, K.H.M. Kwok, S. Lammel, D. Lincoln, R. Lipton, T. Liu, C. Madrid, K. Maeshima, C. Mantilla, D. Mason, P. McBride, P. Merkel, S. Mrenna, S. Nahn, J. Ngadiuba, V. O'Dell, V. Papadimitriou, K. Pedro, C. Pena[58], O. Prokofyev, F. Ravera, A. Reinsvold Hall, L. Ristori, E. Sexton-Kennedy, N. Smith, A. Soha, W.J. Spalding, L. Spiegel, S. Stoynev, J. Strait, L. Taylor, S. Tkaczyk, N.V. Tran, L. Uplegger, E.W. Vaandering, H.A. Weber

University of Florida, Gainesville, Florida, U.S.A.
D. Acosta, P. Avery, D. Bourilkov, L. Cadamuro, V. Cherepanov, F. Errico, R.D. Field, D. Guerrero, B.M. Joshi, M. Kim, E. Koenig, J. Konigsberg, A. Korytov,

JHEP05(2022)014

K.H. Lo, K. Matchev, N. Menendez, G. Mitselmakher, A. Muthirakalayil Madhu, N. Rawal, D. Rosenzweig, S. Rosenzweig, J. Rotter, K. Shi, J. Wang, E. Yigitbasi, X. Zuo

Florida State University, Tallahassee, Florida, U.S.A.

T. Adams, A. Askew, R. Habibullah, V. Hagopian, K.F. Johnson, R. Khurana, T. Kolberg, G. Martinez, H. Prosper, C. Schiber, O. Viazlo, R. Yohay, J. Zhang

Florida Institute of Technology, Melbourne, Florida, U.S.A.

M.M. Baarmand, S. Butalla, T. Elkafrawy[90], M. Hohlmann, R. Kumar Verma, D. Noonan, M. Rahmani, F. Yumiceva

University of Illinois at Chicago (UIC), Chicago, Illinois, U.S.A.

M.R. Adams, H. Becerril Gonzalez, R. Cavanaugh, S. Dittmer, O. Evdokimov, C.E. Gerber, D.A. Hangal, D.J. Hofman, A.H. Merrit, C. Mills, G. Oh, T. Roy, S. Rudrabhatla, M.B. Tonjes, N. Varelas, J. Viinikainen, X. Wang, Z. Wu, Z. Ye

The University of Iowa, Iowa City, Iowa, U.S.A.

M. Alhusseini, K. Dilsiz[91], L. Emediato, R.P. Gandrajula, O.K. Köseyan, J.-P. Merlo, A. Mestvirishvili[92], J. Nachtman, H. Ogul[93], Y. Onel, A. Penzo, C. Snyder, E. Tiras[94]

Johns Hopkins University, Baltimore, Maryland, U.S.A.

O. Amram, B. Blumenfeld, L. Corcodilos, J. Davis, M. Eminizer, A.V. Gritsan, S. Kyriacou, P. Maksimovic, J. Roskes, M. Swartz, T.Á. Vámi

The University of Kansas, Lawrence, Kansas, U.S.A.

A. Abreu, J. Anguiano, C. Baldenegro Barrera, P. Baringer, A. Bean, A. Bylinkin, Z. Flowers, T. Isidori, S. Khalil, J. King, G. Krintiras, A. Kropivnitskaya, M. Lazarovits, C. Le Mahieu, C. Lindsey, J. Marquez, N. Minafra, M. Murray, M. Nickel, C. Rogan, C. Royon, R. Salvatico, S. Sanders, E. Schmitz, C. Smith, J.D. Tapia Takaki, Q. Wang, Z. Warner, J. Williams, G. Wilson

Kansas State University, Manhattan, Kansas, U.S.A.

S. Duric, A. Ivanov, K. Kaadze, D. Kim, Y. Maravin, T. Mitchell, A. Modak, K. Nam

Lawrence Livermore National Laboratory, Livermore, California, U.S.A.

F. Rebassoo, D. Wright

University of Maryland, College Park, Maryland, U.S.A.

E. Adams, A. Baden, O. Baron, A. Belloni, S.C. Eno, N.J. Hadley, S. Jabeen, R.G. Kellogg, T. Koeth, S. Lascio, A.C. Mignerey, S. Nabili, C. Palmer, M. Seidel, A. Skuja, L. Wang, K. Wong

Massachusetts Institute of Technology, Cambridge, Massachusetts, U.S.A.

D. Abercrombie, G. Andreassi, R. Bi, W. Busza, I.A. Cali, Y. Chen, M. D'Alfonso, J. Eysermans, C. Freer, G. Gomez Ceballos, M. Goncharov, P. Harris, M. Hu,

JHEP05(2022)014

M. Klute, D. Kovalskyi, J. Krupa, Y.-J. Lee, C. Mironov, C. Paus, D. Rankin, C. Roland, G. Roland, Z. Shi, G.S.F. Stephans, J. Wang, Z. Wang, B. Wyslouch

University of Minnesota, Minneapolis, Minnesota, U.S.A.

R.M. Chatterjee, A. Evans, J. Hiltbrand, Sh. Jain, M. Krohn, Y. Kubota, J. Mans, M. Revering, R. Rusack, R. Saradhy, N. Schroeder, N. Strobbe, M.A. Wadud

University of Nebraska-Lincoln, Lincoln, Nebraska, U.S.A.

K. Bloom, M. Bryson, S. Chauhan, D.R. Claes, C. Fangmeier, L. Finco, F. Golf, C. Joo, I. Kravchenko, M. Musich, I. Reed, J.E. Siado, G.R. Snow[†], W. Tabb, F. Yan, A.G. Zecchinelli

State University of New York at Buffalo, Buffalo, New York, U.S.A.

G. Agarwal, H. Bandyopadhyay, L. Hay, I. Iashvili, A. Kharchilava, C. McLean, D. Nguyen, J. Pekkanen, S. Rappoccio, A. Williams

Northeastern University, Boston, Massachusetts, U.S.A.

G. Alverson, E. Barberis, Y. Haddad, A. Hortiangtham, J. Li, G. Madigan, B. Marzocchi, D.M. Morse, V. Nguyen, T. Orimoto, A. Parker, L. Skinnari, A. Tishelman-Charny, T. Wamorkar, B. Wang, A. Wisecarver, D. Wood

Northwestern University, Evanston, Illinois, U.S.A.

S. Bhattacharya, J. Bueghly, Z. Chen, A. Gilbert, T. Gunter, K.A. Hahn, Y. Liu, N. Odell, M.H. Schmitt, M. Velasco

University of Notre Dame, Notre Dame, Indiana, U.S.A.

R. Band, R. Bucci, M. Cremonesi, A. Das, N. Dev, R. Goldouzian, M. Hildreth, K. Hurtado Anampa, C. Jessop, K. Lannon, J. Lawrence, N. Loukas, D. Lutton, J. Mariano, N. Marinelli, I. Mcalister, T. McCauley, C. Mcgrady, K. Mohrman, C. Moore, Y. Musienko[51], R. Ruchti, A. Townsend, M. Wayne, A. Wightman, M. Zarucki, L. Zygala

The Ohio State University, Columbus, Ohio, U.S.A.

B. Bylsma, L.S. Durkin, B. Francis, C. Hill, M. Nunez Ornelas, K. Wei, B.L. Winer, B.R. Yates

Princeton University, Princeton, New Jersey, U.S.A.

F.M. Addesa, B. Bonham, P. Das, G. Dezoort, P. Elmer, A. Frankenthal, B. Greenberg, N. Haubrich, S. Higginbotham, A. Kalogeropoulos, G. Kopp, S. Kwan, D. Lange, D. Marlow, K. Mei, I. Ojalvo, J. Olsen, D. Stickland, C. Tully

University of Puerto Rico, Mayaguez, Puerto Rico, U.S.A.

S. Malik, S. Norberg

Purdue University, West Lafayette, Indiana, U.S.A.

A.S. Bakshi, V.E. Barnes, R. Chawla, S. Das, L. Gutay, M. Jones, A.W. Jung, S. Karmarkar, D. Kondratyev, M. Liu, G. Negro, N. Neumeister, G. Paspalaki, S. Piperov, A. Purohit, J.F. Schulte, M. Stojanovic[16], J. Thieman, F. Wang, R. Xiao, W. Xie

JHEP05(2022)014

Purdue University Northwest, Hammond, Indiana, U.S.A.
J. Dolen, N. Parashar

Rice University, Houston, Texas, U.S.A.
A. Baty, T. Carnahan, M. Decaro, S. Dildick, K.M. Ecklund, S. Freed, P. Gardner, F.J.M. Geurts, A. Kumar, W. Li, B.P. Padley, R. Redjimi, W. Shi, A.G. Stahl Leiton, S. Yang, L. Zhang[95], Y. Zhang

University of Rochester, Rochester, New York, U.S.A.
A. Bodek, P. de Barbaro, R. Demina, J.L. Dulemba, C. Fallon, T. Ferbel, M. Galanti, A. Garcia-Bellido, O. Hindrichs, A. Khukhunaishvili, E. Ranken, R. Taus

Rutgers, The State University of New Jersey, Piscataway, New Jersey, U.S.A.
B. Chiarito, J.P. Chou, A. Gandrakota, Y. Gershtein, E. Halkiadakis, A. Hart, M. Heindl, O. Karacheban[24], I. Laflotte, A. Lath, R. Montalvo, K. Nash, M. Osherson, S. Salur, S. Schnetzer, S. Somalwar, R. Stone, S.A. Thayil, S. Thomas, H. Wang

University of Tennessee, Knoxville, Tennessee, U.S.A.
H. Acharya, A.G. Delannoy, S. Fiorendi, S. Spanier

Texas A&M University, College Station, Texas, U.S.A.
O. Bouhali[96], M. Dalchenko, A. Delgado, R. Eusebi, J. Gilmore, T. Huang, T. Kamon[97], H. Kim, S. Luo, S. Malhotra, R. Mueller, D. Overton, D. Rathjens, A. Safonov

Texas Tech University, Lubbock, Texas, U.S.A.
N. Akchurin, J. Damgov, V. Hegde, S. Kunori, K. Lamichhane, S.W. Lee, T. Mengke, S. Muthumuni, T. Peltola, I. Volobouev, Z. Wang, A. Whitbeck

Vanderbilt University, Nashville, Tennessee, U.S.A.
E. Appelt, S. Greene, A. Gurrola, W. Johns, A. Melo, H. Ni, K. Padeken, F. Romeo, P. Sheldon, S. Tuo, J. Velkovska

University of Virginia, Charlottesville, Virginia, U.S.A.
M.W. Arenton, B. Cardwell, B. Cox, G. Cummings, J. Hakala, R. Hirosky, M. Joyce, A. Ledovskoy, A. Li, C. Neu, C.E. Perez Lara, B. Tannenwald, S. White

Wayne State University, Detroit, Michigan, U.S.A.
N. Poudyal

University of Wisconsin — Madison, Madison, WI, Wisconsin, U.S.A.
K. Black, T. Bose, C. Caillol, S. Dasu, I. De Bruyn, P. Everaerts, F. Fienga, C. Galloni, H. He, M. Herndon, A. Hervé, U. Hussain, A. Lanaro, A. Loeliger, R. Loveless, J. Madhusudanan Sreekala, A. Mallampalli, A. Mohammadi, D. Pinna, A. Savin, V. Shang, V. Sharma, W.H. Smith, D. Teague, S. Trembath-Reichert, W. Vetens

JHEP05(2022)014

†: Deceased
1: Also at TU Wien, Wien, Austria
2: Also at Institute of Basic and Applied Sciences, Faculty of Engineering, Arab Academy for Science, Technology and Maritime Transport, Alexandria, Egypt
3: Also at Université Libre de Bruxelles, Bruxelles, Belgium
4: Also at Universidade Estadual de Campinas, Campinas, Brazil
5: Also at Federal University of Rio Grande do Sul, Porto Alegre, Brazil
6: Also at The University of the State of Amazonas, Manaus, Brazil
7: Also at University of Chinese Academy of Sciences, Beijing, China
8: Also at Department of Physics, Tsinghua University, Beijing, China
9: Also at UFMS, Nova Andradina, Brazil
10: Also at Nanjing Normal University Department of Physics, Nanjing, China
11: Now at The University of Iowa, Iowa City, Iowa, U.S.A.
12: Also at Institute for Theoretical and Experimental Physics named by A.I. Alikhanov of NRC 'Kurchatov Institute', Moscow, Russia
13: Also at Joint Institute for Nuclear Research, Dubna, Russia
14: Now at British University in Egypt, Cairo, Egypt
15: Also at Zewail City of Science and Technology, Zewail, Egypt
16: Also at Purdue University, West Lafayette, Indiana, U.S.A.
17: Also at Université de Haute Alsace, Mulhouse, France
18: Also at Tbilisi State University, Tbilisi, Georgia
19: Also at Erzincan Binali Yildirim University, Erzincan, Turkey
20: Also at CERN, European Organization for Nuclear Research, Geneva, Switzerland
21: Also at RWTH Aachen University, III. Physikalisches Institut A, Aachen, Germany
22: Also at University of Hamburg, Hamburg, Germany
23: Also at Isfahan University of Technology, Isfahan, Iran
24: Also at Brandenburg University of Technology, Cottbus, Germany
25: Also at Forschungszentrum Jülich, Juelich, Germany
26: Also at Physics Department, Faculty of Science, Assiut University, Assiut, Egypt
27: Also at Karoly Robert Campus, MATE Institute of Technology, Gyongyos, Hungary
28: Also at Institute of Physics, University of Debrecen, Debrecen, Hungary
29: Also at Institute of Nuclear Research ATOMKI, Debrecen, Hungary
30: Also at MTA-ELTE Lendület CMS Particle and Nuclear Physics Group, Eötvös Loránd University, Budapest, Hungary
31: Also at Wigner Research Centre for Physics, Budapest, Hungary
32: Also at IIT Bhubaneswar, Bhubaneswar, India
33: Also at Institute of Physics, Bhubaneswar, India
34: Also at Punjab Agricultural University, Ludhiana, India
35: Also at Shoolini University, Solan, India
36: Also at University of Hyderabad, Hyderabad, India
37: Also at University of Visva-Bharati, Santiniketan, India
38: Also at Indian Institute of Technology (IIT), Mumbai, India
39: Also at Deutsches Elektronen-Synchrotron, Hamburg, Germany
40: Also at Sharif University of Technology, Tehran, Iran
41: Also at Department of Physics, University of Science and Technology of Mazandaran, Behshahr, Iran
42: Now at INFN Sezione di Bari, Università di Bari, Politecnico di Bari, Bari, Italy
43: Also at Italian National Agency for New Technologies, Energy and Sustainable Economic Development, Bologna, Italy

JHEP05(2022)014

44: Also at Centro Siciliano di Fisica Nucleare e di Struttura Della Materia, Catania, Italy
45: Also at Scuola Superiore Meridionale, Università di Napoli Federico II, Napoli, Italy
46: Also at Università di Napoli 'Federico II', Napoli, Italy
47: Also at Consiglio Nazionale delle Ricerche — Istituto Officina dei Materiali, Perugia, Italy
48: Also at Riga Technical University, Riga, Latvia
49: Also at Consejo Nacional de Ciencia y Tecnología, Mexico City, Mexico
50: Also at IRFU, CEA, Université Paris-Saclay, Gif-sur-Yvette, France
51: Also at Institute for Nuclear Research, Moscow, Russia
52: Now at National Research Nuclear University 'Moscow Engineering Physics Institute' (MEPhI), Moscow, Russia
53: Also at Institute of Nuclear Physics of the Uzbekistan Academy of Sciences, Tashkent, Uzbekistan
54: Also at St. Petersburg Polytechnic University, St. Petersburg, Russia
55: Also at University of Florida, Gainesville, Florida, U.S.A.
56: Also at Imperial College, London, United Kingdom
57: Also at P.N. Lebedev Physical Institute, Moscow, Russia
58: Also at California Institute of Technology, Pasadena, California, U.S.A.
59: Also at Budker Institute of Nuclear Physics, Novosibirsk, Russia
60: Also at Faculty of Physics, University of Belgrade, Belgrade, Serbia
61: Also at Trincomalee Campus, Eastern University, Sri Lanka, Nilaveli, Sri Lanka
62: Also at INFN Sezione di Pavia, Università di Pavia, Pavia, Italy
63: Also at National and Kapodistrian University of Athens, Athens, Greece
64: Also at Ecole Polytechnique Fédérale Lausanne, Lausanne, Switzerland
65: Also at Universität Zürich, Zurich, Switzerland
66: Also at Stefan Meyer Institute for Subatomic Physics, Vienna, Austria
67: Also at Laboratoire d'Annecy-le-Vieux de Physique des Particules, IN2P3-CNRS, Annecy-le-Vieux, France
68: Also at Şırnak University, Sirnak, Turkey
69: Also at Near East University, Research Center of Experimental Health Science, Nicosia, Turkey
70: Also at Konya Technical University, Konya, Turkey
71: Also at Piri Reis University, Istanbul, Turkey
72: Also at Adiyaman University, Adiyaman, Turkey
73: Also at Ozyegin University, Istanbul, Turkey
74: Also at Necmettin Erbakan University, Konya, Turkey
75: Also at Bozok Universitetesi Rektörlügü, Yozgat, Turkey
76: Also at Marmara University, Istanbul, Turkey
77: Also at Milli Savunma University, Istanbul, Turkey
78: Also at Kafkas University, Kars, Turkey
79: Also at Istanbul Bilgi University, Istanbul, Turkey
80: Also at Hacettepe University, Ankara, Turkey
81: Also at Istanbul University — Cerrahpasa, Faculty of Engineering, Istanbul, Turkey
82: Also at Vrije Universiteit Brussel, Brussel, Belgium
83: Also at School of Physics and Astronomy, University of Southampton, Southampton, United Kingdom
84: Also at Rutherford Appleton Laboratory, Didcot, United Kingdom
85: Also at IPPP Durham University, Durham, United Kingdom
86: Also at Monash University, Faculty of Science, Clayton, Australia
87: Also at Università di Torino, Torino, Italy
88: Also at Bethel University, St. Paul, Minnesota, U.S.A.

JHEP05(2022)014

89: Also at Karamanoğlu Mehmetbey University, Karaman, Turkey
90: Also at Ain Shams University, Cairo, Egypt
91: Also at Bingol University, Bingol, Turkey
92: Also at Georgian Technical University, Tbilisi, Georgia
93: Also at Sinop University, Sinop, Turkey
94: Also at Erciyes University, Kayseri, Turkey
95: Also at Institute of Modern Physics and Key Laboratory of Nuclear Physics and Ion-beam Application (MOE) — Fudan University, Shanghai, China
96: Also at Texas A&M University at Qatar, Doha, Qatar
97: Also at Kyungpook National University, Daegu, Korea

JHEP05(2022)014